Use of Diffuser Fibres in the Treatment of Prostate Cancer by Interstitial Photodynamic Therapy

Master's Thesis

Shaineze Afir

SpectraCure AB and
Centre for Mathematical Sciences at Lund University

Supervisors: Ida Arvidsson,
Niels Christian Overgaard and Johannes Swartling

January-August 2018

Abstract

SpectraCure AB is a start-up company aiming at treating internal solid tumours such as prostate tumours with an innovative technology called 'Interstitial Photodynamic Therapy'. This treatment requires the use of optical fibres to deliver the amount of light required to activate a drug injected to the patient which leads to the destruction of the tumours. This treatment is patient-based which means that the amount of light, modulated by the irradiation time, is dependent on the characteristics of the tissue for each patient. In order to do so, the critical parameters to estimate are the optical properties and among them, a particular attention will be given to the effective attenuation coefficient μ_{eff}, which characterises the tissue to be treated. Those parameters are then used as inputs of an algorithm calculating the appropriate irradiation time for each light delivery fibre based on the minimal dose the tissue is supposed to receive to permit the activation of the drug. So far, SpectraCure AB has been using 400 µm core diameter bare end fibres assumed to be point sources to perform the light delivery; eighteen of those are required to have a good estimation of the optical properties of the tissue and enough light in all the region to be treated. The idea now is to introduce diffuser fibres, modelled as an array of point sources, to be able to increase the power delivered by the fibres and in the meantime reducing the number of fibres. The aim of this thesis is to evaluate the performance of diffuser fibres in interstitial photodynamic therapy. A finite element method (FEM) solver called Nirfast for near IR (Infrared) fluorescence and spectral tomography has been used. The study has shown that the properties of the tissue remain well determined for 5 and 7 mm diffuser fibres while they become less accurate for a higher fibre length. Furthermore, the diffusion approximation, which is the simplest approximation for the light propagation in homogeneous tissues, has been applied in the case we have a heterogeneous medium and has lead to correct enough results to enable the treatment with the P18 system developed by SpectraCure AB. We intended to change the power delivered by the fibre but no satisfying conclusion could be drawn.

Acknowledgements

I would like to thank my supervisors Ida Ardvidsson for her patience, help and availability throughout my thesis, Johannes Swartling for giving me the opportunity to do this master thesis, and Niels Christian Overgaard for his continuous feedback. I would also like to give special thanks to Björn Thomasson for his continuous help and moral support during this project. Finally, I would like to thank all the people at SpectraCure AB for their kindness and benevolence.

Contents

Chapter 1: Introduction

1.1 General Overview on Prostate Cancer

According to the World Health Organization (WHO), cancer is the second leading cause of death worldwide: one in six deaths is due to cancer. In 2012, the International Agency for Research on Cancer (IARC) has launched a project called Globocan. The purpose of the project was to evaluate the incidence and mortality of cancer in 184 countries. The incidence is related to the probability for a given medical condition to occur within a population. It has been shown that prostate cancer is the second most common type of cancer in men. Nonetheless, prostate cancer is less deadly than some other cancers and therefore constitutes the fifth leading cause of death by cancer worldwide for men. Even though prostate cancer presents a high survival rate in comparison with other types of cancers, the treatments currently available on the market show several drawbacks.

First, it should be highlighted that the prostate is a gland which is part of the reproductive male system. Its main role is to secrete a fluid which represents 30% of the male semen along with spermatozoa and other constituents. It surrounds part of the urethra and is near the rectum. This proximity to the rectum is convenient in the sense that doctors can perform an examination of the gland through the rectum if they have some suspicion of disease. On the other side, it presents some serious downsides when it comes to treatments. The growing of prostate with age is a natural process but might induce some discomfort such as problems of urination due to the compression of the urethra.

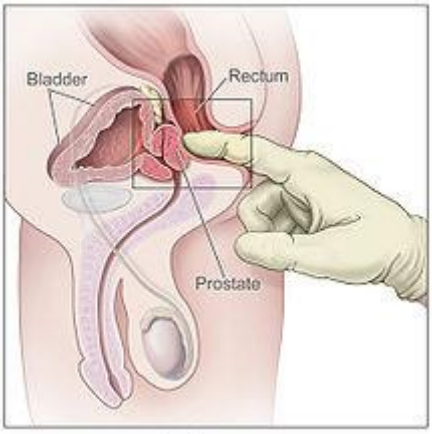

Figure 1.1: Prostate (reference [1]).

The current available treatments are surgery and radiation therapy. The surgical procedure is called prostatectomy and consists in the ablation of the prostate gland. The radiation can be divided into external beam radiation therapy or internal therapy in which a radioactive substance is directly introduced inside the prostate. One of the remarkable characteristic of prostate cancer which justifies the ablation of the gland is that it is often a homogeneous cancer. In other words, cancer is usually spread in the whole prostate.

As said previously, those treatments might have serious side effects such as damaging the nerves leading to erectile dysfunctions or creating a recto-urethra fistula which may generate incontinence or leakage. Those side effects are so important that patients with a slow evolving cancer or old patients are recommended to be maintained under active surveillance instead of starting a treatment, which includes regular testing and monitoring, until new signs show up. Therefore, there is a need for new technical solutions which will help to eliminate the cancer while avoiding the downsides of the treatment.

1.2 Current and Future SpectraCure Solution

Photodynamic therapy (PDT) or interstitial photodynamic therapy (iPDT) are relatively new fields. The combination of the phototoxic and tumor localizing properties of some agents such as porphyrins was exploited for the first time in a paper released in the early 70's. Nonetheless, the first clinical approval are granted twenty years later, first in Canada in 1993.

PDT involves the use of light as treatment. It requires the use of a photosensitizer agent, whose uptake is high by cancerous cells, that absorbs light of certain wavelengths. Then, the excited photosensitizer reacts with molecular oxygen to create radicals that are extremely reactive substances. Those radicals can induce the death of the cells. The surrounding normal tissues are given negligible damage. Furthermore, no obvious mechanism of acquiring resistance to PDT has been observed. It is recognized as a minimally invasive procedure employed for different domains, for example in the treatment of acne. It is under clinical trial for the treatment of different types of cancer such as lung, prostate and bladder cancer.

The need for less harmful treatment combined to the neglectable damages due to PDT have brought SpectraCure AB to choose to develop a product that would use PDT as the technical solution for cancer treatment with a great focus on prostate cancer. They combine state-of-the-art technologies in different science sectors to offer a complete product. Their system integrates an interstitial ultrasound device (see Figure 1.2) that acquires an image of the prostate by inserting a ultrasound probe in the rectum and sending ultrasound pulses towards the prostate (the rectum and prostate are in vicinity as explained in Section 1.1). This image helps to guide the surgeon who has to position up to eighteen fibres in pre-calculated locations in the prostate, as seen in Figure 1.3. The fibres are coupled to a laser device that delivers the correct amount of light to each fibre. The treatment of the patient with the Spectracure system is divided into two steps. The first step consists in determining the initial optical properties to offer an individual treatment for each patient. In this step, the fibres act as both emitters and receivers to analyse the light coming out from each other fibre. The second step is the dose delivery and corresponds to the part where the fibres are only used as emitters to provide the correct amount of light, as seen in Figure 1.4. Those two steps are repeated several times to allow for a tracking in time of the optical properties which permits to avoid overexposure of the tissues while ensuring that the treatment is successful. One of the main challenges is to direct the light in the prostate while minimizing the dose in the surrounding sensitive tissues, more particularly the urethra and the rectum. We assume for simplicity that the optical properties in these tissues are the same than in the prostate since no direct evaluation of the optical properties are made in these tissues.

To simulate the estimation of the optical properties, we will need some initial data. Normally, during the treatment, those data are obtained by litting up one fibre after the other. The other fibres are recording the signal coming out from the lit fibre. In this master thesis, we have chosen to use a FEM solver, nirfast, to simulate this. To calculate the simulated data, the software uses a simplified version of the radiative transfer equation which governs the transport of light in scattering media. After setting out the optical properties and positioning the fibres, it will give us some data that correspond to the signal recorded by the other fibres when each of them is lit on one after the other. Therefore, these data constitute our ground truth and constitute the data with which we perform the evaluation of the optical properties. If the evaluation is good, then the estimated optical properties should be very close to the set optical properties before proceeding to the FEM simulation. In this estimation part, the radiative transfer equation used by nirfast is even more simplified. Indeed, as we will be able to see in equation (3.10), we will use the approximation that the medium is homogeneous to have a simple solution of the light delivered in the tissue.

Once we have the estimated optical properties, beyond the absolute comparison between the estimated optical properties and the ones set at the beginning to obtain the original data, we are more interested on the effects of the differences between the estimated and real optical properties on the dose delivery phase. Therefore, most of the time, we will analyse the dose received in the prostate to quantify the performance of the estimation of the optical properties. One more time, the light propagation will be assumed to follow the homogeneous approach of the radiative transfer equation.

So far, Spectracure AB has used bare end fibres, delivering light at the tip of the fibre and which are assumed to be point sources fibres. It has permitted to restrict most of the light to the prostate by calibrating the power output and duration time at each fibre. Nonetheless, some limits have appeared such as the formation of thermal gradients inside the tissue that might damage the surrounding tissues and limits the optical transmission of light. Consequently, in order to deliver a sufficient amount of light while limiting the power output of each fibre to avoid the damages mentioned before, eighteen bare end fibres are currently used. However, the time needed for the insertion procedure of the fibres increases the cost of the surgery and also the risks for the patient who has to be maintained for a longer time under anesthesia. These are the main reasons why the next step for cancer treatment with iPDT might involve diffuser fibres which deliver light along part of their length. The aim of this thesis is to study, in a 3D realistic model of the prostate, the effects of substituting bare end fibres by diffusers fibres or in other words to state the differences between the use of single point sources fibres and the use of fibres which are simulated as arrays of point sources. The idea is that we might save time and money by decreasing the number of fibres if we use diffusers fibres instead of bare end fibres.

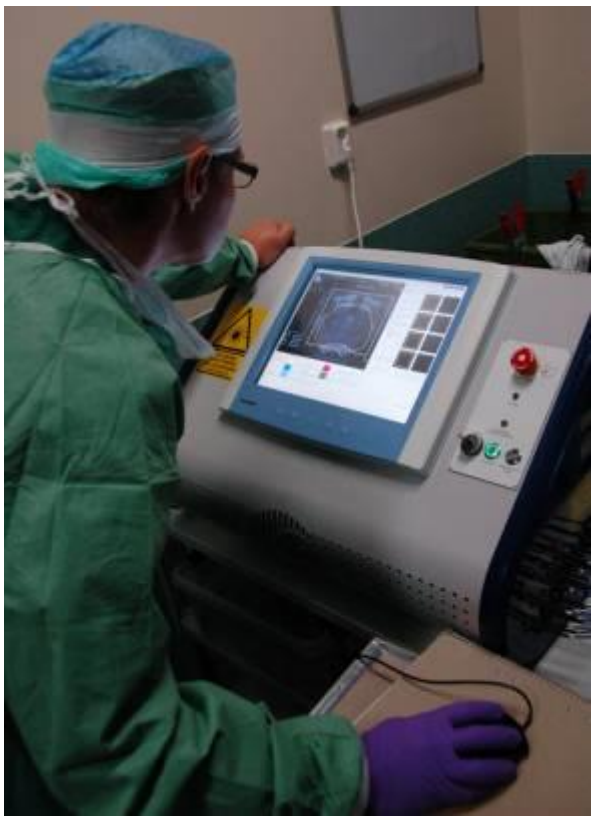

Figure 1.2: Spectracure system: The surgeon first obtains an image of the prostate and of the surrounding tissues before using an algorithm to calculate the fibre positions.

Figure 1.3: The surgeon is inserting the optical fibres at the positions indicated by the algorithm.

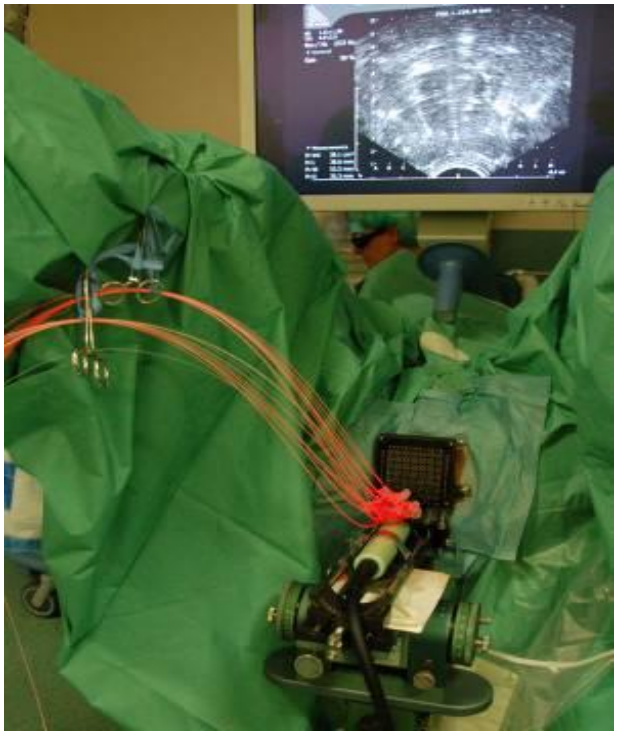

Figure 1.4: Evaluation of the optical properties and Treatment

1.3 Main Challenges

A study case was made in a previous diploma work [2] with four diffuser fibres and a simplistic model of prostate. In this work, the focus is on using the data collected by Spectracure AB on a patient to model a realistic 3D prostate and compute the light distribution in the prostate by solving a (variable coefficient) partial differential equation (PDE) using a FEM solver such as Comsol or NIRFAST. We will have a wide set of parameters to play with: the diffuser position, the diffuser length, the diffuser resolution (i.e the number of point sources used to approximate the diffuser fibre as an array of point sources), the heterogeneity of the prostate, etc.

The main questions that we would like to give an answer to are:

- Is it possible to decrease the number of fibres while permitting the same efficiency in the treatment?
- What are the best choices in terms of parameters for the fibres; such as diffuser length, delivered power and number of fibres.
- Will the optical properties still be correctly determined or will some problems arise from the use of diffuser fibres?
- Will we be able to control the amount of light delivered in the rectum and in the other surrounding tissues?

In the first part, the reader will be briefly introduced to the technique of photodynamic therapy. In the second and third part, this report will expose the theory used to solve the problems of light propagation in tissue by focusing on the different approximations made. Then, in a third part, the results of the simulation will be presented to the reader. The first step would be to present the case of bare end fibres, which can also be called point source fibres, before dealing with the case of diffuser fibres. This last part will hopefully bring us the answers to the questions mentioned in the previous paragraph.

Chapter 2: Photodynamic Therapy

This chapter will help the reader to have a better understanding of the biological and biochemical mechanisms hidden behind the name photodynamic therapy.

2.1 History

Even though photodynamic therapy was known since ages ago, it has only been recently rediscovered and developed. This therapy involves three key components: a photosensitizer, a light source and tissue oxygen. The combined action of those three factors has been discovered and understood through more than one century of experiments.

Phototherapy started in the ancient times, back to about 3000 BC. People in Ancient Egypt, in Greece or even India were believing in the virtues of heliotherapy that they were using to cure skin disorders such as psoriasis or vitiligo.

Later on, the romans invented the 'therms' which were baths exposed to sunlight, especially appreciated for the treatment of skin conditions. With the decline of the Roman Empire, the therms and the concept of heliotherapy disappeared.

Phototherapy appeared again at the end of the XIXth century thanks to a Swiss natural healer and physician called A.Rikli that brought back to the world the concept of light as a curative treatment, concept that had been forgotten for centuries. A.Rikli is often considered as the pioneer of modern phototherapy and dedicated his life to find natural therapies, sticking to his motto 'Water is good, Air is better and Light is best of all'.

At the beginning of the XXth century, light was used in northern Europe and in northern cities of North America to cure lupus vulgaris (cutaneous tuberculosis skin lesions), pulmonary tuberculosis and rickets (soft bones in children due mainly to a vitamin D deficiency). One of the main contributor to the development of phototherapy was a Danish doctor N. Finsen (1860-1904) that showed the benefits of using UV (ultraviolet) lights and received a Nobel Prize in medicine for using UV radiation from the carbon arc lamp in the treatment of skin tuberculosis.

In the mean time, a German professor in Pharmacology in Munich, H.Tappeiner, was developing the field of photobiology. In 1904, he invents the term of Photodynamic Action after noticing the impact of sunlight on the activation of the acridine dye drug.

One of the main discovery in the Pharmacology field is the development of hematoporphyrin (hp). Discovered in 1841, it was first tested on humans around 1910 and was suggested to be used for treatment cancer due to his high affinity towards rapidly dividing cells in 1948. Later on, S.Schwartz discovered that it was not hp that was responsible for the localized action but hematoporphyrin derivatives (hpD) and used it for tumour diagnosis in the year 1960. At the end of the 70's, a first commercial drug, called Photofrin (see Figure 2.1), appeared on the market after some studies was made on human tumor by Dougherty and his coworkers. This period is considered as the beginning of the new era of PDT.

Nowadays, three families of photosensitizers are used: Porphyrin (hp and its derivatives commercialized under the label Photofrin, Photocan or Photosan), Chlorines and Dyes. The chlorines are substances coming from the degradation of chlorophyll in bacteria and algae, which possess photosensitizing properties. Each kind of drug possess its own benefits.

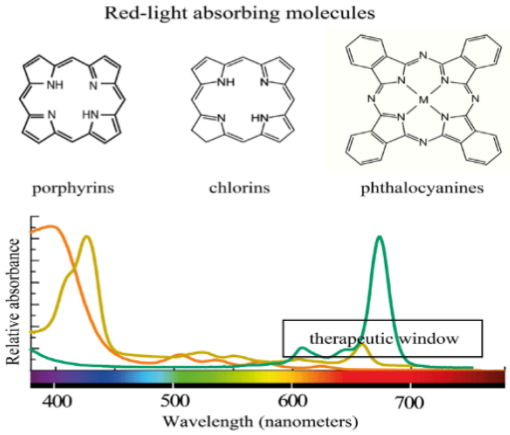

Photosensitizer	Chemical structure	Absorption coefficient $M^{-1}cm^{-1}$	Wavelength (nm)
Porfimer sodium (Photofrin)	porphyrin	3,000	632
Temoporfin (mTHPC, Foscan)	chlorin	35,000	652
Verteporfin (BPD-MA, Visudine)	chlorin	34,000	690
HPPH	chlorin	47,000	665
Chlorin e_6 (C e6)	chlorin	59,000	660
Silicon phthalocyanine (Pc4)	phthalocyanine	200,000	675
Aluminum phthalocyanine tetrasulphonate	phthalocyanone	150,000	676
Zn(II)-phthalocyanine	phthalocyanine	243,000	675
Palladium bacteriopheophorbide (Tookad)	Bacteriochlorin	88,000	762

mTHPC, *meta*-tetra(hydroxyphenyl)chlorine; BPD-MA, benzoporphyrin derivative monoacid ring A; HPPH, 2-(1-hexyloxyethyl)-2-devinyl pyropheophorbide.

Figure 2.1 Optical windows and example of Photosensitizers drugs ([3]).

2.2 Absorption and Scattering

2.2.1 Historic

In the early 1800, Fraunhofer noticed that dark lines appear systematically in the solar spectrum. 45 years later, Kirchoff and Bunsen noticed that those dark lines coincide with emission light of chemical elements and explained that the Fraunhofer lines come from the absorption of chemical elements in the solar atmosphere. This absorption phenomenon has been theorized in 1900 by Planck as the quantum theory.

Einstein used the concept developed by Planck some years before to extend it to the case of light. In 1905, Einstein provides an explanation of the photoelectric effect by postulating the existence of quanta of light: light is therefore constituted by particles called photons. This postulate is called the wave-particle duality. Before Einstein, light was seen as a wave that propagates an electromagnetic field. Einstein's theory is at the origin of the interaction between light and matter.

Matter is constituted by atoms which are neutral. Nonetheless, this neutrality is due to the balance of positive and negative charges. The atom's nucleus is composed of positive and neutral particles called respectively, protons and neutrons. Negative particles called electrons surround the nucleus. Consequently, a photon with a certain energy can exchange energy with those atom's particles. This concept is at the core of spectroscopy. The atom is an organized structure in the sense that its particles can only have certain discrete values of energies. This atomic structure was theorized mathematically by Schrödinger in 1925. In the case of the interaction between matter and light, photons can only be absorbed if they have a certain energy that matches the energy difference between two electronic levels that are solutions of the Schrödinger's equation. This absorption could be represented by a simple diagram as in Figure 2.2.

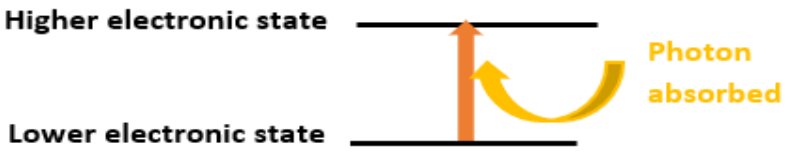

Figure 2.2: Schema of the absorption of a photon

Light in the visible and in the ultraviolet (UV) promotes electrons from one low lying energy level to a higher one. Furthermore, in molecules (and not in atoms) each electronic level is associated with many vibrational levels. To those vibrational levels, rotational levels are superimposed which turns the total level scheme to an almost continuum of states. But the transitions between different vibrational-electronic-rotational are not equally probable.

A chromophore, which is a feature of a molecule describing which wavelengths it can absorb, might also receive light that provokes such a transition. Usually, light in the infrared (IR) domain induces those types of excitations, or in other words following Figure 2.3, which induces a vibrational transition.

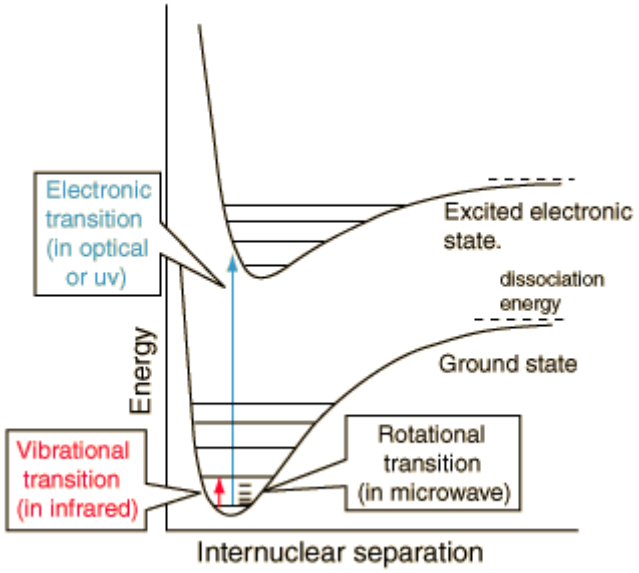

Figure 2.3: Electronic, vibrational and rotational levels in a molecule ([4]).

2.2.2 Optical Window

As explained before, the absorption of light in tissue is linked to the excitation of one electron to a higher state of energy. The main chromophores in the body are blood and water. Other components may contribute to absorption such as melanin or fat. Minor chromophores can also be present but they usually do not perturb the light transport, so for the present study, we can neglect them. The absorption is represented in Figure 2.4 where the vertical axis represents the absorbance which is defined as the fraction of light which is absorbed in logarithmic units ($A = \log\left(\frac{I_{absorbed}}{I_{sent}}\right)$). We can see that there is a domain of wavelengths in which the absorption of the chromophores is minimum. This band of wavelengths, between 600 nm and 1200 nm, is called the optical window. Before the optical window, the absorption by blood and more precisely by haemoglobin is really important. After the optical window, the absorption by water becomes considerable and the infrared light can not propagate in an efficient way in the body. This domain usually limits the choice of wavelength selected to perform photodynamic therapy. We want the light to propagate as far as possible, to be able to treat a large volume.

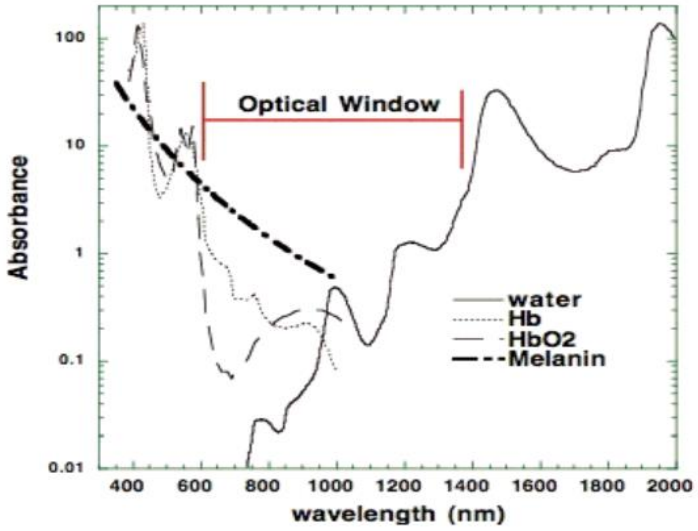

Figure 2.4: Absorption of different chromophores ([5]).

2.2.3 Optical coefficients

Usually, the absorption in tissue is expressed via a coefficient called the absorption coefficient and denoted μ_a. It can be measured indirectly by measuring the intensity of the light.

$$I = I_0 * \exp(-\mu_a * r)$$

Here, I denotes the intensity of the light after passing through the matter, I_0 the initial intensity and r is the distance travelled by the light.

To understand the signification of this absorption coefficient, one can imagine an ideal spherical chromophore characterized by a dimension A which blocks certain rays of light and ends up having an effective cross-section given by $\sigma_a = Q * A$, where Q is just a proportionality constant. The relation between the cross section and the absorption coefficient is linear and only involves N_a, a constant corresponding to the number of chromophores molecules in the medium. In fact, $\mu_a = N_a * \sigma_a$. We can also interpret this absorption coefficient as the inverse of the mean free path which is the distance that a photon travels before being absorbed.

The stopping of some fraction of light is not the only phenomenon that is to consider when talking about light propagation in tissue. In reality, as mentioned in the beginning of this chapter, because we select a wavelength such that we end up in the optical window to allow light propagation, there is another important parameter to take into account, which is the scattering coefficient. The scattering is due to the deviation of the light in the medium because of the heterogeneity of the body tissues. This scattering can be elastic and conserve the energy of the scattered light or inelastic and change the frequency of the light.

Two main types of elastic scattering can be determined: Rayleigh scattering concerns very small particle (compared to the wavelength) and the intensity scattered is proportional to $\frac{1}{\lambda^4}$ (where λ is the wavelength) while Mie scattering which is weakly dependent of the wavelength, concerns large particle or particle in the order of the wavelength and mainly scatter light in the forward direction. In the same way that absorption is described by a coefficient μ_a, scattering is described by a coefficient μ_s (also linked to a scattering cross section by a constant which gives the density of scatterers). However, in the case of scattering, because scattering can be privileged in some directions we also need another parameter to describe it. This preference for some directions is quantified with the parameter g which represents the anisotropy of the scattering, $g = [-1,0,1]$. *g=-1* represents a totally backward scattering, *g=1* a totally forward scattering and 0 a isotropic scattering. For biological tissues, we have essentially forward scattering with values of g between 0.65 and 0.95. A term called

reduced scattering coefficient takes into account that anisotropy value and is given by: $\mu'_s = \mu_s * (1 - g)$.

Finally, a single term called attenuation coefficient, μ_t, summarizes the effect of the absorption and scattering, by simply adding the absorption and scattering coefficient, $\mu_t = \mu_a + \mu'_s$

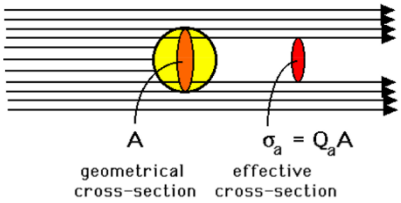

Figure 2.5: Cross-sections of chromophores.

2.3 Theoretical Background

Phototherapy requires three components that we will mention later on. The following part will help us to understand the mechanisms that lead to the destruction of the cancerous cells (necrosis).

2.3.1 A brief introduction to Biochemistry

A photosensitizer is a substance that is sensitive to light. In the previous Section 2.1, we gave the name of some of those commercial agents such as Photofrin. Some are illustrated in the Figure below. Those photosensitizers exhibit a system of conjugated bonds responsible for the absorption of light in the near infrared (NIR) domain. In Section 2.2.1, we have already briefly explained the principle of excitation of a molecule due to the action of light. In the context of photodynamic therapy, the laser light and the photosensitizer are chosen altogether so the exciting light matches the excitation wavelength required to permit the excitation from one energy level to another (see Figure 2.3).

The drug selected by SpectraCure, seen in Figure 2.6, is Verteporfirin (commercialized under the name Visudine and whose active substance is benzoporphyrin derivative monoacid (BPD-MA)). It presents a higher clearance rate from the body than hp and a skin photosensitivity for only a few days which is a great advantage in the treatment of the patient.

To understand the interaction between the electromagnetic field generated by the laser source and the electronic orbitals (which are mathematically represented by the solutions of the Schrödinger equation), we will need to recall some notions of quantum mechanics in biochemistry. This interaction could be described in analogy to the absorption of energy by an oscillating dipole antenna in a radio wave field. Nonetheless, the energy eigenstates of the molecule are stationary and the only source of oscillation is due to the superimposition of different energy eigenstates. This superimposition of state particularly occurs when an electromagnetic field interacts with the molecule.

The highest occupied molecular orbital (HOMO) and lowest unoccupied molecular orbital (LUMO) theory helps to predict the strength of a transition between two energy states. This theory helps to understand the intensity of the electronic absorption bands and the reason why all the transitions are not equiprobable. Some calculations (based on Hückel method applied to conjugated

systems) helps to predict, based on the atomic orbitals, the distribution of electrons in the molecular orbitals when the atoms bond in a molecule.

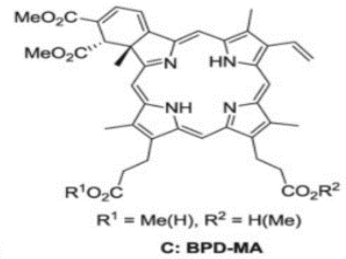

Figure 2.6: Verteporfirin ([6]).

Figure 2.7 shows those coefficients; the radius are representative of the values of those coefficients: big for high Hückel coefficients, small for low Hückel coefficients. The colors black and white are just there to indicate the sign of those coefficients (positive for black and negative for white). But only the absolute values of those coefficients matters. Here, in the transition charge density, we can see that there are four partial dipoles represented by red arrows. The strongest dipoles are pointing upwards, and the smallest downwards in the direction of the short axis of the molecule. This indicates that the HOMO-LUMO transition will be very likely if an electric field polarized parallel to the direction of the short axis will come. Therefore, we understand that depending on the values of those coefficients between the different energy eigenvalues, and given a certain field with a certain polarization, some transitions will be preferred and therefore have a high probability which results in a strong 'light' signal released by the molecule after de-excitation.

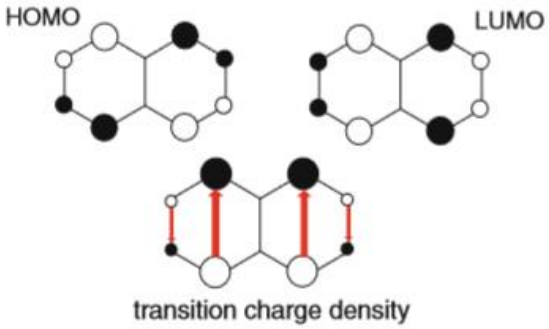

Figure 2.7: HOMO-LUMO theory of naphthalene ([7]).

2.3.2 Photophysical processes in molecules

The photosensitizer in the drug is under its fundamental stable configuration that is usually called ground state. Each electronic state has a spin multiplicity which corresponds to the sum of all the spins of the electrons that populate that certain state. The spin for an elementary particle corresponds to an intrinsic form of angular momentum. For the electron, the spin number S is equal to 1/2, and this spin is also related to another quantity which is the projection of this spin on a certain axis and usually results in two configurations for the electron: spin up (+1/2) and spin down (-1/2).

The multiplicity of the spin is a number given by the formula 2S+1. For normal molecules with an even number of electrons, the spin is generally 0, the multiplicity is therefore equal to 1 and explains the term of singlet state often heard in the literature. If the spin is equal to 1, the multiplicity is 3 and the reference term for the state is triplet.

The ground state configuration is usually a singlet state denoted by S_0. This can be seen in Figure 2.8 representing the different processes in the molecules following the absorption of light by the molecule. Each S_i system represents an excited electronic states while the light lines represent vibrational levels. As one can see, the absorption is followed by a fast radiationless process called vibrational relaxation and corresponds to the distribution to the molecule's surroundings of some excessive energy to end up in the most vibrationless excited electronic state of the system S_i. The

molecule can also undergo internal conversion which transfers electronic energy to vibration energy that is, one more time, dissipated to the surroundings.

The conversion from a singlet state to a triplet one can only happen if an effective magnetic field approaches the electron in the state. This can be due for example to collisions which will break the pairs of electrons and permits the flipping of an electron to get a spin of 1.

The return to the ground state after a certain time is called photoluminescence. This is particularly noticeable in a laboratory since it produces a spontaneous undirected emission of light, rather independent of the absorbed wavelength but which is specific to the emitting molecule. In reality this term includes two other phenomena: fluorescence and phosphorescence. The fluorescence follows quasi immediately the absorption: this is due to a state with a very short life time.

On the other hand, the triplet state has a longer lifetime. The fluorescent signal has a high intensity while the phosphorescent signal is weak. This is due to the fact that the ground state is a singlet state and the fluorescent signal, coming from the de-excitation from another singlet state to the ground state, is more likely to happen compared to the de-excitation from a triplet state (T_1 for example) to the ground state, giving the phosphorescent signal. This latter type of transition is qualified of forbidden transition because an allowed transition should preserve the spin multiplicity.

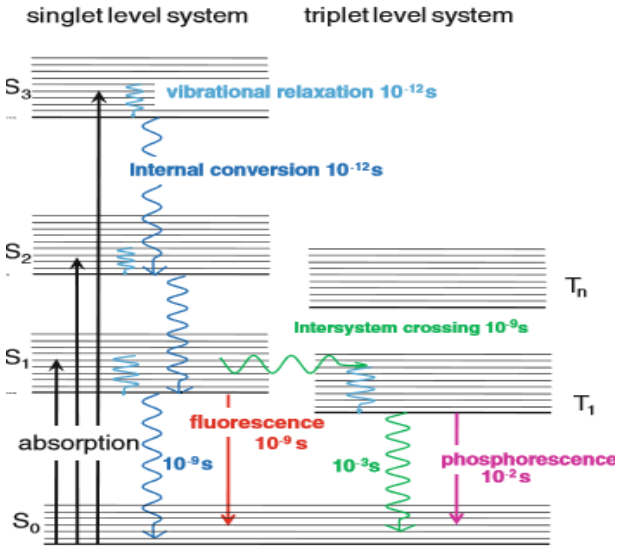

Figure 2.8: Jablonski scheme with the typical photophysical processes in molecules ([8]).

2.3.3 Mechanism of action of the photosensitizer

As mentioned above, the lifetime of the triplet state is longer than the singlet state. Consequently, the chance that they transfer energy is higher.

Now, we should give more attention to the dioxygen O_2 molecule. In the theory of HOMO-LUMO mentioned in part 2.3.1, the ground state of O_2 is shown to be a triplet state, whose molecular diagrams can be seen in the Figure below. We can see in the HOMO, the presence of two electrons with spins up (represented in the molecular orbitals called π^*). The singlet state can be formed by energy transfer. In the Molecular orbital (MO) diagram (see Figure 2.9), this would consist in pairing the electrons of the HOMO in the LUMO (which is called σ^* in the MO diagram). This configuration is unstable since it leaves a vacant orbital. Hence, this instability will induce a fast return to the triplet ground state (the lifetime of the singlet state is estimated to be about 100 ns). During that time the dioxygen can only diffuse less than 50 nm which indicates a localized action of the PDT treatment. The de-excitation will permit to have a photosensitizer in its ground state and therefore the drug is not consumed during that process.

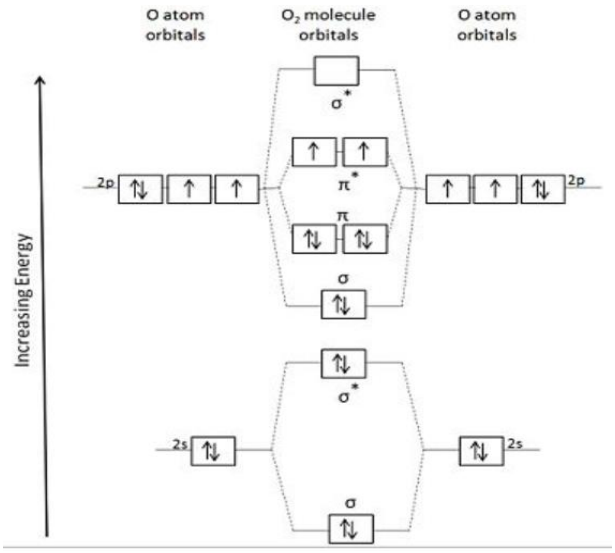

Figure 2.9: Molecular orbital (MO) diagram of dioxygen ([7]).

Nonetheless, there is a small probability that the singlet state of O_2 reacts with the ground state of the photosensitizer which results in a permanent loss of the photosensitizer. This phenomenon is called photobleaching. Drugs that favour type II reaction (reaction by formation of a singlet O_2 state) are more common but another mechanism called type I reaction can also lead to the necrosis of the cancerous cells. The excited triplet state of the PS substance can react with a substrate present in the tissue directly which will also result in the formation of oxidized products as shown in the Figure below.

One of the conclusion that we could come up with is the importance of choosing a drug with a high intersystem crossing yield.

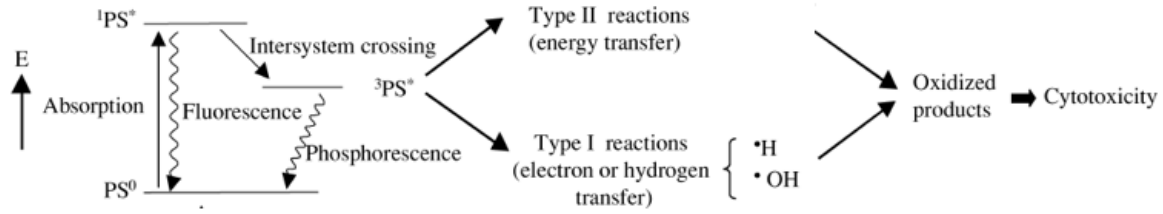

Figure 2.10: PDT Mechanism([8]).

2.4 SpectraCure AB System P18

2.4.1 Dosimetry

The photodynamic therapy is a complex process that involves the interdependence between three factors that can be seen in Figure 2.11: oxygen, light and photosensitizer. To give a measure of the efficacy of the treatment, three approaches are possible: explicit, implicit or indirect dosimetry. The concept of implicit and explicit photodynamic therapy dosimetry was introduced in the 90s by Wilson et al [17]. Well-defined physical quantities such as the fluence rate or the photosensitizer concentration can be measured with the explicit dosimetry. Since those quantities are physical, they can be measured and used in a dose model to estimate the singlet oxygen production. In implicit dosimetry, one can use a measurable quantity sensitive to some or all of the factors influencing photodynamic efficacy but that does not require independent measurements of each of these quantities.

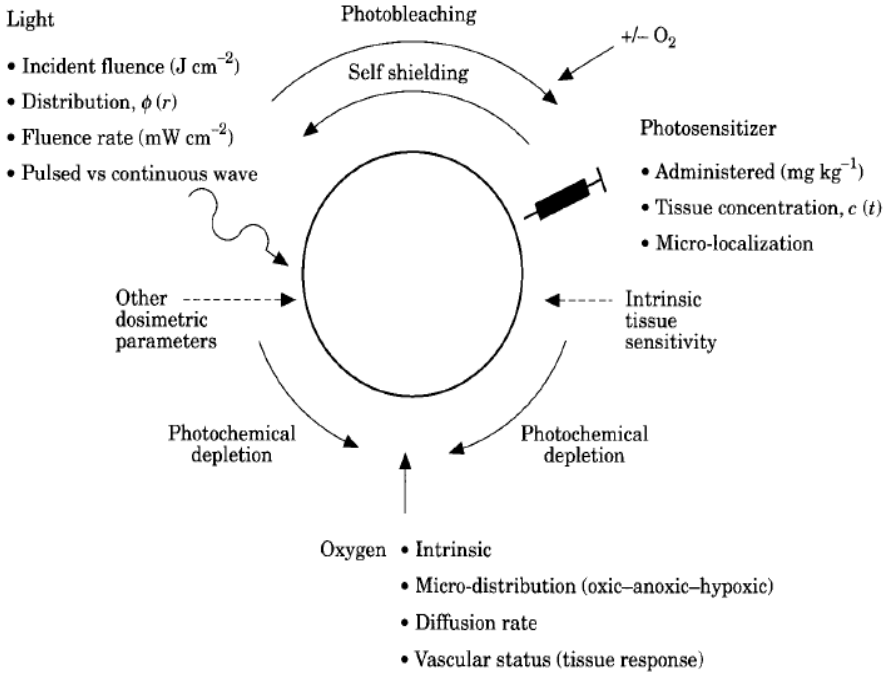

Figure 2.11: Interdependency of different dosimetry factors in PDT ([17]).

2.4.1.1 Explicit Dosimetry

A definition of explicit PDT dose from the physics point of view could be: 'the light energy deposited to photosensitizer', in other words, it is proportional to the product of the absorption coefficient of the photosensitizer and light fluence. The photosensitizer absorption coefficient is proportional to the photosensitizer concentration. In its simplest form, the explicit approach to PDT dosimetry consists of measuring the average photosensitizer concentration in or around the target tissue just prior to light treatment and the light fluence rate at some points within or around the target volume. In this approach, one of the a priori assumption is that the tissue response can be predicted by the local product of the light fluence rate and photosensitizer concentration. In some studies, it was found nonetheless that those measurements were not good predictors of the tissue response because it does not account for the oxygenation of the tissue.

Technically, explicit dosimetry can be a complex challenge, especially if we want to obtain a complete set of dose factor measurement. The main downside of explicit dosimetry is that it does not take into account microdosimetric factors.

2.4.1.2 Implicit Dosimetry

In implicit dosimetry, the purpose is to measure quantities that integrate all the response determining treatment factors and their interdependencies. Therefore, there is no need to measure all the factors independently. For example, one of the indices we can use in implicit dosimetry is the photobleaching effect. This photobleaching is caused by the reaction of the singlet oxygen formed with the photosensitizer itself, which leads to the destruction of the photosensitizer (see Section 3.2.3). Indeed, if that photobleaching is caused by reactions with singlet oxygen, it is reasonable to think that the rate of photobleaching will be a good index of the rate of deposition of singlet oxygen mediated damage in tissue. On the other hand, other physical processes such as oxygen transport and light diffusion complicate the correlation between photobleaching and PDT induced damage.

2.4.1.3 Direct Dosimetry

This dosimetry method consists in detecting the weak phosphorescence peak emitted at 1270nm when singlet oxygen returns to the ground state (see Figure 2.8). This method constitutes a real advantage since it especially reduces the complexity, a single measurement is used to evaluate the efficiency of the treatment. However, the singlet oxygen is extremely weak. Furthermore, in the near infrared (NIR) spectral region (where this signal is detected), the dark-count background of the photomultipliers (PMTs) detectors is considerable in comparison to the singlet oxygen signal and those PMTs are more expensive than PMTs used for visible spectrum analysis. Furthermore, other sources of luminescence such as endogenous cell/tissues might also make this identification harder. Finally, the monitoring by direct $^1O_2$ is difficult and cost effective if we compare it to some simpler techniques such as implicit and explicit dosimetry.

2.4.2 Light delivery system

In interstitial PDT, lasers are often used because they enable a good fibre coupling efficiency. The choice of the wavelength must match the absorption peak of the photosensitizer chosen. Therefore, Spectracure AB has chosen 690nm wavelength laser. The fibres, which are 400µm bare end fibres, deliver a power output of 150mW. The number of fibres used so far has been set to 18 (which explains the name P18 of the device) with the previous conditions of size and power output given before. The fact of having bare end fibres limit the power output due to a high accumulation of energy density at the tip of the fibres (only delivery point). That is the reason why diffuser fibres which can emit and receive light all along their length are preferred in order to be able to increase the light power output. Indeed, bare end fibres are usually preferred for the treatment of lesions within a hollow organ while cylindrical/diffuser fibres would be used for solid organs.

Chapter 3: Methodology Models of Light Propagation in Tissue

In biological tissue, the monitoring of optical properties is required to be able to predict quantitatively the light propagation. In general, near infrared light is used because of its low absorption by the living tissues. Nonetheless, because the body constitutes a complex medium with a high number of constituents, the light is scattered multiple times. Therefore, we need a model that accounts for this multi-scattering of the light. In such medium, the model that seems to describe this situation best is based on the theory of radiative transfer, presented in [13]. This chapter aims at presenting the main equations that govern the propagation of light in tissue to understand how the estimation of the optical properties can be made based on measurements of light distribution in certain locations of space. The equations will also be used when evaluating the performance of the estimation by calculating the light dose predicted in the tissue based on the estimated optical properties.

3.1 Light Transport in Tissue

3.1.1 Definitions

The prediction of light propagation in tissues is done thanks to the Radiative Transfer equation (RTE). Before deriving this equation based on conservation of energy, we need to introduce some quantities.

- **Spectral radiance L_ν** – is the energy flow per unit normal area per unit solid angle per unit time per unit temporal frequency bandwidth
- **Radiance L** – is defined as the spectral radiance integrated over a narrow frequency range [ν,ν+Δν].

  $$L(\vec{r},\hat{s},t) = L_\nu(\vec{r},\hat{s},t) * \Delta\nu$$

  Where r denotes the position, $\hat{s}$ a unit direction vector and *t* the time.
- **Fluence Rate or intensity** – is the energy flow per unit area per unit time:

  $$\phi = \int_{4\pi} L(\vec{r},\hat{s},t)d\Omega$$

  where Ω is the solid angle.
- **Current density J** – is the net energy flow per unit area per unit time:

  $$J(\vec{r},t) = \int_{4\pi} \hat{s} * L(\vec{r},\hat{s},t)d\Omega$$

In the optical window, the light transport is governed by the diffusion approximation which is based on the fact that, for this window of wavelengths, $\mu_a \ll \mu'_s$. This approximation is valid in optically thick media (i.e on media for which the optical thickness is defined by $\tau = \int_0^l \mu_{eff}(z)dz \gg 1$, with $\mu_{eff} = \sqrt{3\mu_a(\mu_a + \mu_s')}$ and z the thickness). It has been shown that this diffusion approximation is a suitable model to describe the RTE in scattering-dominated materials such as biological tissues.

3.1.2 Derivation of the Radiative transfer equation

The RTE seen in equation 3.1 is derived via conservation of energy. It states that the beam of light loses energy through divergence and extinction (due to absorption and scattering away from the beam) and gains energy from light sources in the medium and scattering towards the beam.

$$\frac{\partial L(\vec{r},\hat{s},t)/c}{\partial t} = -\hat{s} * \nabla L(\vec{r},\hat{s},t) - \mu_t * L(\vec{r},\hat{s},t) + \mu_s \int_{4\pi} L(\vec{r},\hat{s},t) P\left(\widehat{s'}.\hat{s}\right) d\Omega' + Q(\vec{r},\hat{s},t) \quad (3.1)$$

It is derived from the following equation:

$$dP = -dP_{div} - dP_{ext} + dP_{sca} + dP_{src} \quad (3.2)$$

The different terms in equation (3.2) can be expressed as following:

- **The energy diverging out of the volume element dV:**
$$dP_{div} = \hat{s} * \nabla L(\vec{r},\hat{s},t) d\Omega \mathrm{dV} \quad (3.3)$$
- **Extinction:**
$$dP_{ext} = (\mu_t ds) * (L(\vec{r},\hat{s},t) d\Omega \mathrm{dA}) \quad (3.4)$$

  Where $(\mu_t ds)$ denotes the probability of extinction with $\mu_t = \mu_a + \mu_s$
- **Scattering** - Energy coming in the volume dV and due to scattering from any direction $\hat{s}'$ and scattered into $d\Omega$ around direction $\hat{s}$ per unit time:
$$dP_{sca} = (N_s dV) * [\int_{4\pi} L(\vec{r},\hat{s},t) P(\widehat{s'},\hat{s}) \sigma_s \, d\Omega'] d\Omega \quad (3.5)$$

  N_s is the density of scatterers and σ_s is the scattering cross-section as explained in Section 2.1.3. The phase function $P(\widehat{s'},\hat{s})$ is the probability function so that $L(\vec{r},\hat{s},t)P(\widehat{s'},\hat{s})\sigma_s \, d\Omega'$ is the energy intercepted by a single scatterer within solid angle $d\Omega'$ per unit time. In fact, $P(\widehat{s'},\hat{s}) \, d\Omega$ is the probability that a light propagating in the direction $\widehat{s'}$ is scattered into $d\Omega$ around direction $\widehat{s}$. This phase function only depends on the angle between the incident and scattered direction and therefore, we can re-write the scattering quantity as:
$$dP_{sca} = (\mu_s dV) * [\int_{4\pi} L(\vec{r},\hat{s},t) P(\widehat{s'}.\hat{s}) \, d\Omega'] d\Omega \quad (3.6)$$
  With $\mu_s = \sigma_s * N_s$.

- **Source**- the energy produced by a source in the volume element within the solid angle element per unit time:
$$dP_{src} = Q(\vec{r},\hat{s},t) dV \, d\Omega \quad (3.7)$$

With $Q(\vec{r},\hat{s},t)$ the power produced by a source, per unit angle and per time.
The change in energy in the volume dV within the solid angle dΩ is given by:

$$\mathrm{dP} = \frac{\partial L(\vec{r},\hat{s},t)/c}{\partial t} dV \, d\Omega \quad (3.8)$$

Here *L/c* is the propagating energy per unit volume per unit solid angle, and c is the speed of light.

3.1.3 The diffusion Approximation

3.1.3.1 General Equation

The solving of the radiative transfer equation can be quite complicated under its form as (3.1). Instead, some approaches help to give reasonable solutions. This is particularly true for the diffusion approximation which gives fairly good results in biological tissues. As explained before, the diffusion approximation is valid in a high scattering medium for which ($\mu'_s \gg \mu_a$).

Furthermore, in our case, the study of the light propagation will be done under the approximation that we have a steady state, which means that all the equations will be time independent.

$$\mu_a \Phi(\vec{r}) - \nabla \left(D(\vec{r}) \nabla \Phi(\vec{r}) \right) = Q(\vec{r}) \quad (3.9)$$

3.1.3.2 Derivation of the Diffusion Approximation Equations

As mentioned before, the radiance is approximated by an expansion of spherical harmonics which leads to:

$$L(\vec{r}, \hat{s}) \cong \sum_{n=0}^{1} \sum_{m=-n}^{n} L_{n.m}(\vec{r}, \hat{s}) Y_{n.m}(\hat{s}) \quad (3.10)$$

$Y_{n.m}$ denotes the spherical harmonics and $L_{n.m}$ the expansion coefficients.

$$Y_{n.m} = Y_{n.m}(\Phi, \theta) = (-1)^m \sqrt{\frac{(2n+1)(n-m)!}{4\pi(n+m)!}} P_{n,m}(\cos\theta) e^{im\phi} \quad (3.11)$$

With $P_{n,m} = \frac{(1-x^2)^{\frac{m}{2}}}{2^n\, n!} \frac{d^{m+n}}{dx^{m+n}} (1-x^2)^n$ the Legendre polynomials.

Those relations permit to rewrite the fluence rate as a function of the fluence rate and of the current density:

$$L(\vec{r}, \hat{s}) = \frac{1}{4\pi} \Phi(\vec{r}) + \frac{3}{4\pi} J(\vec{r}).\hat{s} \quad (3.12)$$

If, in equation (3.1), we neglect the time dependency and introduce the new way of writing the radiance as given in (3.12), we have a new RTE equation:

$$\mu_a \Phi(\vec{r}) + \nabla J(\vec{r}) = Q(\vec{r}) \quad (3.13)$$

In this last equation, we have assumed the source to be isotropic (i.e. independent of $\hat{s}$).

Under the assumption that the fractional change in $J(\vec{r})$ within l_t (the inverse of the mean free path when the free path is defined as $(\mu_t = \mu_a + \mu'_s)$) is small, then we can establish the relation between $J(\vec{r}, t)$ and $\Phi(\vec{r})$:

$$J(\vec{r}) = -D \nabla \Phi(\vec{r}) \quad (3.14)$$

Where $D = \frac{1}{3(\mu_a + \mu_{s'})}$ is called the diffusion coefficient.

By introducing (3.14) in (3.13), we get equation (3.9).

3.1.4 Finite element theory

As we have seen, the diffusion approximation is valid when $\mu_a \ll \mu'_s$ and it assumes that the light propagation is weakly anisotropic. This last assumption is generally not respected near sources and boundaries. However, comparisons with Monte Carlo simulations (approach to solve the radiative transfer equation) showed that the predictions were qualitatively correct around boundaries with the diffusion model as explained in [18].

As we said in Section 1.2, the finite element method (FEM) is used to simulate the initial data needed to estimate the optical properties. It uses the radiative transfer equation in its form as shown in (3.9). But to solve this problem with the FEM, we need to specify appropriate boundary conditions.

If we call Ω the domain of study (prostate), then the final problem in this master thesis can be formulated as:

$$\begin{aligned} &\mu_a \Phi(\vec{r}) - \nabla \left(D \nabla \Phi(\vec{r}) \right) = Q(\vec{r}) \ , \forall\ \vec{r} \in \Omega \\ &\Phi(\xi) + 2DA\, \hat{n}\, .\nabla \Phi(\xi) = 0\,, \quad \forall\, \xi \in \partial\Omega \end{aligned} \quad (3.15)$$

The first element in (3.15) is the diffusion approximation and the second line represents the boundary conditions which are furtherly explained in the next paragraph.

3.1.4.1 Discussion of the boundary conditions

The Dirichlet boundary conditions (DBC) claims that:

$$\Phi(\xi) = 0, \qquad \forall\, \xi \in \delta\Omega \tag{3.16}$$

Where Ω is the domain of interest and δΩ is the boundary of that domain.

The DBC is equivalent to have a perfectly absorbing medium surrounding the domain Ω. That would mean that every photon is absorbed as soon as it crosses the boundary δΩ and that the photon density is equal to 0 outside the domain. This approach seems too strong.

A more realistic approach could be formulated as a Robin boundary condition (RBC) which constrains a linear combination of the photon density and the current at δΩ :

$$\Phi(\xi) + 2\mathrm{D}\,\hat{n}\,.\nabla\Phi(\xi) = 0 \tag{3.17}$$

With $\hat{n}$ the normal vector to δΩ at ξ. Physically, this would be equivalent to have a non scattering medium surrounding Ω with no diffuse surface reflection at δΩ.

Because of some problems concerning a mismatch between refractive indices inside the domain and in the surrounding medium, a reformulation of the RBC can be made:

$$\Phi(\xi) + 2\mathrm{DA}\,\hat{n}\,.\nabla\Phi(\xi) = 0 \tag{3.18}$$

Where $\mathrm{A} = \frac{1+R}{1-R}$ and R a parameter governing the internal reflection at the boundary.

The DBC has the advantage of leading to a more simple mathematical model while the RBC describes a more realistic situation. The compromise is realized by applying a mixt condition. The boundary is extrapolated to $\delta\Omega_{ext}$ on which the DBC will be applied while the RBC will be applied on δΩ (see Figure 3.2).

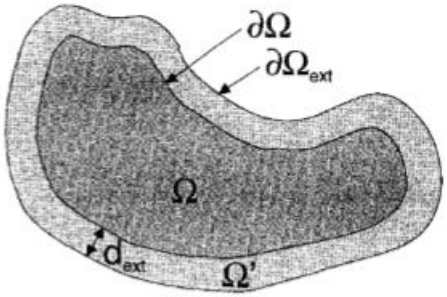

Figure 3.2: Boundaries and domain.

3.1.4.2 Formulation of the finite element problem

We want a continuous and piecewise linear approximation Φ^h of Φ. In order to do so, the domain Ω is divided into *D* nonoverlapping elements τ over which Φ^h is assumed to be linear. Nodes $\mathrm{N_{j\,(j=1\ldots P)}}$ are attached to the element vertices. At each point r within an element τ_i, $\Phi^h$is given by a linear interpolation of nodal values Φ_j.

$$\Phi^h(r,t) = \sum_{j|Nj\in\,\tau\mathrm{i}} \Phi_j(t)\psi_j(r) \tag{3.19}$$

Where ψ_j are linear nodal shape function with support over all elements that have the node $\mathrm{N_j}$ as a vertex and $\psi_j(r_i) = \delta_{ij}$ where r_i is the position of node $\mathrm{N_i}$.

The weak formulation of the for each node j, using Galerkin approach, is given by

$$\int \psi_j(r)\,[\mu_a(\mathrm{r}) - \nabla(\mathrm{D}\,\nabla)]\Phi^h(\vec{r})d\Omega = \int \psi_j(r)\,\mathrm{Q}(\vec{r})\,d\Omega \tag{3.20}$$

The integration by parts of (3.20) and substituting Φ^h by its expression in (3.19) gives us the following expression:

$$\int_\Omega \mu_a(\mathrm{r})\psi_j(r)\psi_i(r)\Phi_i + \nabla\psi_j(r)\,.\,D\,\nabla\psi_i(r)\Phi_i\,d\Omega = \int_\Omega \psi_j(r)\,\mathrm{Q}(\vec{r})\,d\Omega - \frac{1}{c}\int_{\delta\Omega}\psi_j(\xi)\,\Gamma(\xi)\,d(\partial\Omega) \quad (3.21)$$

$\Gamma(\xi)$ is the exitance and is defined by $\Gamma(\xi) = -cD(\xi)\,\hat{n}\,.\nabla\Phi(\xi)$.

A matrix expression of (3.21) is:

$$[K(D) + C(\mu_a)]\Phi = \mathrm{Q}_0 - \beta \quad (3.22)$$

Where K, C, Q_0 and β are matrixes expression for the terms in equation (3.21). In our case, the problem is assumed to be stationary which spared us from doing a finite difference scheme. The solving of equation (3.22) is then direct.

3.1.5 Homogeneous Medium Approximation

The solving of the problem formulated in (3.15) brings us the initial data that we need to evaluate the optical properties. Nonetheless, the solving of equation (3.9) is too complicated in our case and we decide to go further in our analysis so we end up to a simpler form of equation (3.9). We can assume a homogeneous medium in which $D = \frac{1}{3(\mu_a+\mu_{s'})}$, called the diffusion coefficient, is assumed to be constant, i.e independent of $\vec{r}$.
This leads to equation (3.23) which is the Helmholtz equation in the case where the source term Q is due to a point source positioned at the position $\vec{r}_s$ with a power P_0.

$$\mu_a\Phi(\vec{r}) - D\,\nabla^2\Phi(\vec{r}) = P_0\delta(\vec{r} - \vec{r}_s) \quad (3.23)$$

The steady state diffusion approximation can be solved in the frequency domain if the volume is considered infinite and homogeneous. The solution is given by a Green function as expressed in equation (3.24).

$$\Phi(\vec{r}\,,\vec{r}_s) = \frac{3\mu_s{}'\,P_0}{4\pi|\vec{r} - \vec{r}_s|} * e^{-\mu_{eff}*|\vec{r} - \vec{r}_s|} \quad (3.24)$$

With $\mu_{eff} = \sqrt{3\mu_a(\mu_a + \mu_s{}')}$.

In this thesis, the interest will be both on a homogeneous and heterogeneous prostate medium. Nonetheless, we will exclusively use the Green's approximation as if the prostate was homogeneous and we would like to discuss the consequences of such an approximation on the treatment of a heterogeneous prostate.

Furthermore, in the case of the diffuser fibres, the source term in (3.9) is different. Indeed, we have assumed that the continuous diffuser fibres could be approximated by an array of discrete point sources. The number of points is called the fibre resolution and constitutes a parameter to study in the case of diffuser sources. With this assumption, we will also use (3.23), by assuming that each point constituting one fibre, acts independently from one another. Nonetheless, the power in the right hand side of (3.23) will not be equal to P_0 but to $\frac{P_0}{Fibre\ Resolution}$ so that the fibre, when considering all the point sources, still emits a power P_0.

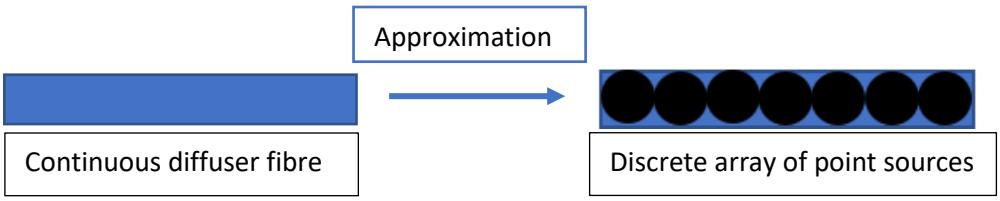

Figure 3.1: Approximation concerning the diffuser fibres.

3.2 Forward and Backward problems

In the following parts, the reader will often encounter the terms of backward or inverse and forward problems. This section is the opportunity to clarify those terms. The forward problem could be expressed as the following : 'Given certain parameters, which data could we expect? '. A simple picture of those terms is provided in Figure 3.3. This question will require to establish a physical model.

The inverse problem is the previous problem taken in the opposite way. It could be formulated as 'Given a set of data, what are the parameters which would lead to such data?'.

The terms of forward and backward problems can be used in various fields of science. In the context of light propagation in tissues, and more generally medical imaging, the solving of the backward problems consists in estimating the optical properties of tissues from which we have e.g. ultrasound, MRI, PET-scan images.

In the case of this master thesis, we will solve both a forward and backward problem. Indeed, the forward problem will consist in generating data thanks to a finite element software (NIRFAST slicer 3D). Afterwards, we will use that data to solve the inverse problem and estimate how good is the solving of that backward problem with different methods.

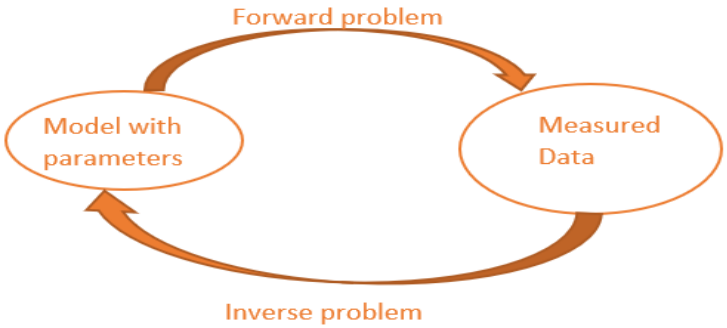

Figure 3.3: Inverse and forward problem.

3.2.1 Linear Least Square Method

In equation (3.11), we can introduce an attenuation factor (A) which takes into account some dampening effect due to the formation of blood around the fibre when this last one is introduced in the body. Now, if we apply a logarithm on both sides of equation (3.11), we have:

$$log\ \Phi(\vec{r}\ ,\vec{r}_s) = \log(\frac{3 * A * \mu_s{}' P_0}{4\pi|\vec{r}\ - \vec{r}_s|}) - \mu_{eff} * |\vec{r}\ - \vec{r}_s| \qquad (3.25)$$

By rearranging the terms and applying the laws relative to the logarithm, we get:

$$log\ \Phi(\vec{r}\ ,\vec{r_s}) + log|\vec{r}\ - \vec{r_s}| - \log\left(\frac{3*\mu_s{}'\ P_0}{4\pi}\right) = -\mu_{eff} * |\vec{r}\ - \vec{r_s}|\ + \log(A) \quad (3.26)$$

Which can be written as:

$$log\ (\Phi(\vec{r}\ ,\vec{r_s})|\vec{r}\ - \vec{r_s}|) - \log(\frac{3*\mu_s{}'\ P_0}{4\pi}) = -\mu_{eff} * |\vec{r}\ - \vec{r_s}|\ + \log(A) \quad (3.27)$$

We remind the reader that $\mu_s{}'$ is assumed to be constant and was estimated to be 900 m^{-1}, that the delivery power is 150 mW for the point sources fibres and that the fluence rate was computed by Nirfast. Therefore, if we denote y the left side of equation (3.27), we have a linear equation whose undefined coefficients are, for each fibre, μ_{eff} and *A* (see equation (3.28)). Indeed, each fibre is assumed to have independent behaviours from each other which turns into having a number of undefined coefficients equal to two times (due to a μ_{eff} and *A*) the number of fibres. So if we have 18 fibres, then we will have 36 unknowns.

$$y = -\mu_{eff} * |\vec{r}\ - \vec{r_s}|\ + \log(A) \quad (3.28)$$

Equation (3.25) can be written under its matrix form.

$$y_{LLSQ} = X_{LLSQ}\beta_{LLSQ} \quad (3.29)$$

If we assume to have N sources is the matrix with the distances between different fibre sources whose size is *(N-1)N* x *2N*. The N first columns of X_{LLSQ} contains a 1 only if the two sources considered are interacting. The last N columns contain the values $|\vec{r}\ - \vec{r_s}|$.

β_{LLSQ} is a vector whose first N coefficients are attenuations coefficients corresponding to each source and the N following coefficients are the μ_{eff} corresponding to the *N* sources. So we have 2N unknowns in total.

The solution of the system represented by equation (3.29) is given by

$$\beta = \underset{\beta}{\operatorname{argmin}}(S(\beta))$$

Where $S(\beta) = \left|y_{LLSQ} - X_{LLSQ}\beta_{LLSQ}\right|^2$.

3.2.2 P18 estimation

This time, we do not take into account an attenuation factor. Consequently, we write equation (3.25) as

$$\log \Phi(\vec{r}\ ,\vec{r_s}) = \log(\frac{3 * \mu_s{}'\ P_0}{4\pi|\vec{r}\ - \vec{r_s}|}) - \mu_{eff} * |\vec{r}\ - \vec{r_s}| \quad (3.30)$$

In this case, in comparison to the linear estimation presented in the previous section, the number of unknowns is given by the number of fibres (one μ_{eff} coefficient for each fibre).

The re-writing of equation (3.30) leads to:

$$y_{P18} = -\mu_{eff} * |\vec{r}\ - \vec{r_s}| = X_{P18}\beta_{P18} \quad (3.31)$$

This time X_{P18} is a matrix whose size is *N(N-1)* x *N* and β is a *N* x *1* vector which only contain the N μ_{eff} coefficients.

One more time, we solve a least square problem. However, this method is called P18 in reference to the method currently used in the device realized by Spectracure AB. In other words, the current system used by Spectracure AB does not take into account the attenuation factors.

3.3 Nirfast: Near Infrared Fluorescence and Spectral Tomography

In this master thesis, we will use Nirfast to generate the initial data or ground truth with which we will try to reconstruct the optical properties. Nirfast is an open source, MATLAB-based software package developed by researchers at the university of Exeter and Dartmouth College. A user-friendly interface has been developed in Nirfast but because the needs in this project are quite specific, we will not use this interface but only the functions that this interface calls.

To generate the initial data, we solve a forward problem: we input the optical properties (and, if required, the attenuation coefficients) in the prostate, the positions and power of the fibres and we get the light distribution at each nodes. This light distribution is then used in Matlab to estimate the original properties. We act as if we did not know the set optical properties (and possibly the set dampening (attenuation) coefficients mentioned in Section 3.2.1). This forward problem is represented in Figure 3.4 and corresponds to the black boxes.

The fluence rate is then used to calculate the optical properties with the least square method as explained in Section 3.2. This step is called resolution of the inverse problem. It is represented by blue and green arrows to distinguish the different methods of resolution as detailed in Section 2.3. Those colours will be used also in the results part: the blue for the P18 results (without dampening) and the green for the linear least square results (with dampening).

Now, what we are really interested in, is the influence of the determination of those optical properties on the patient's treatment. In order to study this effect, the next step is to use those estimated parameters to calculate the irradiation times (the time during which each fibre will shine so that the patient receives at least the expected dose of 5 J/cm^2 in the prostate). This is done by a Matlab script using the Cimmino algorithm. This algorithm optimizes, for a given positioning of the fibres, the irradiation times for each fibre so that the light produced permits to have a high amplitude in the prostate while avoiding overexposure of light of the surrounding tissues. A slightly more detailed description will be given of this algorithm in part 4.3.1.

The next step is to use those estimated irradiation times to reconstruct the field in the patient's body, based on the estimated optical properties. Those irradiation times will be the ones used during the treatment. The fluence maps called Estimated Fluence Map are created using Green's diffusion approximation. The maps called Real Fluence map in Figure 4.8 use the data from the FEM simulations (the fluence rate) and multiply those data respectively by the irradiation times corresponding to the real properties.

Once we have the fluence maps, we can calculate the Dose Volume Histograms. Those are histograms which link the proportion of each tissue receiving a certain light dose to the tissue volume. It is simply to determine, for each tissue type, the fraction of tissue that receives a certain dose of light. The tissue type is already known for each voxel element. There are four tissue types which are normal tissue (surrounding tissues around the prostate), prostate, urethra and rectum. The tissues that we want to pay more attention at are the prostate, in which we want the maximum number of voxels to receive a light dose above 5 J/cm^2 (threshold dose) and the rectum in which we want the lowest number of voxels to receive that threshold dose.

The focus will be on the differences between the case of diffuser fibres and the case of bare end fibres (point sources) and the consequences on the patient's health if the treatment is realized with estimated quantities in comparison with the real quantities.

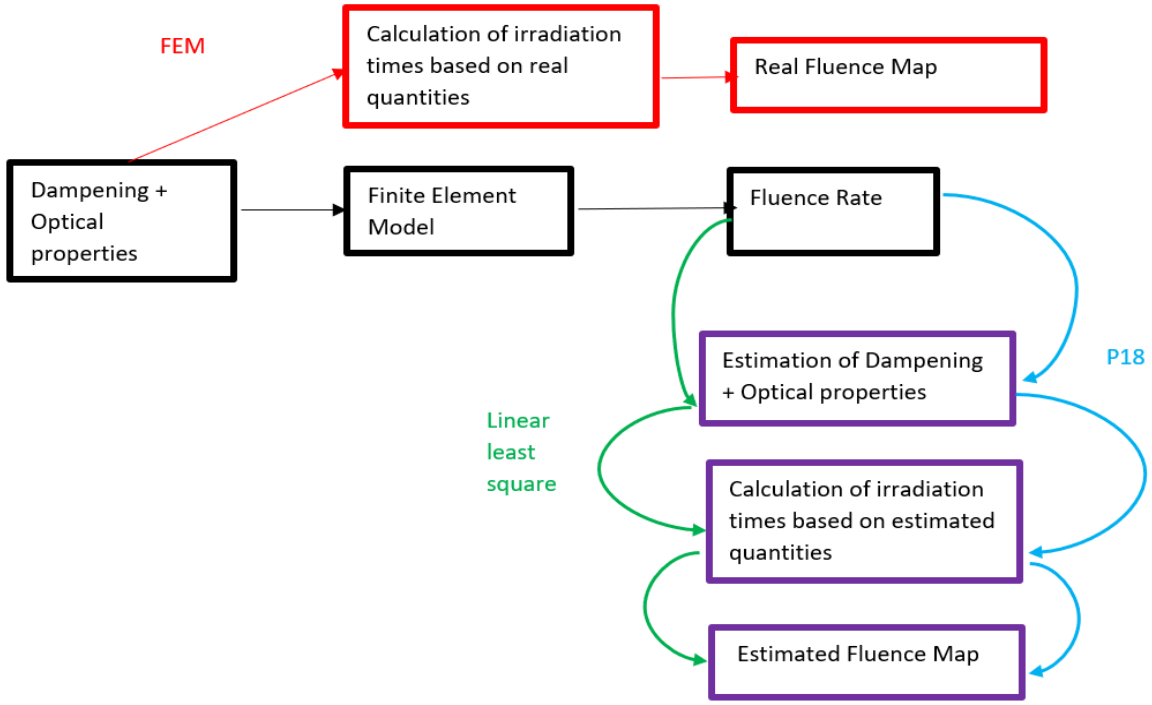

Figure 3.4: Scheme method resolution.

Chapter 4: Simulation of light propagation in prostate via fibres

In this chapter, we will present the results after applying the method presented in the previous chapter. Because the prostate is the tissue that we would like to treat, the results will often be given in the prostate. Nonetheless, the rectum is a sensitive tissue around the prostate that we would like to spare to avoid any damages and pain to the patient. Therefore, we will often look at the results in the rectum too.

In the first part, we will focus on the establishment of a reference case based on the current device used at Spectracure AB: the use of eighteen 400 µm bare end fibres. Then, we will compare the performance of this reference case to the case where we have diffuser fibres. Some fibres parameters will be changed in a second time.

4.1 Results with the Reference Model

We have to establish a model to which we will compare our results with. We have chosen to use the current model used by the company: eighteen points sources fibres delivering a power output of 150 mW.

We will consider different cases: we can either have a homogeneous medium inside the prostate (with a constant μ_a everywhere) or a heterogeneous medium.

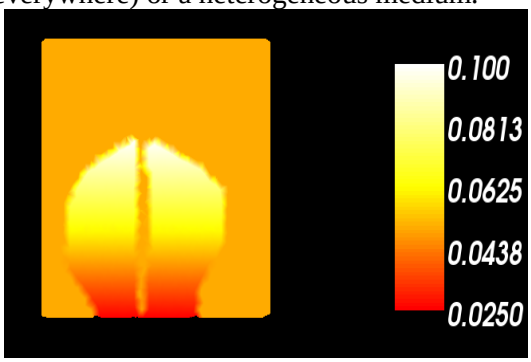

Figure 4.1: Definition of a heterogeneous absorption coefficient in the prostate (the colour bar indicates the values of the μ_a coefficient (mm^{-1})).

To treat the case of a heterogeneous prostate medium, we will consider different situations or cases:

- Case 1: the absorption coefficient varies linearly with the z axis. This situation is represented in Figure 4.1.
- Case 2: we defined some tumours elements around 6 fibres. The absorption coefficient is set to 0.050 mm^{-1} excepted in the tumours. The tumour absorption coefficients can be either higher (it was set to 0.100 mm^{-1}) or lower (set to 0.010 mm^{-1}) than the surrounding environment. The case 2 situation is represented in Figure 4.2.

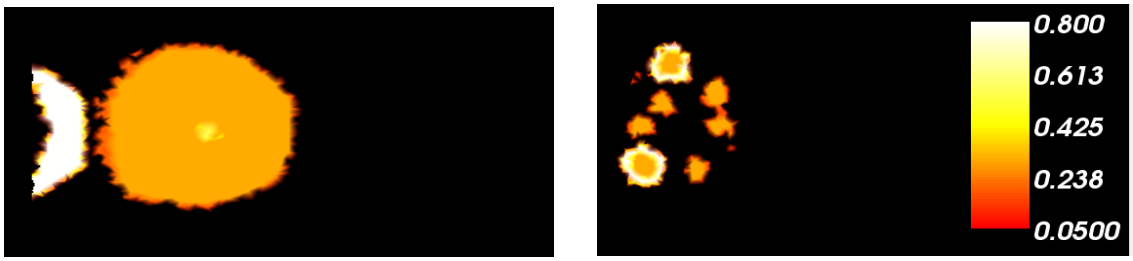

Figure 4.2: Tumours in prostate: The left subfigure is just used to see the position of the prostate. The colours shown in that figure only correspond to the region type (black for surrounding tissues, orange for prostate, yellow for urethra, white for rectum). In the right subfigure, the values correspond to the μ_a values but they have been changed in order to visualize the tumours more clearly. In this right figure, the orange parts represent the fibres while the brightest part represent the tumours around only 2 fibres. In the real case the tumours are 3 mm wide while their width was set to 5 mm to allow a better visualization in the current situation. The legend bar is in mm^{-1}.

4.1.1 Homogeneous Prostate

4.1.1.1 Study of the Mesh Influence

In Figure 4.3, we have plotted the percentage of prostate receiving the light threshold for different number of elements. A number of elements above 200 000 give pretty correct results in a reasonable amount of time. Indeed, the increase of the mesh resolution is increasing the computational time. Therefore, we try to find the lowest number of elements which give the best results as possible. In the remaining study, we will use a number of elements over 200 000 elements to ensure that the mesh does not affect our results.

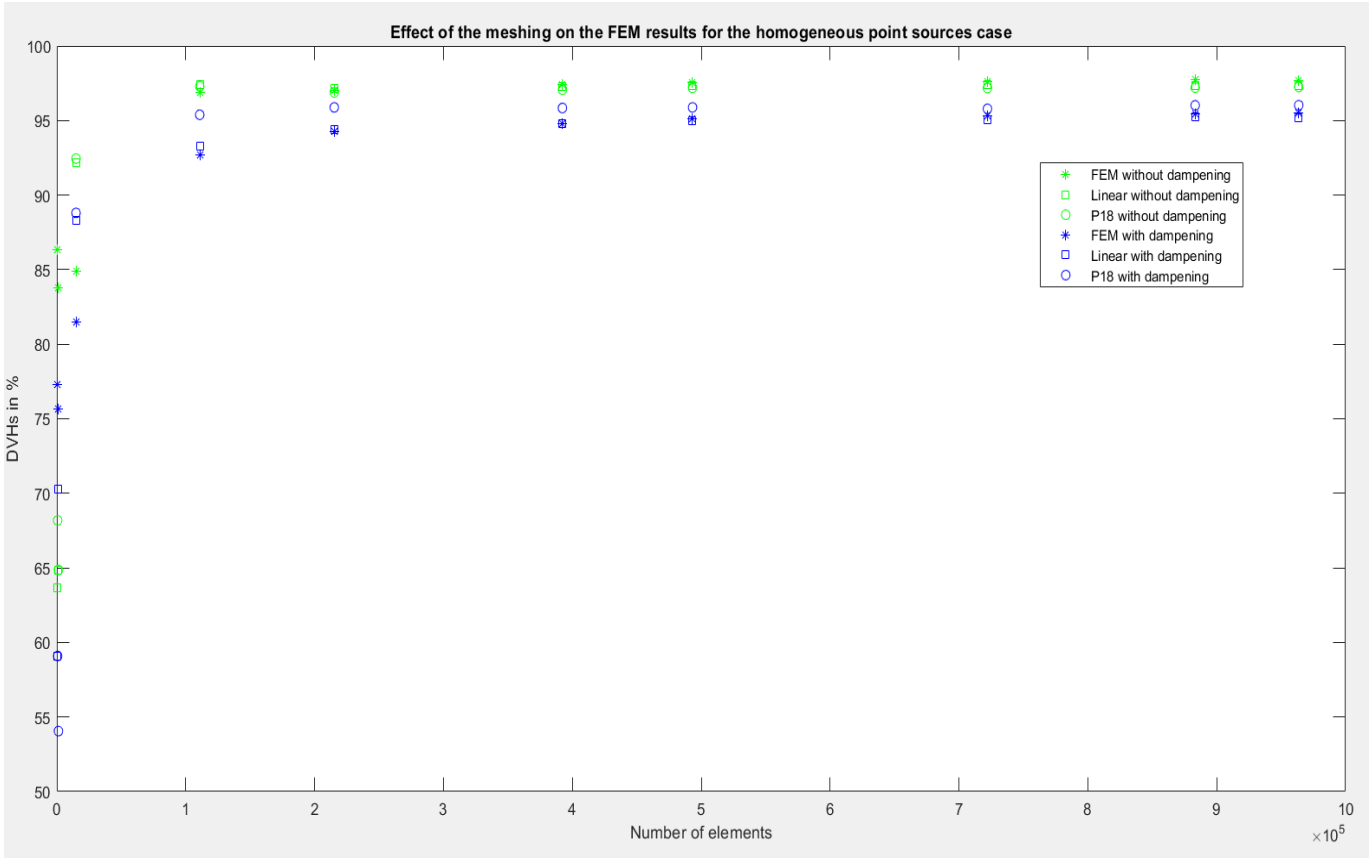

Figure 4.3: Influence of the number of elements of the mesh on the DVHs results (with dampening coefficients set so that the lower fibres number have the highest dampening).

In this section, we will talk about DVH which stands for Dose Volume Histogram. It refers to a quantity of light received by a certain proportion of tissue. Here, when we talk about DVH, it might correspond to two situations:

- If the DVH is plotted as a function of the light dose, it represents the proportion of tissue that is receiving the light dose indicated. This corresponds to the real definition of the DVH
- If the DVH is plotted as a function of some other quantities that are not the light dose, it means that the DVH is evaluated for the minimum light dose of 5 J/cm^2 which is the minimal dose we want the prostate to be exposed to. This last definition is something that we have used only in the context of this master thesis.

4.1.1.2 Study of the Results in Terms of DVHs

In the case of a homogeneous medium inside the prostate, the results, in terms of proportion of prostate exposed to the minimum dose light of 5J/cm^2, are illustrated in Figure 4.4. For this first trial, the dampening coefficients were set in order to have dampening coefficients sparsely spread between 0 and 1, while having a different coefficient for each fibre. They were then chosen so that a fibre with a low number (the number is arbitrarily associated to one fibre) has a high dampening coefficient while the dampening effect is decreasing with the number associated to each fibre; in other words, it gets closer to 1 the higher the fibre number is. Such a configuration is represented in the middle subfigure in Figure 4.4.

The linear and the P18 methods, respectively in green and blue in all the Figures shown and which are more detailed in the Sections 3.2.1 and 3.2.2, give a good estimation of the optical properties in the absence of dampening. With the introduction of dampening, we can see that the optical properties and the dampening coefficients are correctly estimated by the linear model while the P18 model leads to an overestimation of the optical properties. Nonetheless, if we look closer at the results with the P18 model, we can see that this overestimation is diminishing with the increase of the fibre number. We can conclude that the P18 model is interpreting the dampening effect (which is high for low fibre numbers as explained before) as a change in μ_{eff}. To see the influence of this estimation of the dampening effect as a variation in $\mu_{eff,}$ we need to look at the values of the light dose calculated based on the estimated optical properties that will be delivered to the patient.

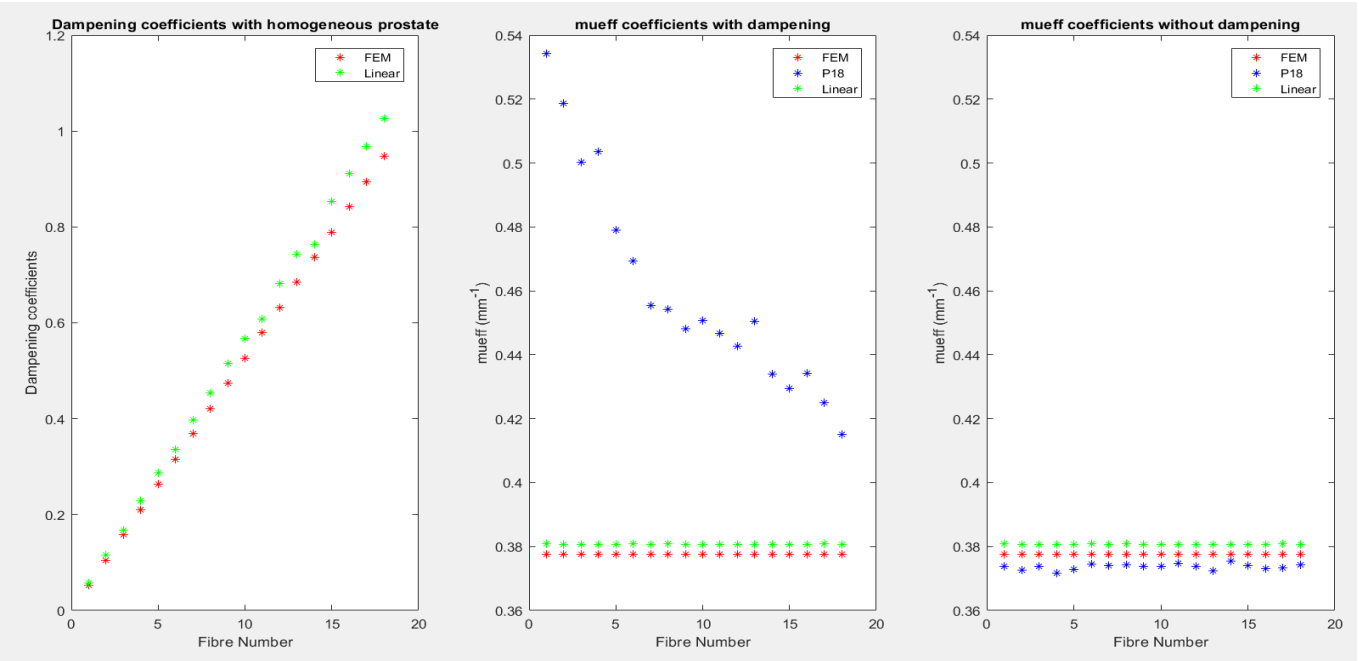

Figure 4.4: μ_{eff} coefficients and dampening coefficients in the case of a homogeneous prostate.

It appears that both of the estimations end up with good results in comparison with the DVH results corresponding to the ideal situation (in red in Figure 4.5), where the irradiation times correspond exactly to the times needed for the treatment.

We can also see that in the prostate, we expect values for the FEM results (in red) that are higher than the linear results (in green) because the optical properties with the linear method are close to the real properties (the ones used to calculate the red data) but not exactly equal and therefore the treatment should be more efficient with the FEM data. On the other hand, the results obtained with the P18 method can be either higher or lower depending on how the estimation is made. The expression of the dampening as a variation in the absorption coefficient might lead either to an overestimation or underestimation of the DVHs values. This situation is seen in Figure 4.6. We also have to keep in mind that having a higher DVH in the prostate does not necessarily mean that the results are better. We have to take into account the results in the rectum, in the urethra and in the surrounding tissues. In order to see more precisely the way the P18 method is performing in comparison with the linear method, we have chosen to set randomly the values of the dampening on the point sources. The results are seen in Figure 4.6. As said previously, the P18 method results in comparison with the FEM results are varying quite randomly (one time, the blue points are above the red data, the other time they are under). The problem with this method is that for some values of dampening, the results are really close or under the 95% bar whereas the results never get that low for the linear estimation.

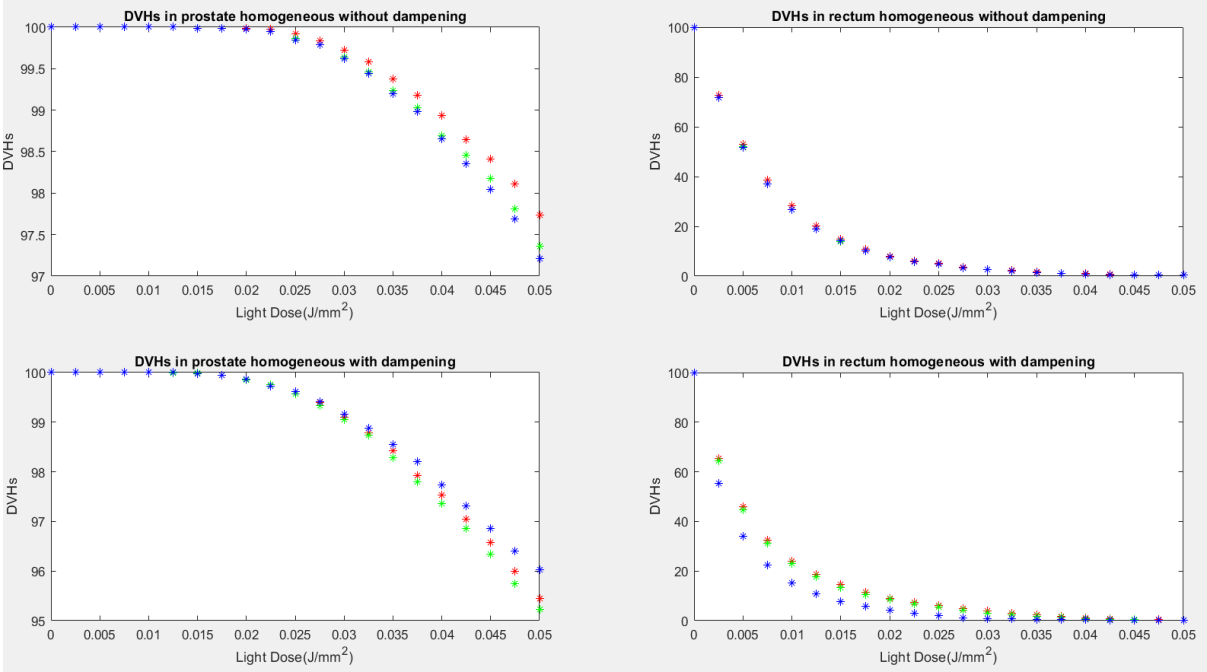

Figure 4.5: ***proportion of prostate and rectum receiving a light dose for different conditions****. As always the P18 results are given in blue, the linear method is represented in green and the FEM data in red.*

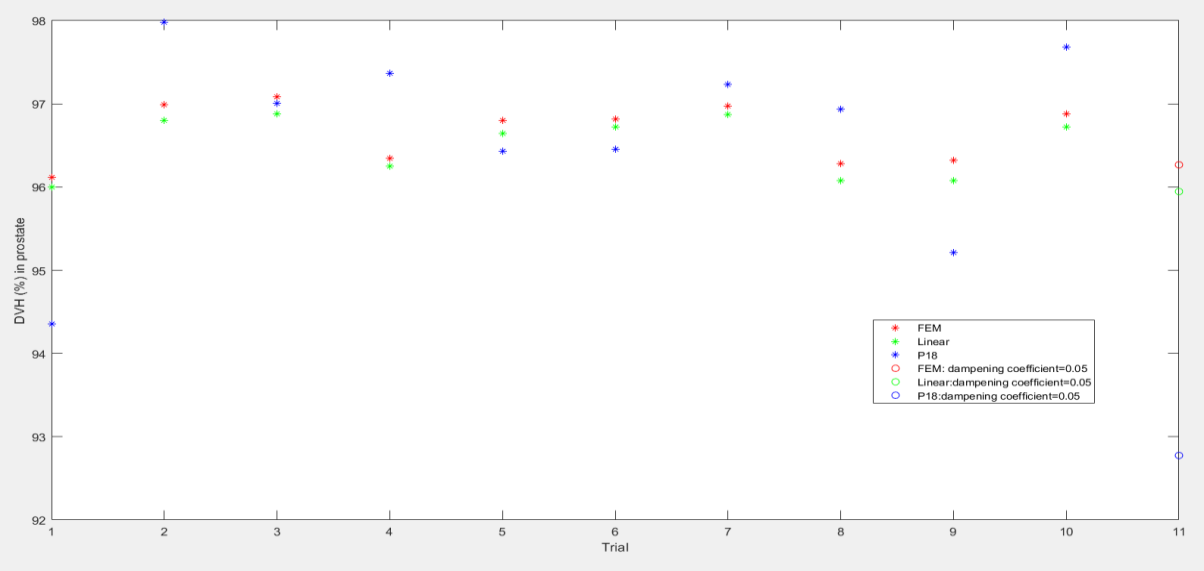

Figure 4.6: ***proportion of receiving the threshold light dose for different conditions.*** *As always the P18 results are given in blue, the linear method is represented in green and the FEM data in red. The results with stars illustrate the case where the dampening coefficients were set randomly for all the fibres. The circles represent the case where we have set all the dampening coefficients to 0.5 for all the fibres.*

4.1.2 Heterogeneous Prostate

As mentioned in the beginning of this section, we will consider two different heterogeneous situations. The one with tumours around some fibres and the one with a gradient.

In the case where we have a heterogeneous medium, the red data corresponding to the more precise FEM-calculation must no longer be taken as the reference since the values of μ_a at the fibre positions must be evaluated based on the values set at the nodes (which are set by us). Therefore, to attribute a value of μ_a where the fibre are positioned, we imagine a sphere around the fibre and we take a mean of the values of μ_a at the nodes inside that sphere as shown in Figure 4.7. But the radius of the sphere of evaluation matters since the optical properties are based on the mean value of the optical properties at the nodes around the fibres and therefore influences the results. In Figure 4.8, we can see the results for μ_{eff} for different values of radius selected. In the bottom subfigures, we can clearly see the presence of the 6 tumours around fibres 1,4,7,10,13 and 16. The increase of the radius of the evaluation sphere for this case 'dilutes' the importance of those tumours and we do not see them anymore.

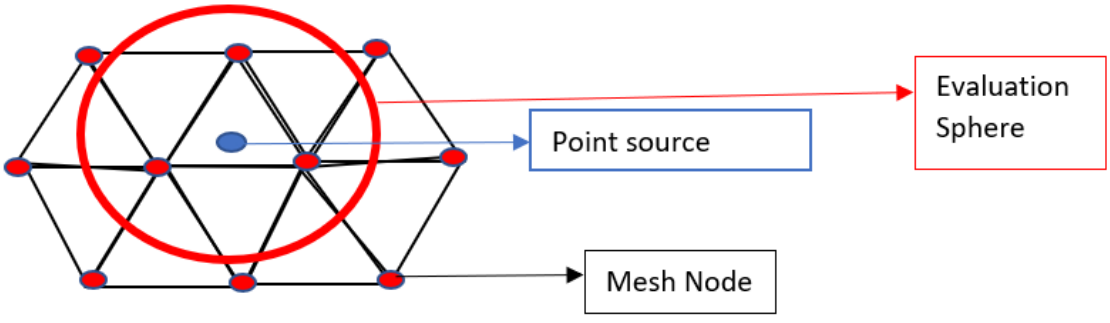

Figure 4.7: Evaluation of the optical properties within a sphere for the FEM data.

In the case of a heterogeneous prostate, the linear model expresses the heterogeneity in the μ_{eff} as a change in the dampening coefficients. As we can see in the middle and bottom subfigures, the green values corresponding to the linear model describe a flat line whereas the blue and red, respectively the P18 and FEM models, are sloppy. This is explained by the reason we just gave.

Because the red values are biased, we will not pay more attention to those values later on. On the other hand, the dampening coefficients seen in Figure 4.8 are set at each fibre and therefore the FEM data make sense and are not biased for those values.

We expect the linear dampening coefficients in the heterogeneous case to be similar to the linear dampening coefficients in the homogeneous case but because the heterogeneity is expressed as a change in dampening coefficients, those values are different. In fact, if we compare the black and green squares which respectively represent the case where we have a heterogeneous tissue with tumours and a homogeneous tissue, we can see that for the fibres where we have tumours (1,4,7,10,13,16), the black and green squares differ in positions while they are in the same positions for other fibres.

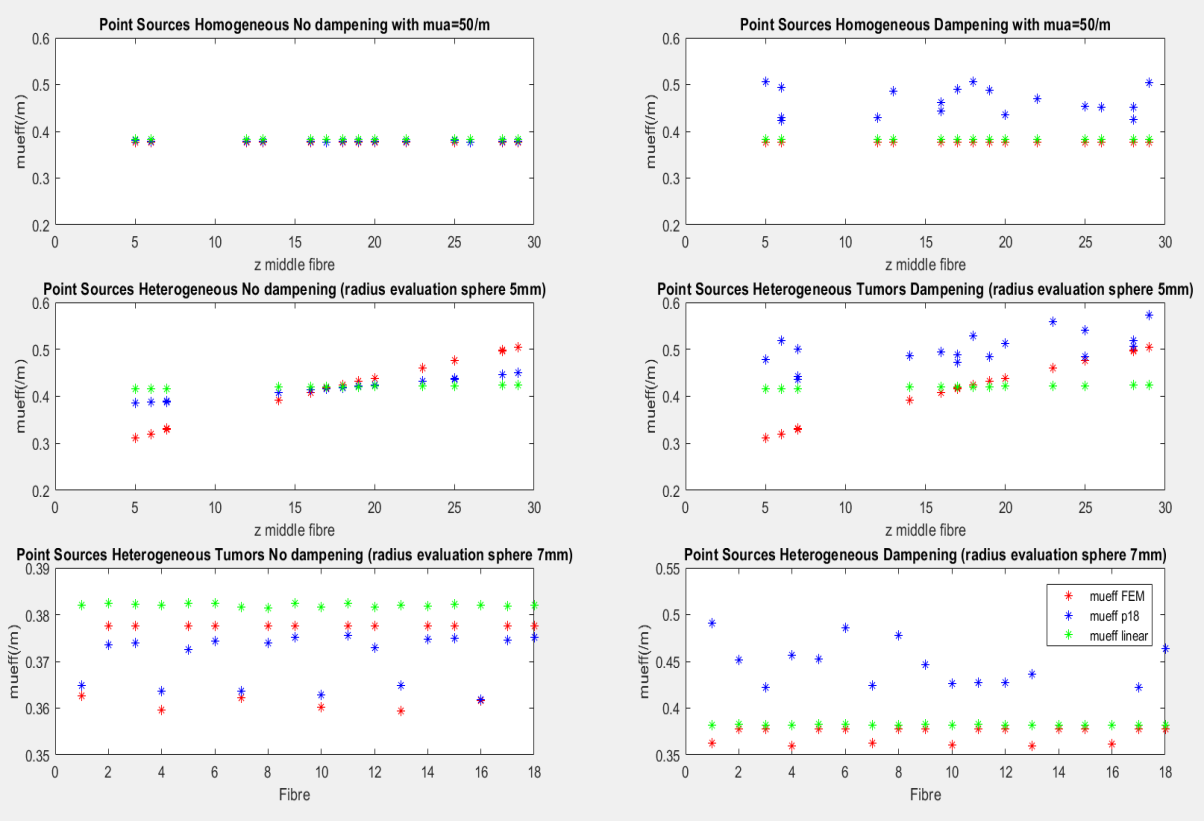

Figure 4.8: ***Comparison of the estimations of the optical properties for the homogeneous and heterogeneous cases (random dampening coefficients).*** *The figures on the top correspond to the homogeneous case, the middle figure to the case where we have a gradient for the absorption coefficient in the prostate and the bottom figures correspond to the presence of tumours around 6 fibres with a lower absorption coefficient (μ_a=10 instead of 50 m^{-1}).*

In terms of estimation of the dampening coefficients, it seems that the gradient case, in pink in Figure 4.9 is the most difficult case. The dampening coefficients are often off compared to the FEM data, in red in Figure 4.9 (which are this time real values and no doubt is permitted concerning their value).

In Figure 4.10, the percentage of prostate nodes exposed to a certain light amount is represented. The green and blue data are data calculated with the data coming from the FEM model and consequently, their value is not dependent on the evaluation sphere of the μ_{eff}. So we can state with confidence that the P18 method ends up to quite bad DVHs results due to the approximation of the dampening coefficient as a variation in μ_{eff} (case called Point sources heterogeneous dampening in Figure 4.10).

The important things to remember is that for all the cases (homogeneous or heterogeneous), we end up with DVHs results above the threshold of 95% of prostate being treated. In the absence of dampening, the estimations with the linear or P18 method are both equivalent in terms of DVHs.

However, in the presence of dampening, especially in the case of the gradient of μ_a in the tissues, the linear model seems the most appropriate one in terms of DVHs in the prostate (even though it is going to estimate the heterogeneity in μ_{eff} as a change in dampening coefficients).

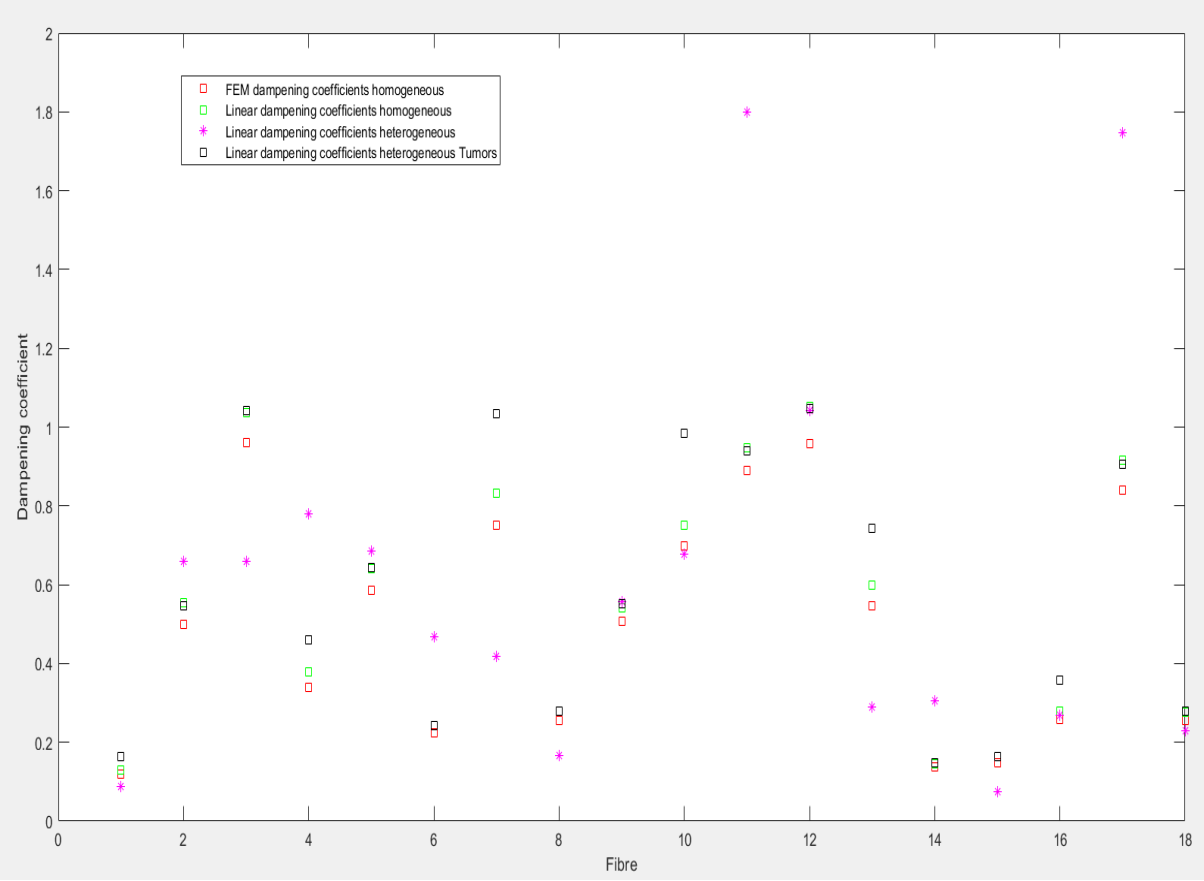

Figure 4.9: ***Comparison of the estimations of the dampening coefficients for the homogeneous and heterogeneous cases (random dampening coefficients).*** *Only the linear and FEM results are presented because the P18 method does not take into account those dampening coefficients. The linear dampening coefficients in the heterogeneous case are the coefficients with the gradient case.*

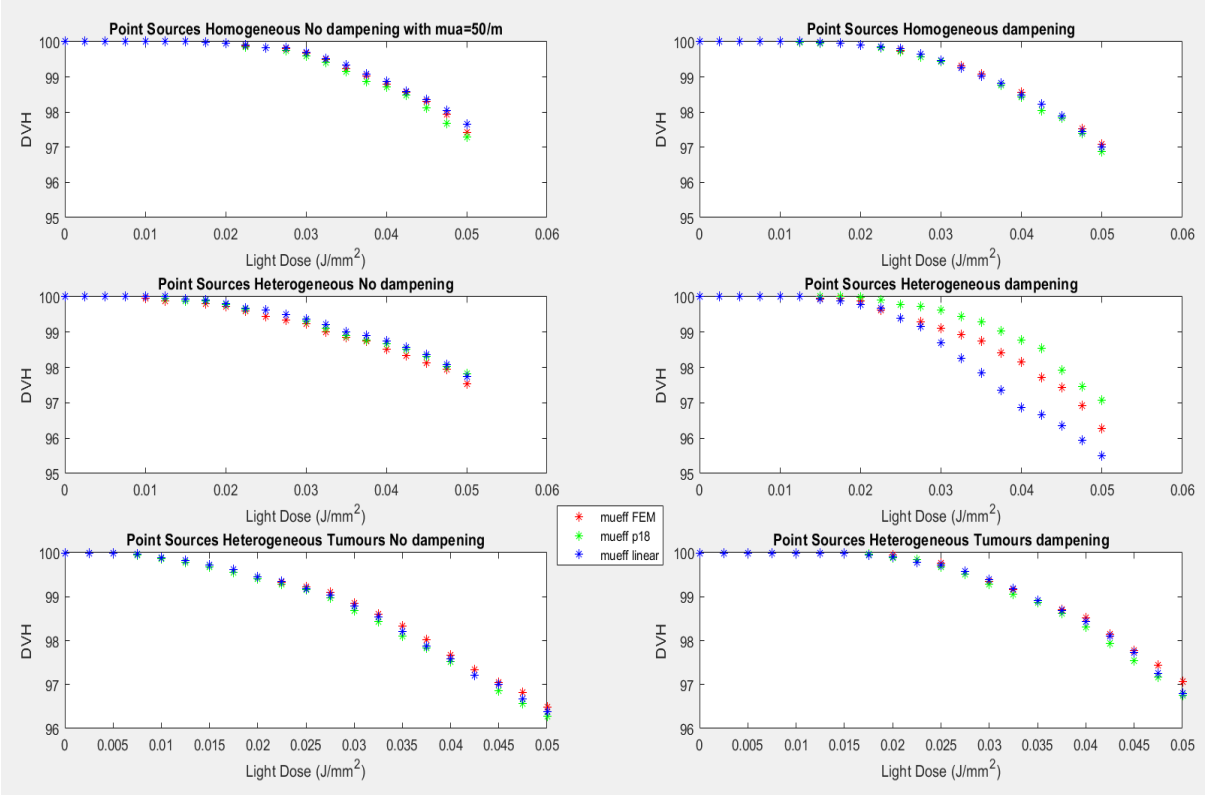

Figure 4.10: Comparison in terms of DVHs in the prostate between the different cases.

4.2 Introduction of Diffuser Fibres

Compared to the reference model, some additionnal challenges will arise from the use of diffuser fibres.We have made some approximations:

- The diffusers fibres are considered as an array of point sources
- To determine the μ_{eff} for each fibre, we first determine the values at each point of the fibres and we take the mean over those points. The μ_{eff} for each fibre is then determined. We assume that each point of the fibre see the medium around with this value of μ_{eff}.
- Each point source of the array is considered as a point source and therefore, the light emitted by the fibre is the sum of green functions due to every point of the fibre. In other words, we consider every point of the fibre as an independent point source. In reality, those points sources are not independent because every point source belonging to the same fibre will not receive the same amount of light when the fibre are used as receivers.

4.2.1 Study of the Mesh Resolution

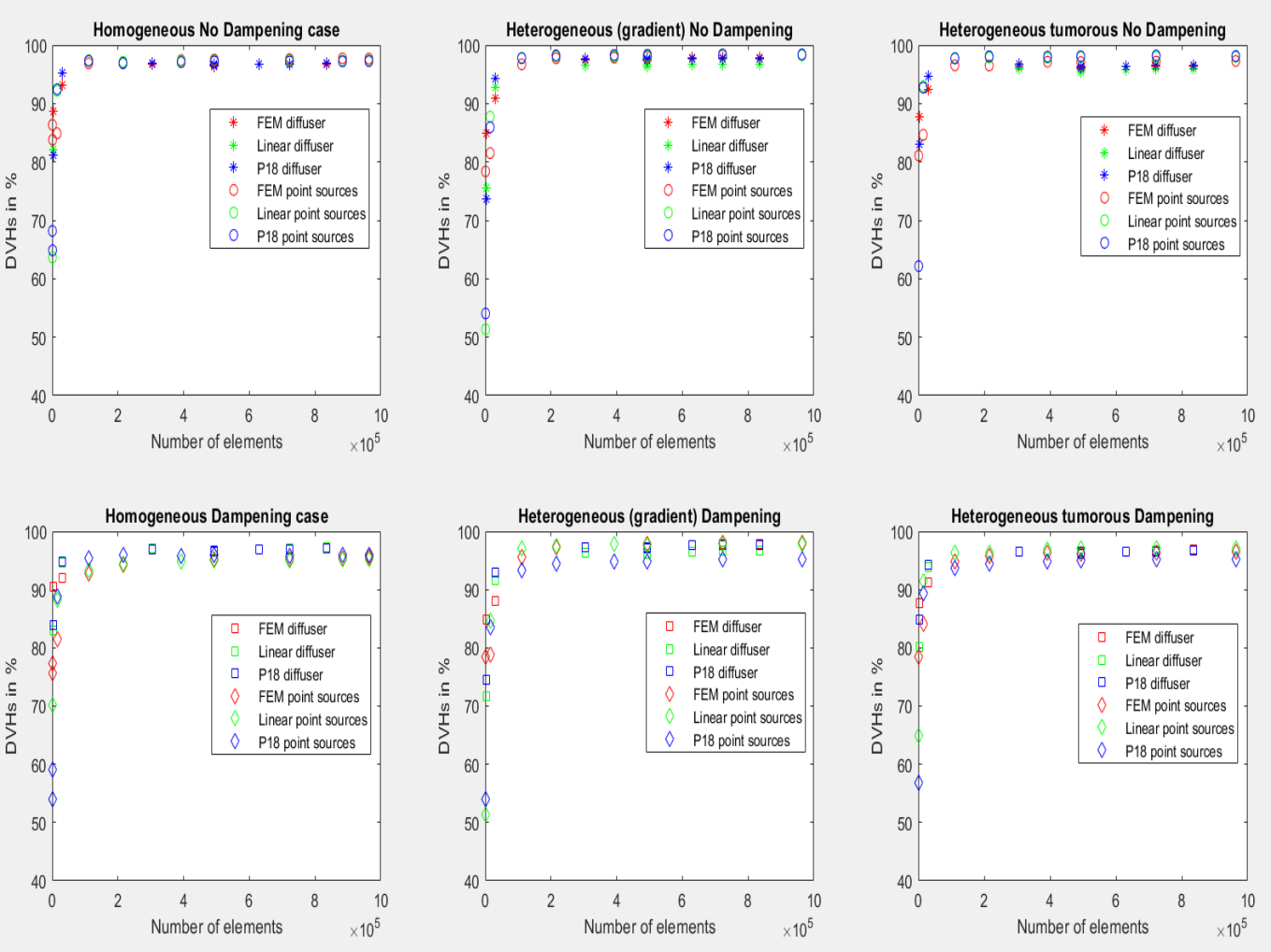

Figure 4.11: DVHs in prostate (number of prostate nodes receiving at least 5J/cm^2) in different situations (homogeneous, heterogeneous, with or without dampening) for 5 mm diffuser fibres.

In Figure 4.11, we can see the values of the DVHs in the prostate for the different cases of prostate medium with 5 mm diffuser fibres. The fibre resolution for the 5 mm fibres was set to 10 (following the criterium previously found when studying the fibre resolution): each diffuser fibre is represented by 10 points. The fraction of prostate nodes is represented as a function of the number of elements used to discretize the prostate during the meshing phase realized by Nirfast. There does not seem to be any difference of convergence between the point source case and the diffuser case nor between the different situations (homogeneous/heterogeneous). A number of elements between 200000 and 300000 seems reasonable. This is the number of elements used in all the following simulations.

4.2.2 Study of fibre resolution and fibre length

Since we said that the FEM data was biased in the point source case and it is even more valid in the diffuser case, we will only focus on the P18 and linear methods.

With diffuser fibres, one parameter that might influence the results obtained is the choice of the fibre resolution. As mentioned earlier, we have made the hypothesis that the line diffuser was approximated by an array of points sources. In Figure 4.12 and 4.13, we varied the number of point sources for 5 mm diffusers from 5 to 31. We can note that the difference between the fibre resolutions is really more important in presence of dampening and that, for a fibre resolution superior to 8 points, we do not have a big change in the DVHs of the prostate. The fibre resolution does not seem to influence the results in the rectum.

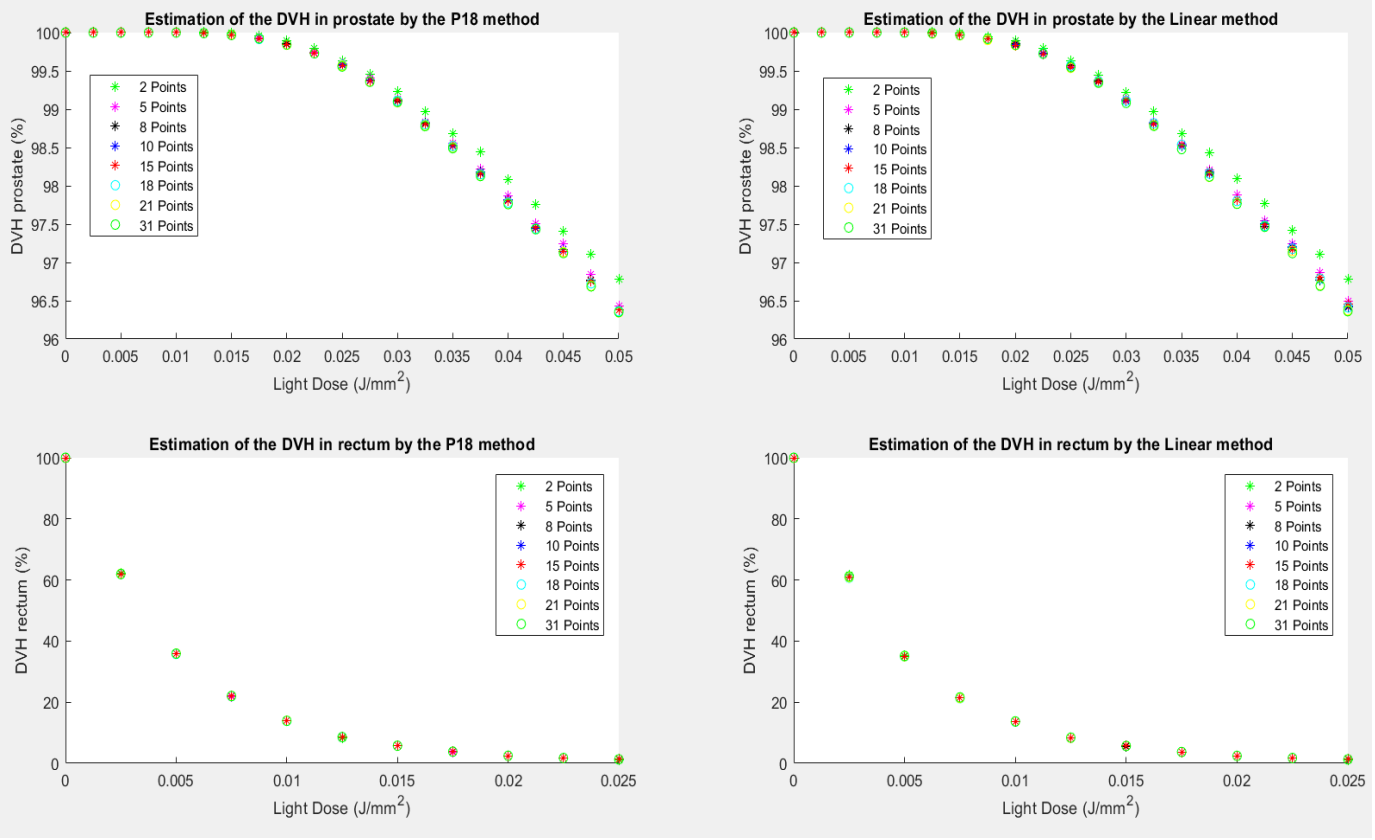

Figure 4.12: Fibre resolution for 5 mm diffusers in homogeneous prostate (No dampening).

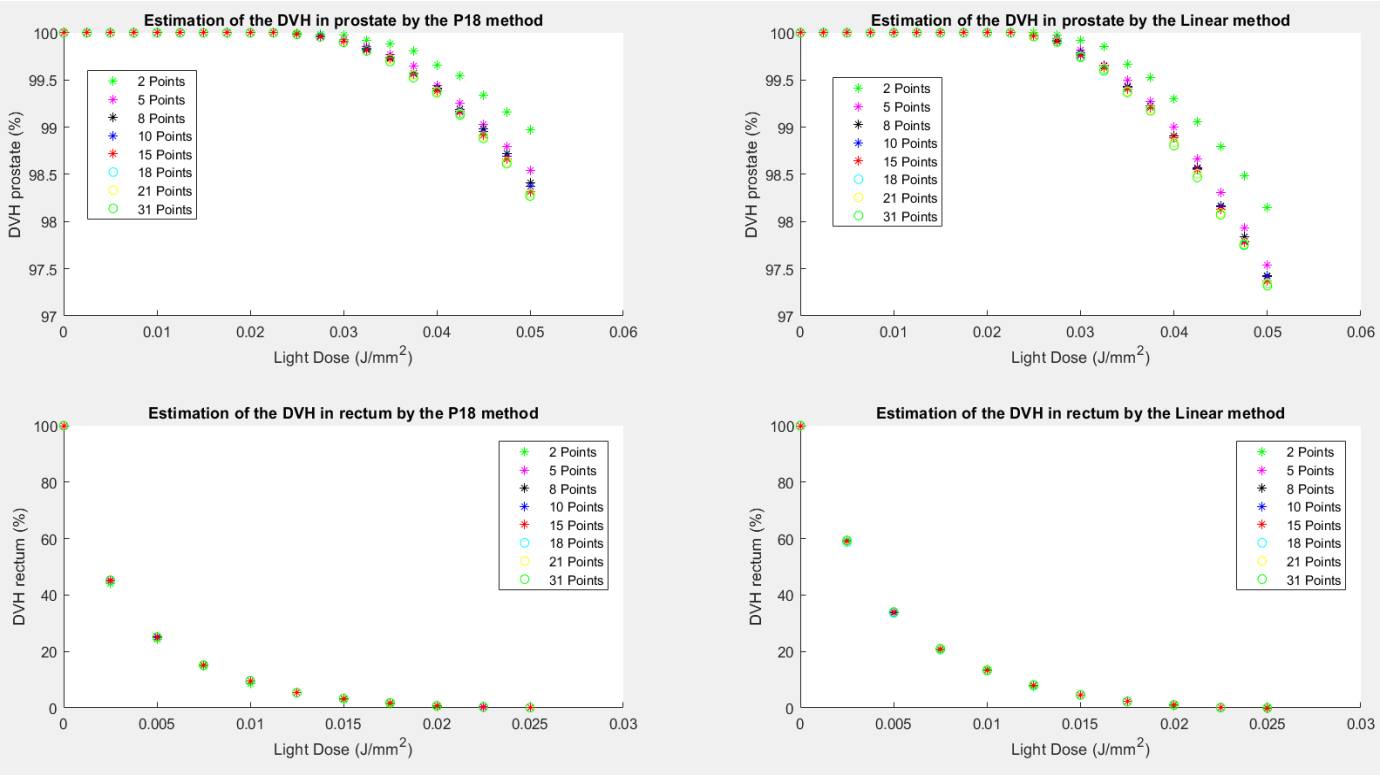

Figure 4.13: Fibre resolution for 5 mm diffusers in homogeneous prostate (Dampening).

We want the lowest fibre resolution to save computation time while having correct enough results even though we used the approximation from continuous line diffuser to discrete point sources. Therefore, we decided that a fibre resolution that was at least twice the fibre length was good enough. In the case of 5 mm diffuser, that means we have to choose a fibre resolution of at least 10 points.

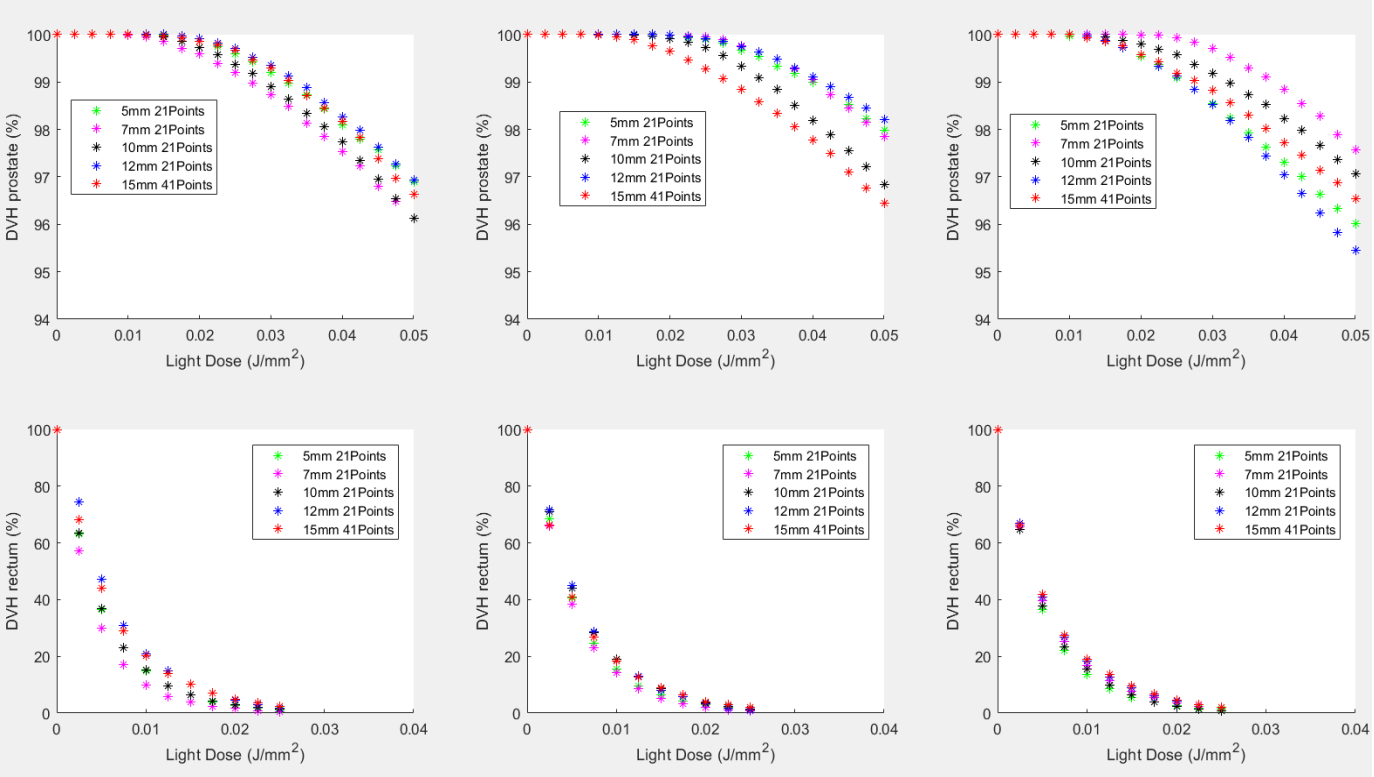

Figure 4.14: DVHs in prostate and rectum for different fibre positions in a homogeneous medium (No dampening).

We also need to study the difference between different fibres lengths. In Figure 4.14, we have plotted for three different fibre positions, the values of the DVHs in the prostate and the rectum in a homogeneous medium. As we can see, the values of the DVHs are really dependent on the positioning of the fibres and no real difference can be observed between the fibres with different lengths in the homogeneous case. The choice of the fibre resolution (21 points or 41points) was made following the criterium that there is no change in DVHs with a fibre resolution that is twice the fibre length.
With Figures 4.14 to 4.16, we can draw several conclusions concerning the evolution of the DVHs in the prostate for different fibre lengths. The different subfigures in those Figures correspond to different fibre positionings. In Figure 4.16, we can see more clearly that fibre with a long length (especially the 15 mm fibres) lead to worse results more often than shorter fibres. The DVHs can be lower than the 95% threshold or really close to it. In 3 cases out of 6, the 10 and 12 mm also perform poorly. The 7 and 5 mm fibres never end up with a DVH lower than 96% in the 6 cases treated in Figure 4.16. The case with a tumorous medium seems to have pretty similar results excepted that the fact that the difference with the different fibres is less clear but we can still see the tendency that the long fibres perform slightly more poorly than the short fibres.

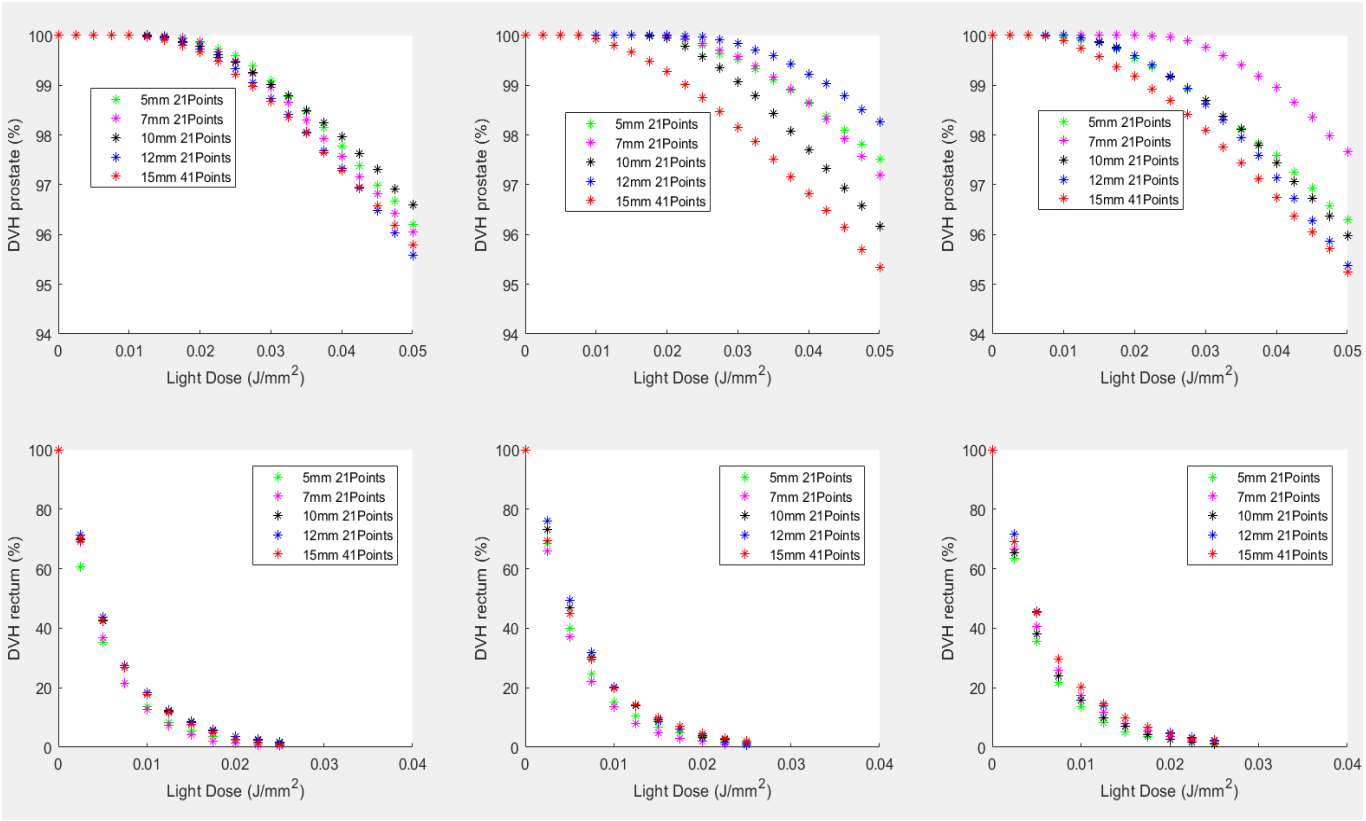

Figure 4.15: DVHs in prostate and rectum for different fibre positions in a heterogeneous tumorous medium (No dampening).

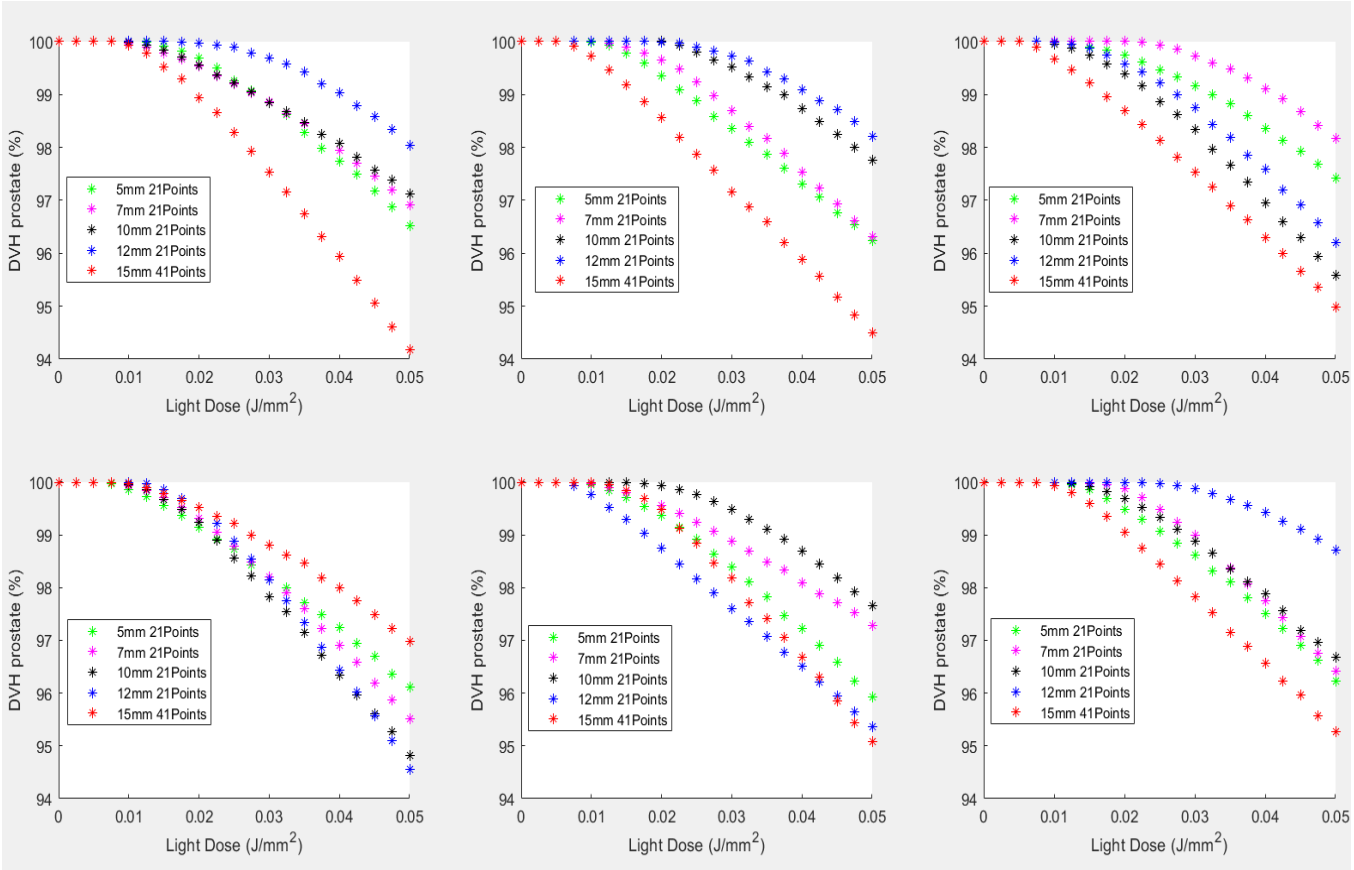

Figure 4.16: DVHs in prostate for different fibre positionings in a heterogeneous medium with gradient (No dampening).

4.2.3 Conclusion with Diffuser Fibres

We can summarize the previous results in few points:

- In order for the fibre resolution not to have an influence on the results, this one must be set to twice the fibre length (if the fibre is 5 mm the resolution must be of 10 points at least).
- The DVHs results are really dependent on the fibre positionings. A previous report has shown that for a certain length the fibre positioning variations could induce a 2% variation in the DVHs.
- The fibre length has some influence on the results. A fibre length of 5 or 7 mm limits the risk of reaching low values of DVHs for some fibre positionings. Nonetheless, we would like to take that fibre as long as possible in order to increase the output power delivered to the tissue while avoiding the possible damages (boiling, etc) due to a high power density in the tissue.
- The linear method seems to have slightly less fluctuations in the DVHs results in comparison with the P18 method which will estimate any variation (including the dampening effect) as a variation in μ_{eff}.
- A mesh constituted by a number of elements between 200 000 and 300 000 elements is sufficient to predict the results with a good accuracy while avoiding long computational time.
- One of the question that we were wondering at the beginning was if we could predict, with a good enough accuracy, the optical properties in the tissue. For the 5 and 7 mm, we have shown that the DVHs results were similar to the ones obtained with point sources fibres.
- Another answer has also been given to whether or not it is a problem if we do not apply the required irradiation times but irradiation times based on the estimations of the optical properties. In that case, the results remain as high as wanted (above the 95% threshold).
- We still obtain good results in the case of a heterogeneous medium even though we use the diffusion approximation which is not valid in the case of a heterogeneous medium to estimate the irradiation times required.

4.3 Variation of output power

The purpose of changing the point sources fibres to diffuser fibres was the possibility that we have of increasing the power output without bringing more damages to the surrounding tissues. This would permit to use less fibres and therefore decrease the time needed for the surgical procedure which will be a benefit for both the patient (less risks) and the hospital (cut in the cost of the surgery). However, the current limits in the increase of the power are the one imposed by the range that the current lasers can deliver at. Due to the limitations in the laser device, the maximum output power that can be delivered currently is 700 mW. We will increase the power from 150 to 700 mW and see the effect on the results.

4.3.1 Block Cimmino Algorithm

The study of the power increase has revealed that the parameters chosen in the Cimmino algorithm to calculate the irradiation times needed for the treatment were optimal for the output power 150 mW. Therefore, a change of those parameters was necessary in order to compare the results between different power outputs. Also, a deeper knowledge of the Cimmino algorithm is needed so we can know on which parameter we should act.

Furthermore, we have shown above that the 5 and 7 mm diffuser fibres were the ones which were leading to the best results. Furthermore, no significant difference was observed between those two fibres lengths. Therefore, we will limit this study to the case of 5 mm diffuser fibres.

The Cimmino algorithm, which is more described in the Appendix, is supposed to find the optimal irradiation times given a certain amount of conditions which are:

- The highest proportion of prostate should receive at least 5 J/cm^2
- The lowest proportion of rectum, urethra and surrounding tissue should receive at most 5J/cm^2
- Some weights are applied to each condition, to quantify how important is the condition compared to the other conditions (for example the condition on the prostate is more important than the one on the urethra)

The conditions for each tissue type are transformed to a system of linear inequalities. Mathematically, these hyperplans are defined as the spaces containing the vectors $x \in \mathbb{R}^T$ which verify:

$$< a^j, x >= b_j \qquad j=1,2,\ldots,J. \tag{4.1}$$

Where each vector a^j is T dimensional, $a^j \in \mathbb{R}^T$ and T represents the number of fibres. The components of a^j are assumed to be real numbers. The number J is equal to 4 in our case and corresponds to the number of conditions or tissue type for which we are going to have an inequality concerning the delivered dose. Eventually, each vector b_j represents the maximum or minimum dose delivered in each tissue type. The $< , >$ stands for the usual inner product in $\mathbb{R}^T$:

$$< a^j, x >= \sum_{t=1}^{T} a_i^j * x_i$$

As said before, we try to fulfill different conditions depending on the tissue type: a minimum dose of 5 J/cm^2 must be received by the prostate and a maximum dose that can be received by the other organs is 5 J/cm^2.

4.3.2 Results

4.3.2.1 Effect of the initialisation time

In Figures 4.17 to 4.20, we have plotted the effect of the initialisation time on the results in the prostate and rectum (which are the most important tissues) for an ouput power equal to 700mW. We will compare those results to the ones obtained with an output power equal to 150mW (reference case) in Figures 4.22 to 4.23.

In Figures 4.17 to 4.20, we can note that the lower is the choice of the initial irradiation time, the less the difference between the times applied on the fibres is important. Indeed, if we look at Figures 4.20 and 4.22, we can see that for an initial irradiation time of 100s, all the fibres end up with the same irradiation time which is approximately the initial irradiation time. We remind the reader that the solution obtained is a convergent solution. Instead, if the initial irradiation time is 700s then we have a real distinction between the different fibres. This observation might be relevant when we want to focus on the reduction of the number of fibres by increasing the power. It seems that choosing an initial time high enough is better to allow a real difference between the different fibres. On the other hand, for all the fibres, we can see that the increase of the initial time leads to a converging solution that has a lower percentage of prostate treated.

We can also observe that for a high output power, some really high values are obtained in the rectum if we set the initialisation time to a low value. Indeed, in Figure 4.21, more than 8% of the rectum receives a dose equal to 5 J/cm^2. This phenomenon is not observed with 150mW fibres. Another interesting aspect to note down is the fact that for all the cases, the chosen initial irradiation time constitutes an upper limit for the irradiation times calculated by Cimmino. For example, in Figure 4.19, we can see that if we set the initial time to be 1500s then the maximum Cimmino irradiation time is 1400s and that is the same for all the initial irradiation times tested.

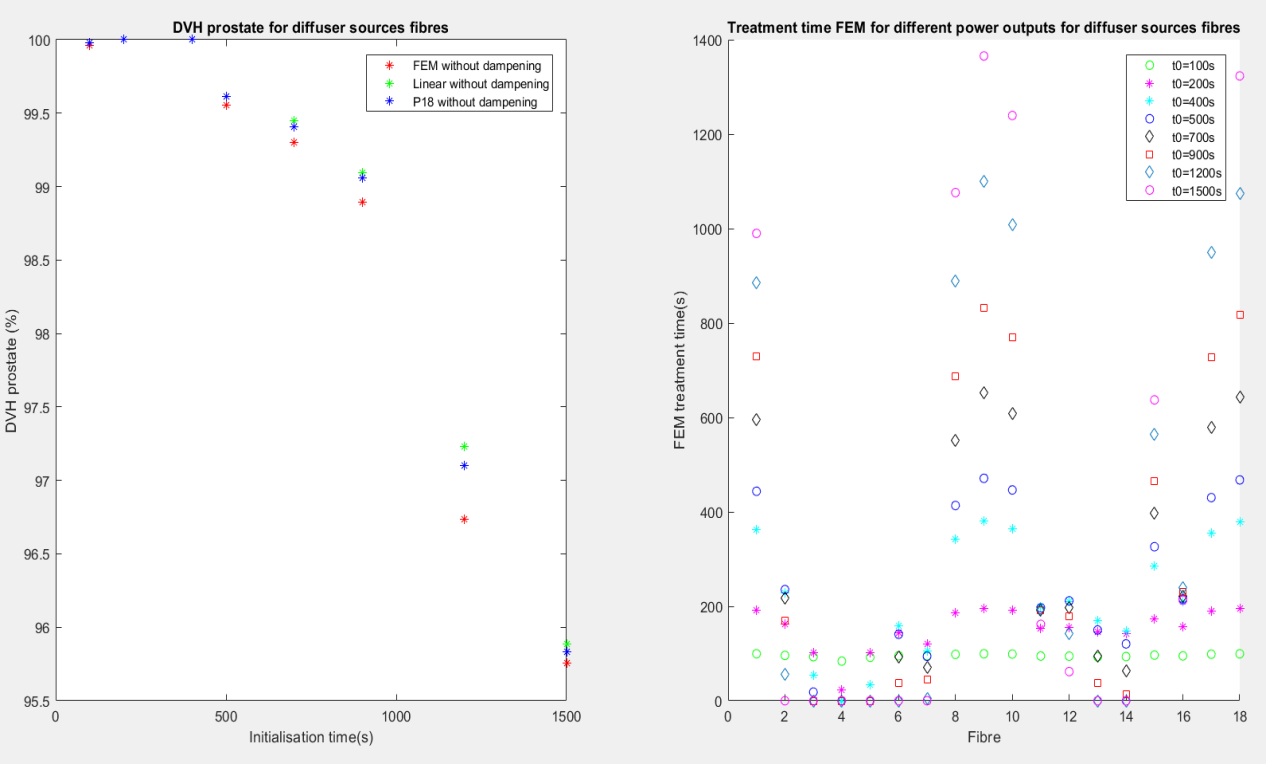

Figure 4.17: Block Cimmino 2: Percentage of prostate receiving the threshold dose when using 18 fibres with different initialisation times for a power output equal to 700mW (random positioning 1).

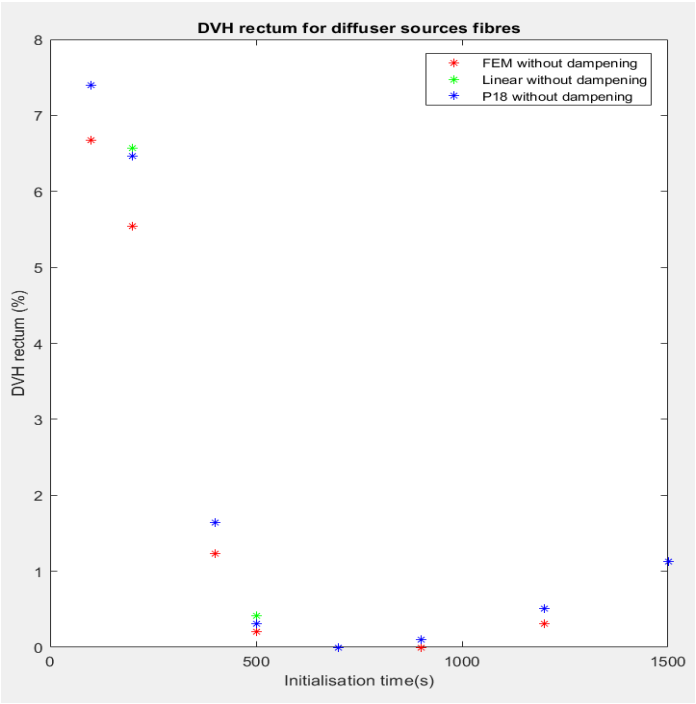

Figure 4.18: Block Cimmino 2: Percentage of rectum receiving the threshold dose when using 18 fibres with different initialisation times for a power output equal to 700mW.

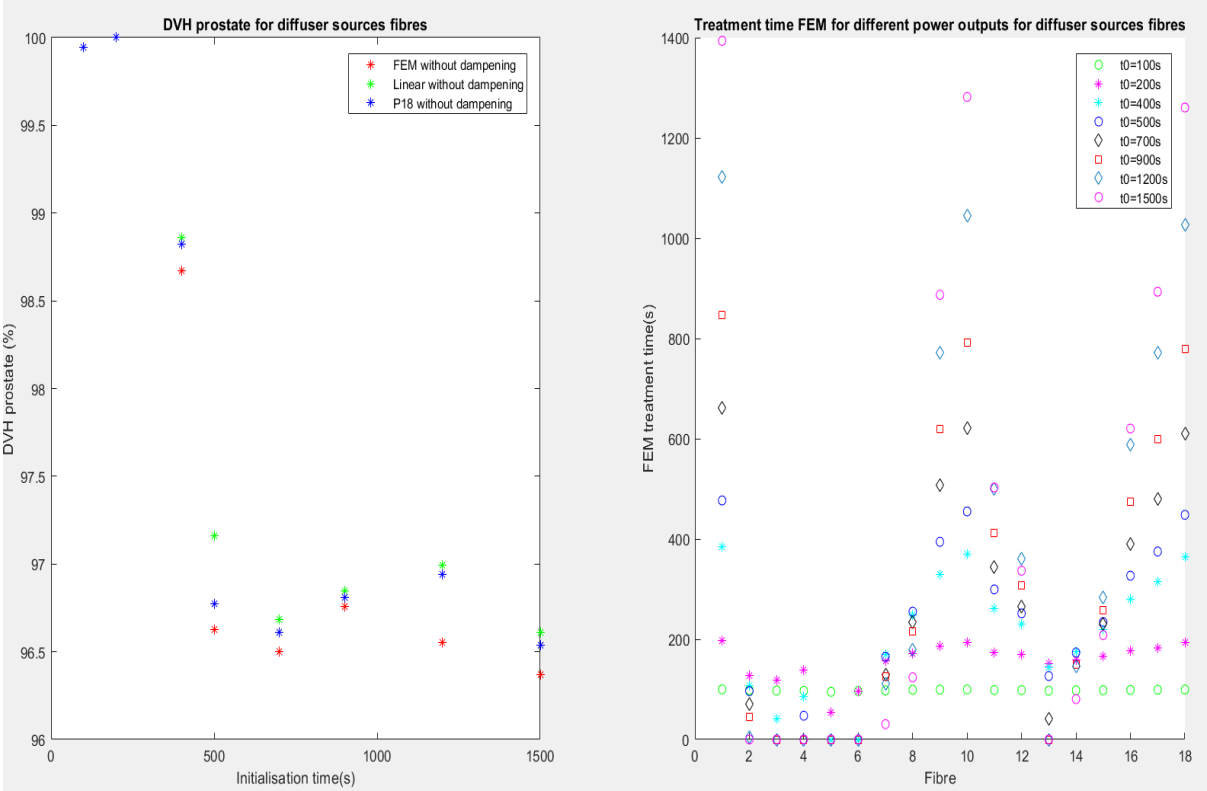

Figure 4.19: Block Cimmino 2: Percentage of prostate receiving the threshold dose when using 18 fibres with different initialisation times for a power output equal to 700mW (random positioning 2).

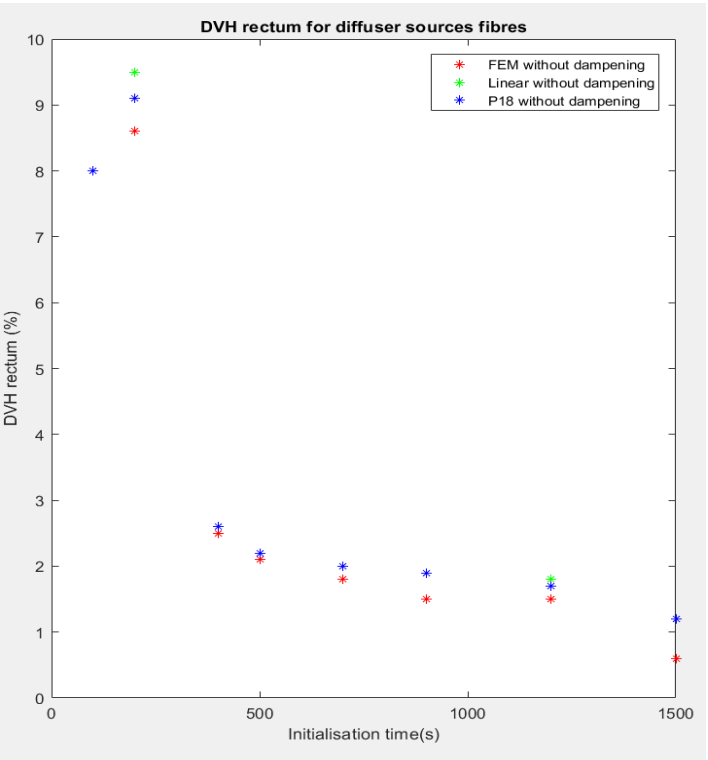

Figure 4.20: Block Cimmino 2: Percentage of rectum receiving the threshold dose when using 18 fibres with different initialisation times for a power output equal to 700mW.

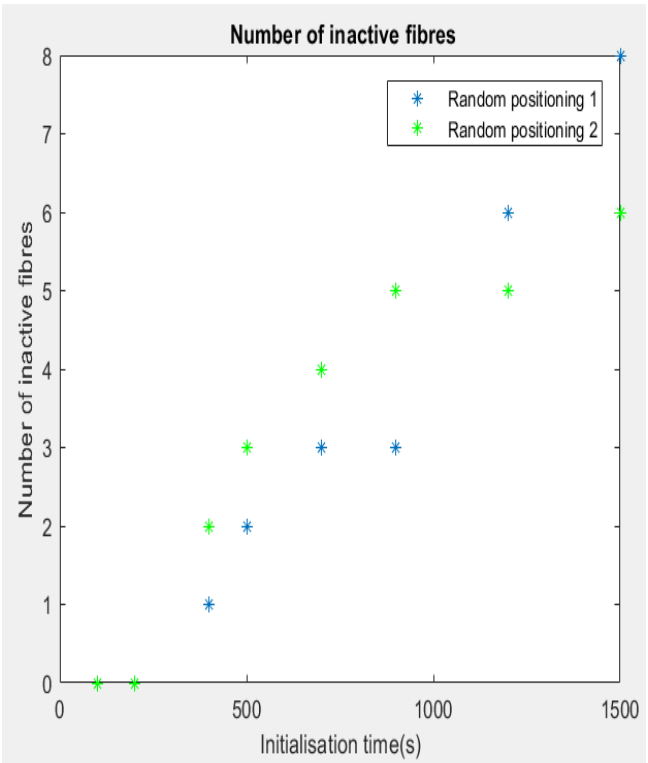

Figure 4.21: Number of unused fibres for which the irradiation times are set to 0s by the Block Cimmino 2 algorithm (Output Power: 150 mW).

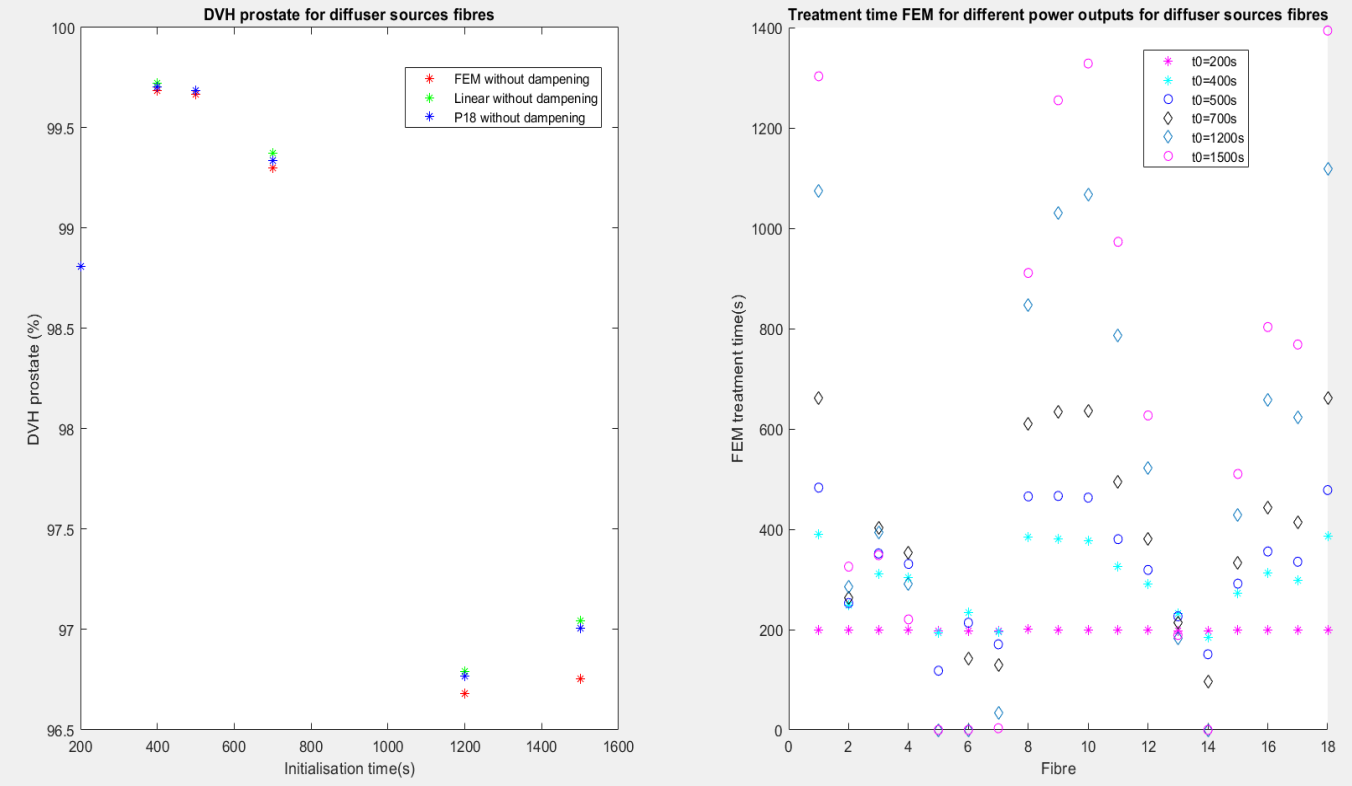

Figure 4.22: Block Cimmino 2: Percentage of prostate receiving the threshold dose when using 18 fibres with different initialisation times for a power output equal to 150mW.

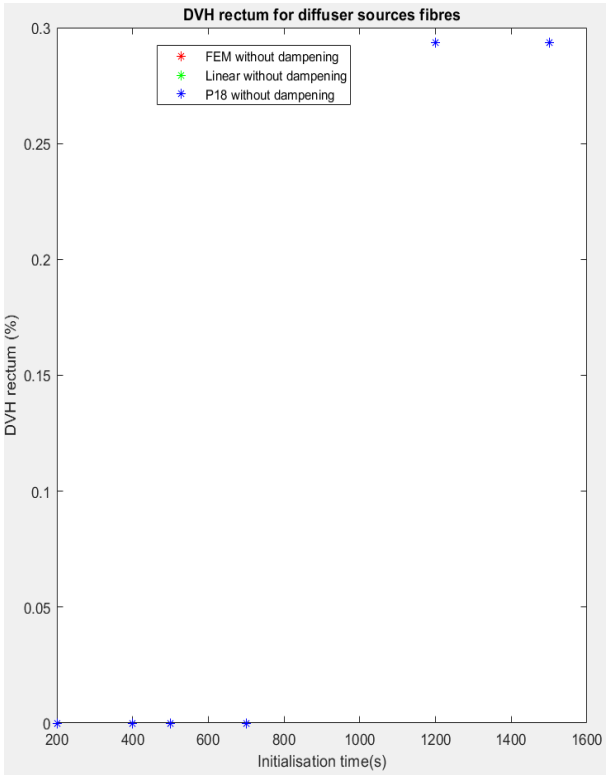

Figure 4.23: Block Cimmino 2: Percentage of rectum receiving the threshold dose when using 18 fibres for a power output equal to 150 mW.

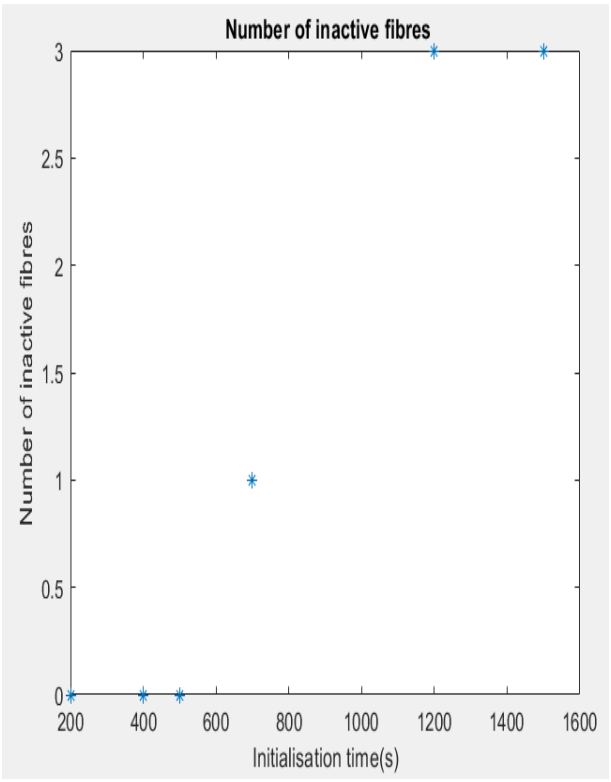

Figure 4.24: Number of unused fibres for which the irradiation times are set to 0s by the Block Cimmino 2 algorithm (Output Power: 150 mW).

In figures 4.21 and 4.24, we have plotted the number of inactive fibres. We can see that in the case where the power is set to 150 mW the number of inactive fibres (whose irradiation times are strictly equal to 0) is lower than in the case where we have a 700mW output power. The fact that we have time that are strictly equal to 0 seems a bit suspicious, in the sense that we would understand to have low irradiation times for some fibres but not strictly equal to 0. Plus, we do not have an explanation concerning the link between the number of inactive fibres and the initialisation time. It seems that the higher is the initialisation time, the more inactive fibres we get.

4.3.2.2 Comparison between Block Cimmino 2 and Block Cimmino 20

The main difference between the Block Cimmino 20 and the Block Cimmino 2 algorithm seems the importance given to the prostate compared to the rectum. The Block Cimmino 2 algorithm values more a high dose in the prostate while the Block Cimmino 20 gives priority to a low value in the rectum.

Because the values achieved by the Block Cimmino 20 (λ_k =20) seem really low in the prostate, we would give preference to the case where λ_k =2 (Block Cimmino 2). Nonetheless, in comparison to Figure 4.22 and 4.23, where we had an output power of 150mW, we can see that the increase of the power is followed by an increase of the dose in the rectum. It seems that at the current time, the settings for Block Cimmino 2 or maybe the Block Cimmino algorithm itself are not able to guarantee as good results as in the case where the power output is equal to 150mW.

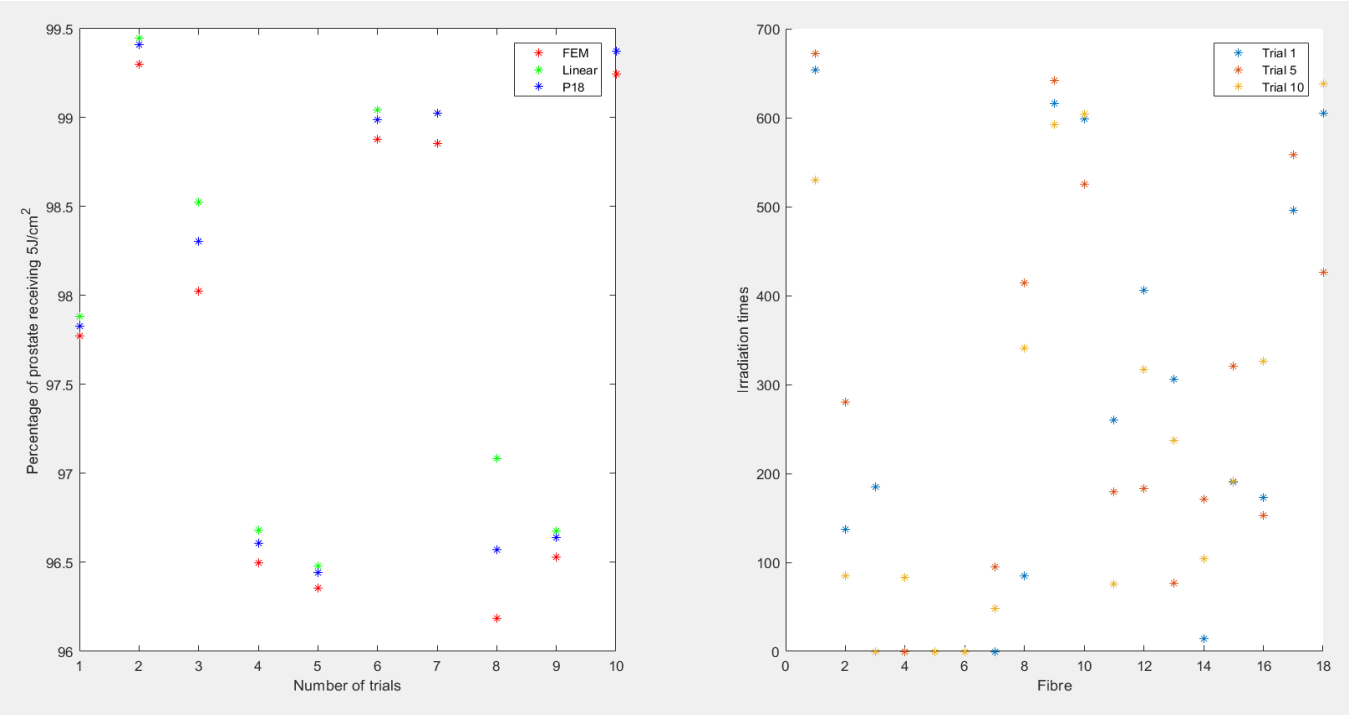

Figure 4.25: Percentage of prostate treated at the threshold dose with the Block Cimmino 2 algorithm (t_0 =700 s and Power=700 mW).

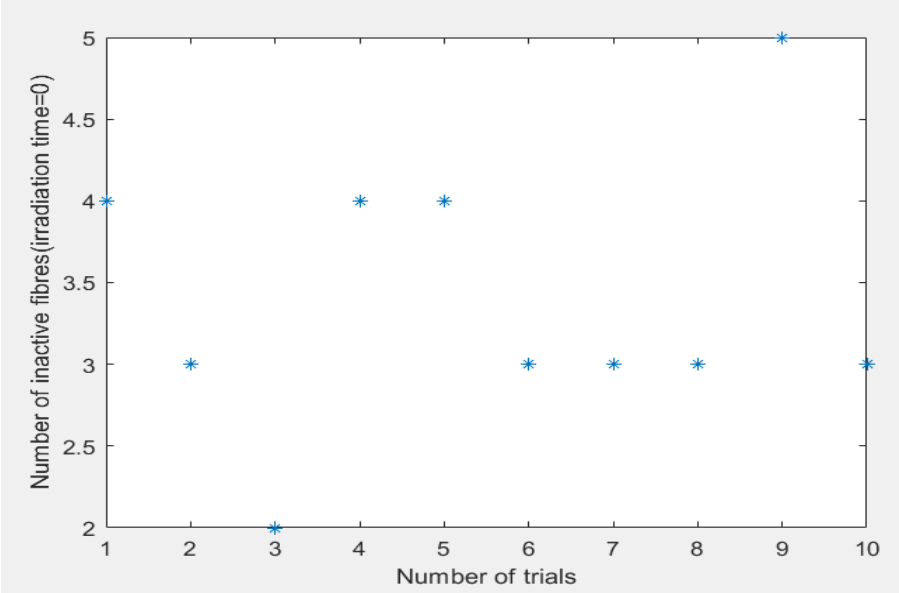

Figure 4.26: Number of inactive fibres or fibres with an irradiation time equal to 0 s.

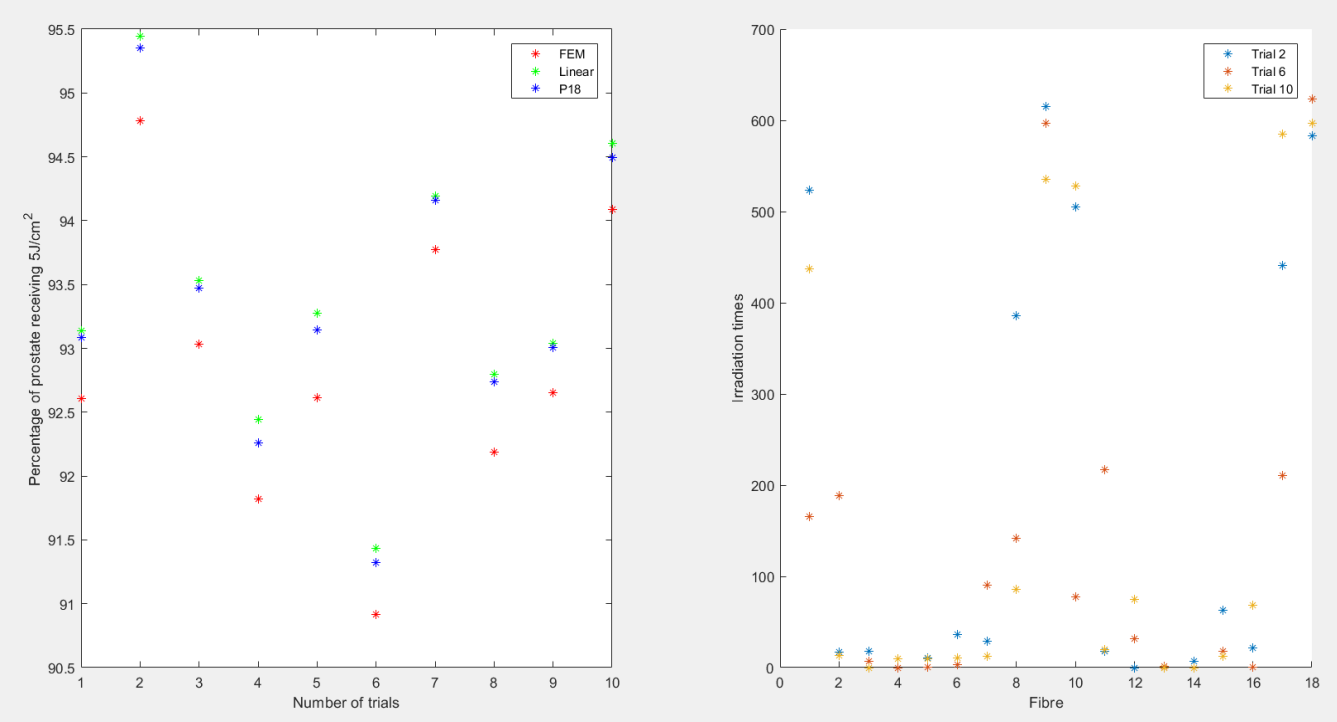

Figure 4.27: Percentage of prostate treated at the threshold dose with the Block Cimmino 20 algorithm (t_0 =700s and Power=700mW).

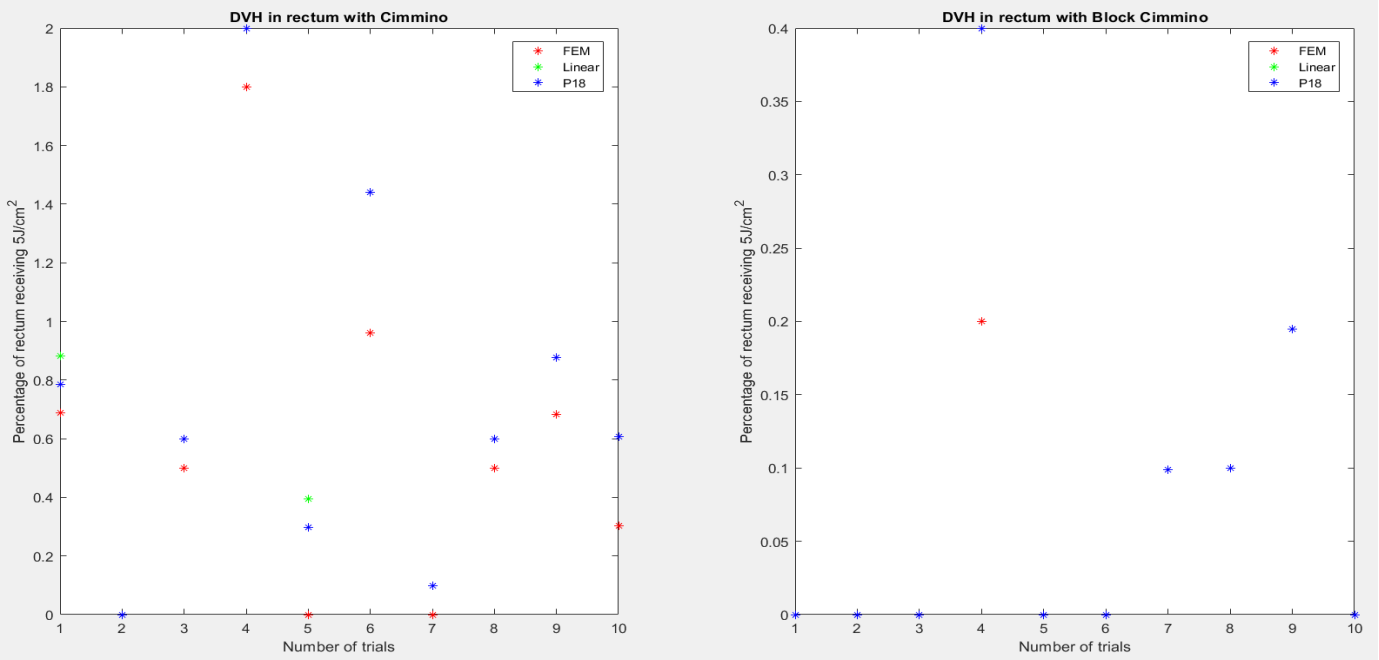

Figure 4.28: Comparison dose in the rectum with Block Cimmino 2 (left) and Block Cimmino 20 (right) algorithms.

4.3.2.3 Use of 15 fibres

Since the average number of inactive fibres was found to be 3, we have reduced the number of fibres to 15. We can see the results in Figures 4.29 and 4.30. The percentage of prostate receiving the threshold dose is slightly inferior to the case where we had 18 fibres (this time we have between 95 and 98% whereas we had between 96% and 99.5% previously). Plus, even though the number of fibre was decreased from 18 to 15, we still end up with an average of 3 inactive fibres.

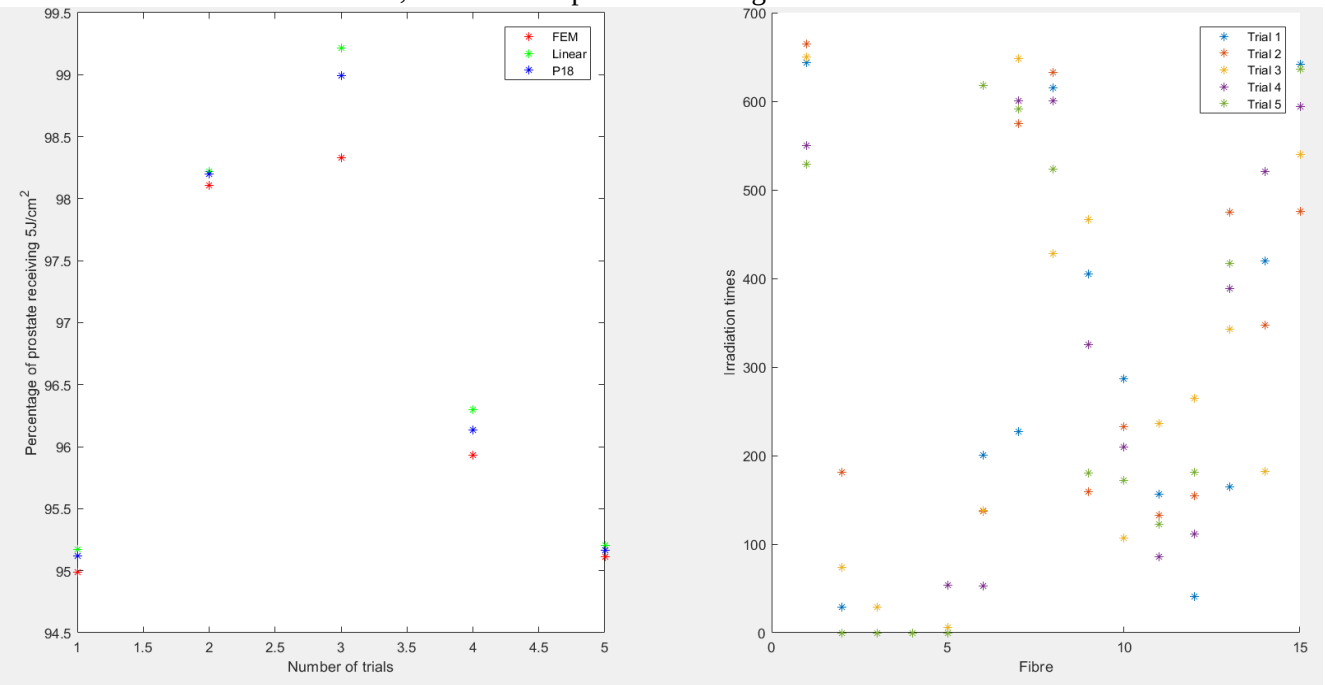

Figure 4.29: Percentage of prostate treated at the threshold dose by using 15 fibres with the Block Cimmino 2 algorithm (t_0 =700s and Power=700mW).

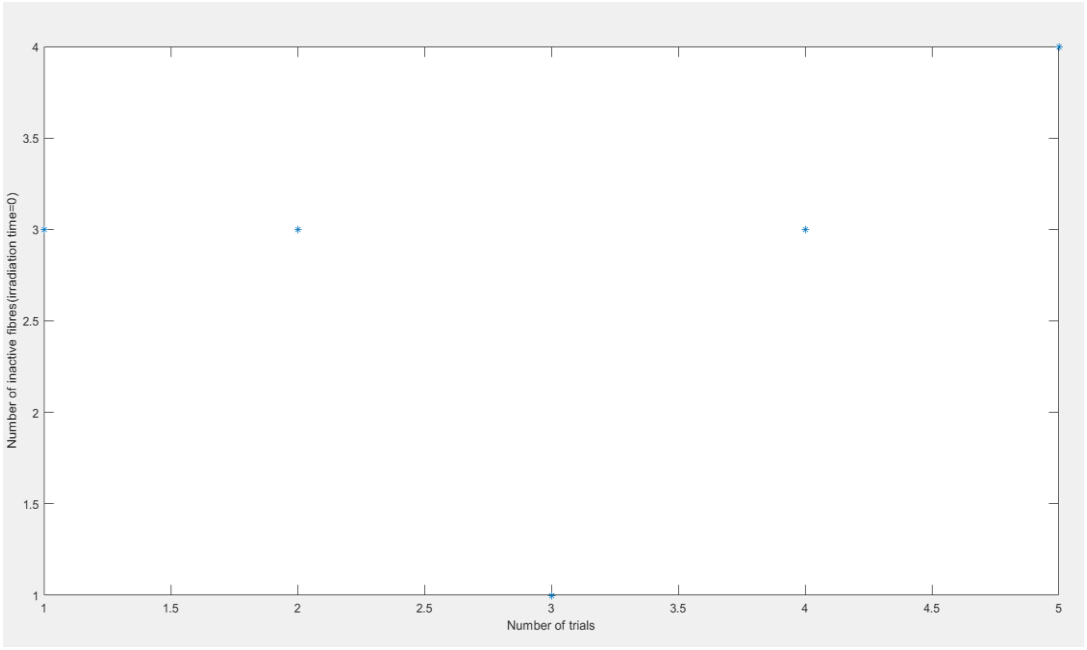

Figure 4.30: Number of inactive fibres or fibres with an irradiation time equal to 0 s (15 fibres).

The main reason to this situation might be the fact that the fibre positioning is done independently of the treatment planning. In fact, everytime that we are decreasing the number of fibres, the positioning of the fibres might change completely and therefore it is hard to compare the results.

One simulation that we could run is to choose the same fibre positions as in the case where we had 18 fibres and just remove the ones which had an irradiation time of 0s as we do in Figure 4.33 to 4.36. For example, we can take the trial numbers 2, 6, 7, 8 and 10 as an example in Figure 4.25 which have an irradiation time set to 0 following Block Cimmino 2's predictions.
The results for the Block Cimmino 2 algorithm are shown in Figure 4.31. As we can see, the values in the prostate are all above 98%. One of the problem that we encounter is that with some position, we reach really high values in the rectum. In order to understand what is happening, we are graphically plotting the fibre positions in Figures 4.33 to 4.36.

We can observe that for trial 2 and trial 8 (Figure 4.25) which correspond to trial 1 and 4 in Figures 4.33 and 4.32, the inactive fibres correspond to fibres close to the rectum. Therefore, we do not understand how by removing those fibres, the dose in the rectum can reach 8%. In Figure 4.33, we can observe with trial 4 that we have high irradiation times for fibres 2, 6 and 7. This situation might be the reason why we have such high value in the rectum. Nonetheless, no explanation can be brought concerning the reason why the irradiation times calculated with the Block Cimmino 2 algorithm can lead to such results. In Figure 4.37, we can see that the distribution of the irradiation times has completely changed due to the removal of the fibres. This is the reason why the values are so high in the rectum. We observe a general increase of the irradiation times when using 15 fibres.

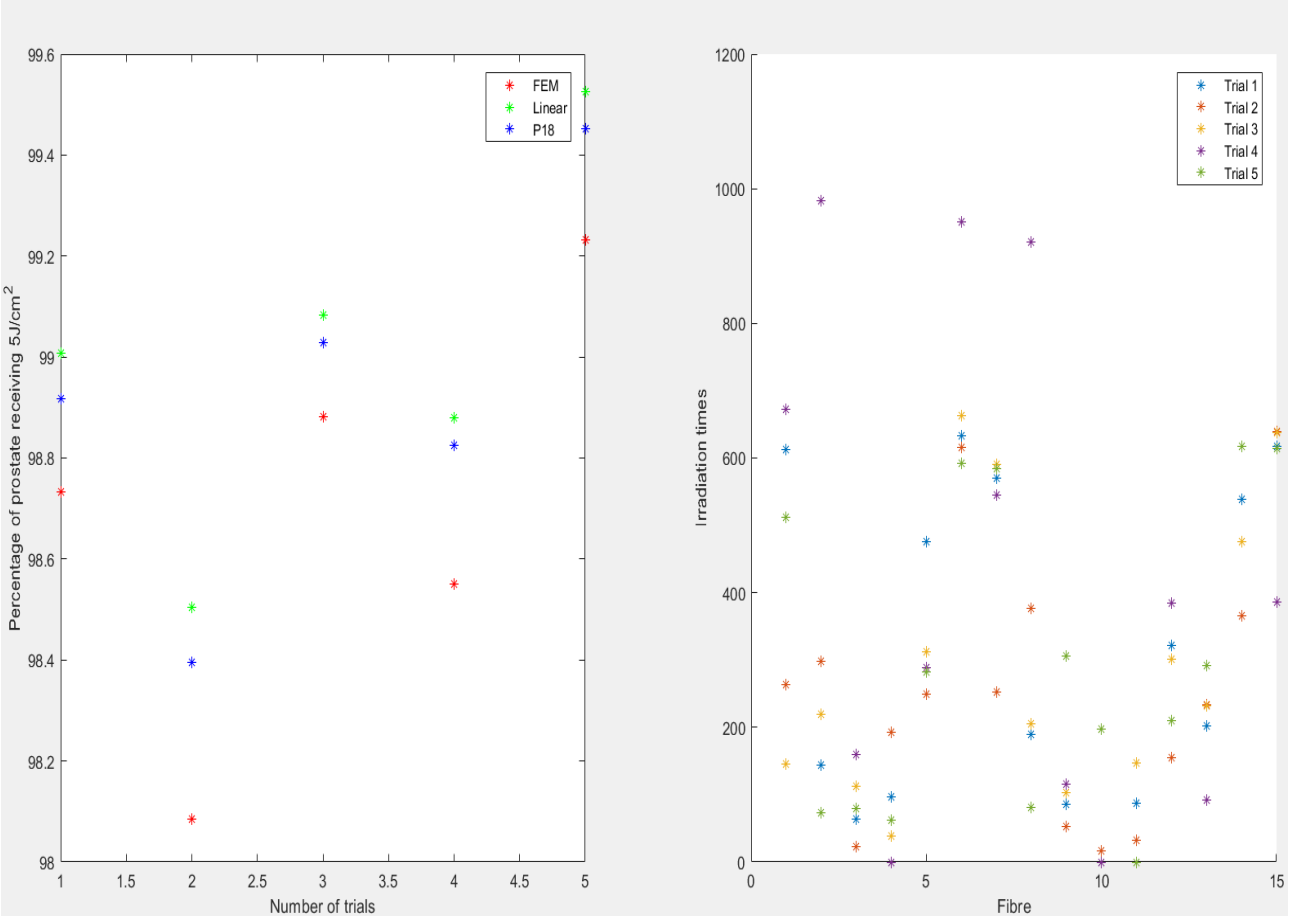

Figure 4.31: Use of the 15 active fibres (out of the 18 initially placed in Figure 7) with Block Cimmino 2.

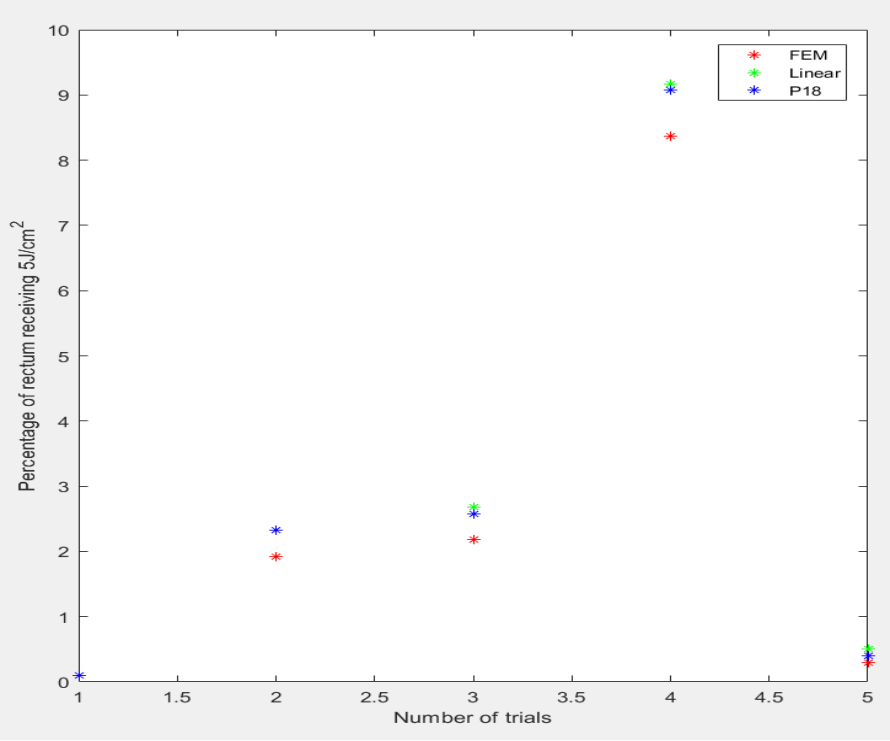

Figure 4.32: Rectum dose received by the use of only 15 fibres as shown in Figure 17 with Block Cimmino 2.

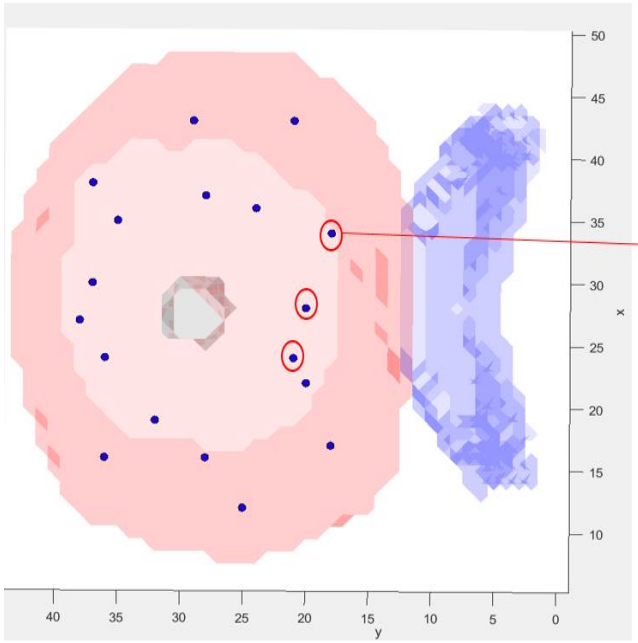

Figure 4.33: positions of the 18 fibres.

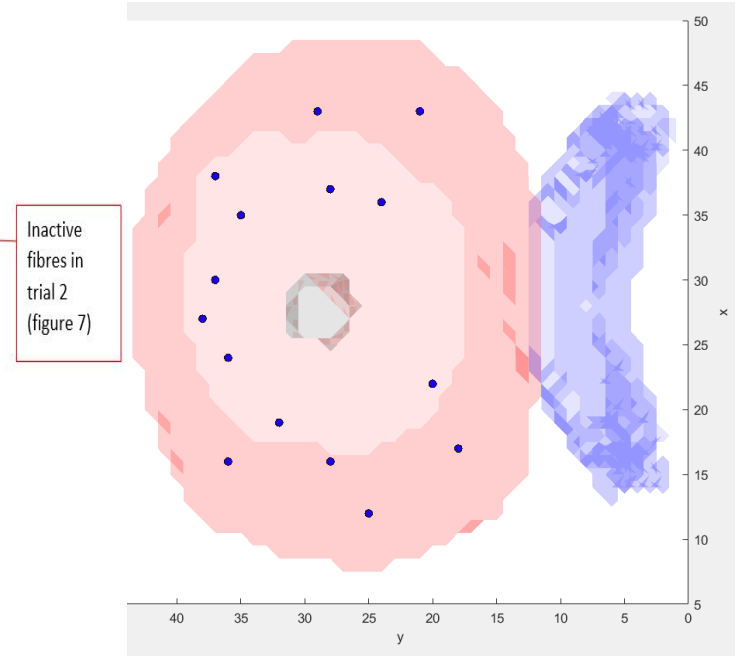

Figure 4.34: Removal of the three inactive fibres from trial 2 in Figure 4.28.

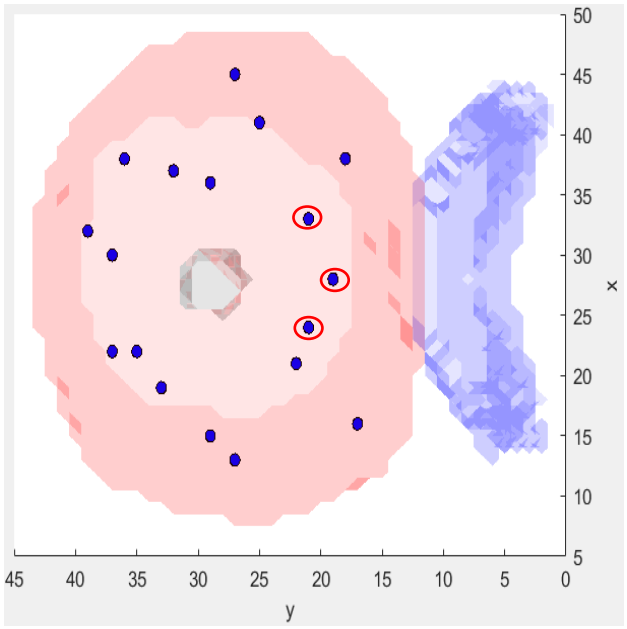

Figure 4.35: position of the fibres with trial 8 in Figure 4.25.

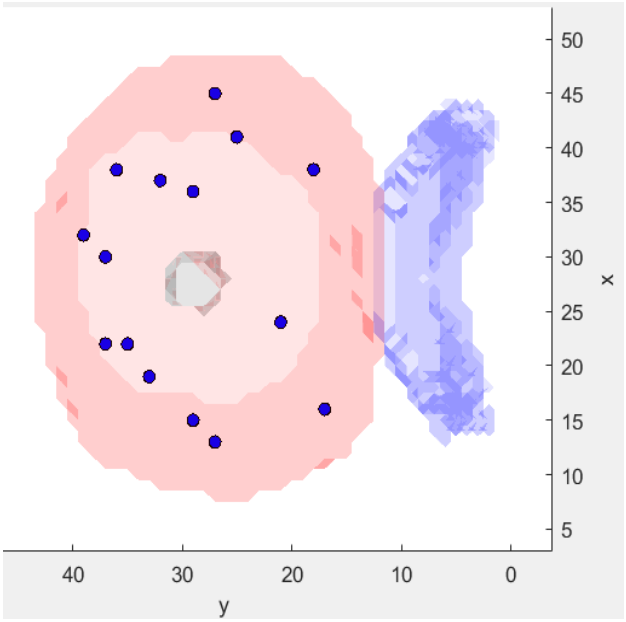

Figure 4.37: Removal of the three inactive fibres from trial 8 in Figure 4.25.

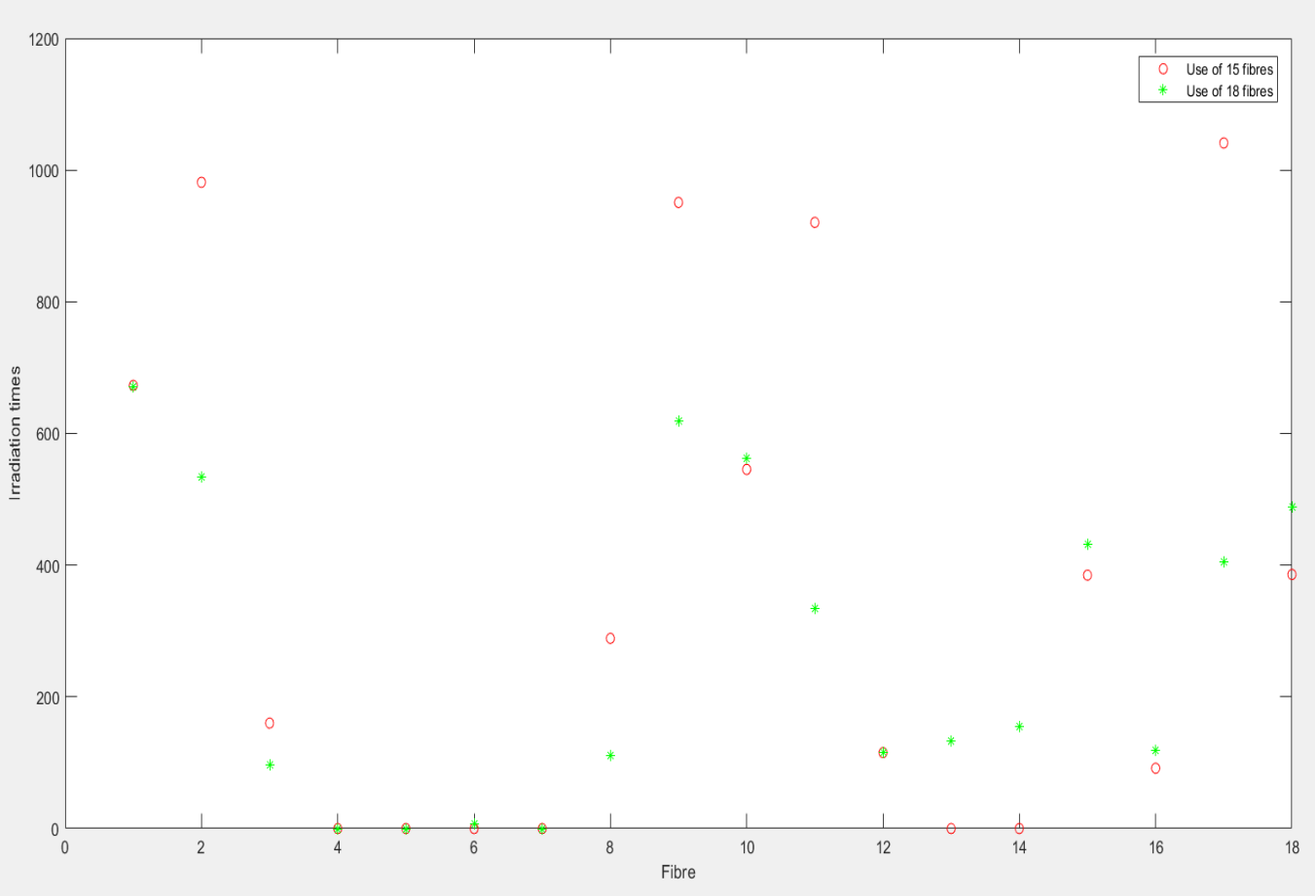

Figure 4.37: Comparison irradiation times with 15 or 18 fibres (fibre 4,5 and 7 were artificially set to 0 in the case where we have 15 fibres for graphical purpose only).

4.3.2.4 Conclusion

The Cimmino algorithm or the Block Cimmino algorithm in our case (we remind the reader that so far we haven't used the Cimmino algorithm but only the Block Cimmino algorithm as explained in the beginning of this report) seems to be dependent of many parameters that appear to have been optimized for the point source case with 150 mW. We have tried to study the dependency on some of those parameters such as the initial irradiation times and we have found some interesting results such as the limitation of the final irradiation times due to that initial irradiation time chosen. However, the study in detail of the Block Cimmino algorithm seems out of the scope of this thesis. No conclusion was achieved concerning the reduction of the number of fibre by the use of diffuser fibres in comparison to the use of point sources fibres.

The incoherent behaviour of the Block Cimmino algorithm has been suggested to be attributed to the fluence model of using a decreasing exponential with a long tail, whereas in reality this tail should be cut.

Chapter 5: Conclusions

In chapter 1, we had mentioned some challenges that we would like to meet.

The first thing that we can confirm is the fact that the change of point sources fibres for diffuser fibres, all the other parameters being constant, guarantees the same level of accuracy in the determination of the optical properties while preserving the surrounding tissues. That last statement is particularly valid for low fibre lengths such as 5 mm and 7mm. For longer diffuser fibres, the efficiency of the treatment is not as great as with bare end fibres. We have also been able to notice that the performance of the fibres is hard to quantify for different fibre lengths because the positioning of the fibres, done by an independent algorithm, makes the DVHs results fluctuate a lot.

Since the 5 mm and 7 mm fibres permit to achieve good results, we wanted to change the delivered power so that we can decrease the number of fibres used. Yet, we have noticed that the Cimmino algorithm, that is the algorithm used to determine the irradiation times for each fibre, was optimized for the delivered power of 150 mW that is used by Spectracure AB at the moment. Some changes in the parameters of the Cimmino algorithm were intended but unfortunately has not allowed us to draw any conclusion concerning the performance of the treatment with a lower number of diffuser fibres delivering a higher power.

We have also tested two different methods concerning the determination of the optical properties. The reason why we had two methods was to see how the blood pooling phenomenon, while inserting the fibres in the prostate, could affect the performance of the treatment. We have seen that both the P18 method and the linear method could lead to good results. Nonetheless, the linear method permits to achieve slightly better results than the P18 method when there is blood pooling.

Another important aspect of this master thesis was to check the validity of the diffusion approximation in the case where we have a heterogeneous prostate and after testing two different cases of heterogeneous prostate media, we can say that the diffusion approximation leads to a satisfying level of treatment though not valid in theory.

This diploma work was a contribution to the will expressed by Spectracure AB to introduce diffuser fibres as a replacement of point sources fibres that the company uses now. The following step would be to check the results by doing some experiments on a phantom model of the prostate and to compare the results between point sources fibres and the 5 and 7 mm diffuser fibres. It could be an interesting extension of this diploma work.

Bibliography

[1]: *https://en.wikipedia.org/wiki/Prostate*: Prostate, in Wikipedia Retrieved 2011-01-24.
[2]: Master Thesis Johan Rengstedt, November 2013
[3]: *http://www.worldscientific.com/doi/pdf/10.1142/S1088424617300014:* Francesca Moret and Elena Reddi, *Strategies for optimizing the delivery to tumors of macrocyclic photosensitizers used in photodynamic therapy (PDT)*, J. Porphyrins Phthalocyanines **21**, 239 (2017).
[4] *http://hyperphysics.phy-astr.gsu.edu/hbase/molecule/molec.html*: ©C.R. Nave, 2017, *Hyperphysics*, website developed by the Georgia State University
[5]: http://photobiology.info/Hamblin.html: Michael R. Hamblin,Mechanisms of low level light therapy, 8/14/08
[6]: Mahmoud H. Abdel-Kader, *Photodynamic Therapy From Theory to Application*, Springer,2014
[7]: ***https://photochemistry.wordpress.com/category/photodynamic-therapy/:*** *Photodynamic Therapy: An overview*, the Photodynamic Portal, December 16, 2012
[8]: *http://cytoluminator.com/rsrch/state-of-the-art-delivery-ps-pdt.pdf:* Yvette Niamien Konan, Robert Gurny, Eric Allemann, *State of the art in the delivery of photosensitizers for photodynamic therapy, Journal of* Photochemistry and Photobiology, *2001*
[9] B. C. Wilson, Megan Elizabeth Patterson, Lothar Lilge, *Implicit and explicit dosimetry in photodynamic therapy: a New paradigm*, Lasers in Medical Science, 1997
[10]: *https://www.sciencedirect.com/science/article/pii/S0006349511054749*Mark T.Jarvi, Michael S.Patterson, Brian C.Wilson, *Insights into Photodynamic Therapy Dosimetry: Simultaneous Singlet Oxygen Luminescence and Photosensitizer Photobleaching Measurements*, Biophysical Journal, 8 February 2012
[11] https://www.aapm.org/meetings/05AM/pdf/18-4025-7778-678.pdf, Timothy C Zhu, Jarod C Finlay, and Brian C Wilson, *Photodynamic Therapy: Fundamentals and Dosimetry*, AAPM Refresher Course, July 28, 2005
[12]:https://books.google.se/books?id=9G5yBgAAQBAJ&pg=PA174&lpg=PA174&dq=bare+end+fibres+in+PDT&source=bl&ots=M8FgnRjEQb&sig=XlOlA6sqc6FJP-F2bGgysXWrgvA&hl=en&sa=X&ved=0ahUKEwjb6IGMxfPaAhWjIpoKHTZyAfgQ6AEILTAB#v=onepage&q=bare%20end%20fibres%20in%20PDT&f=false, Eric Barret, Matthieu Durand,*Technical Aspects of Focal Therapy in Localized Prostate Cancer*, Springer, 2015
[13]:http://www.eng.ucy.ac.cy/cpitris/courses/ECE477/presentations/English/05.%20Tissue%20Optics.pdf, University of Cyprus Biomedical Imaging and Applied Optics, course online
[14]http://appliedmath.ucmerced.edu/sites/appliedmath.ucmerced.edu/files/documents/PHDdocs/ambrocio_2009.pdf, *A Self-Consistent Obstacle Scattering Theory for the Diffusion Approximation of the Radiative Transport Equation*, University of California, Merced, *Elibet Ambrocio* , 2008
[15] Brian C Wilson and Michael S Patterson, *The physics, biophysics and technology of photodynamic therapy*, Physics in Medicine & Biology, 9 April 2008
[16] Yair Censor, Martin D Altschuler and William D Powlis, *On the use of Cimmino's simultaneous projections method for computing a solution of the inverse problem in radiation therapy treatment planning*, Inverse Problems **4,** 1988
[17] Brian C.Wilson, Michael S.Patterson, Lothar Lilge, *Implicit and explicit dosimetry in photodynamic therapy: a New paradigm*, Lasers in Medical Science, *1997*
[18]M.Schweiger, S.R.Arridge, M.Hiraoka and D.T.Delpy, *The finite element method for the propagation of light in scattering media: Boundary and source conditions*, Medical Physics, 1995

Appendix

- Creation of the Mesh by nirfast

The geometry of the prostate is stored as a 3D voxel matrix called classification3DModel. Those data result from the segmentation of medical images by some doctors. This matrix is stored in the matlab format '.mat' that is not readable by Nirfast. The first step is to convert those data in a readable format for Nirfast (vtk file).

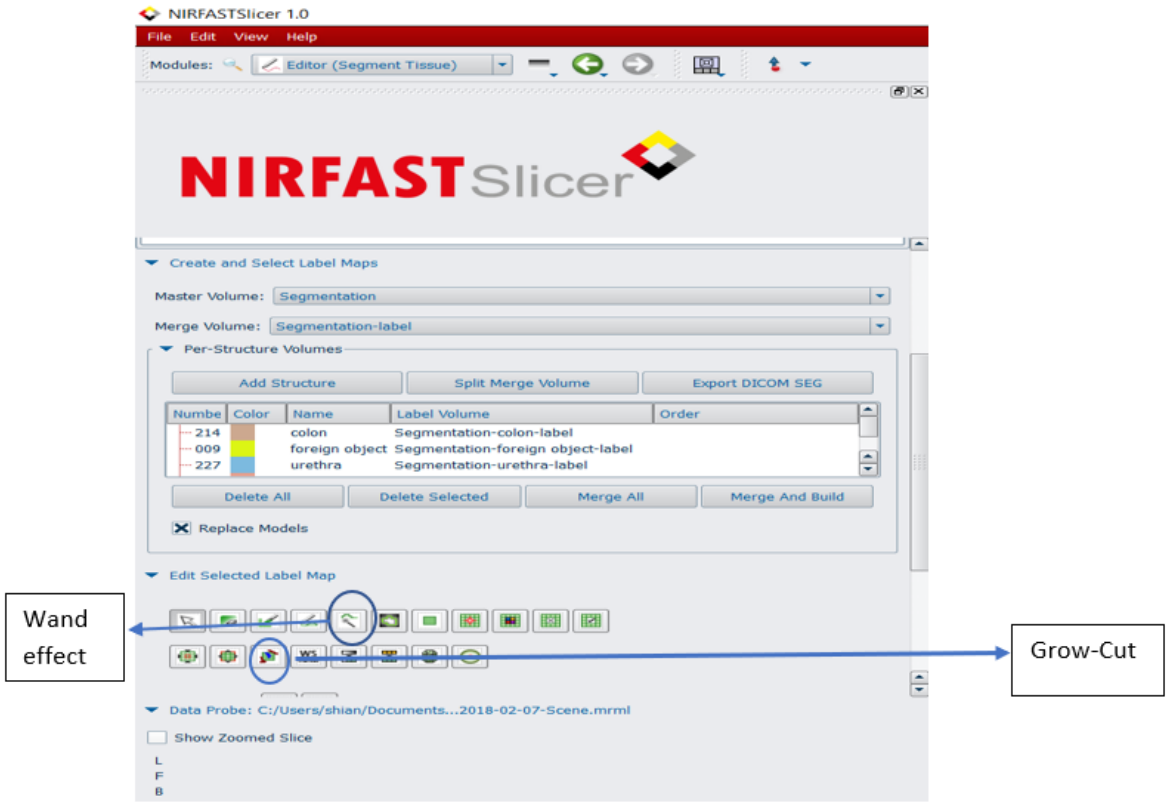

Figure 1: Segmentation with Nirfast.

The second step is to realize the segmentation of the image obtained in Nirfast Slicer. To do that, we use the tools presented in Figure 1. The segmentation map obtained is represented in Figure 2 (segmentation realized on one slice) and 4 (segmentation extended to the whole prostate).

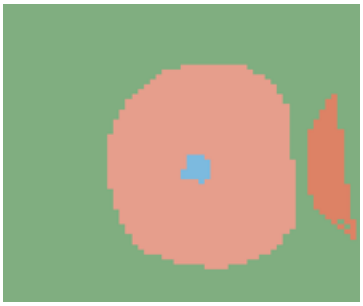

Figure 2: Segmentation Map.

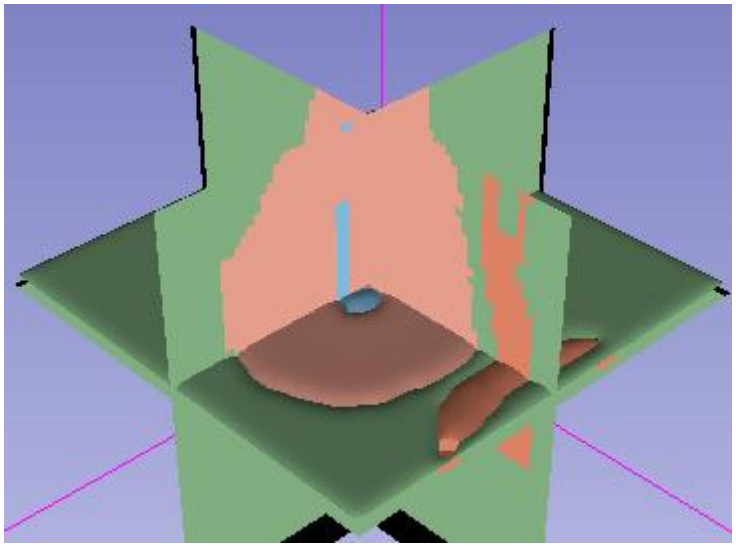

Figure 3: Extension of the segmentation to the whole prostate.

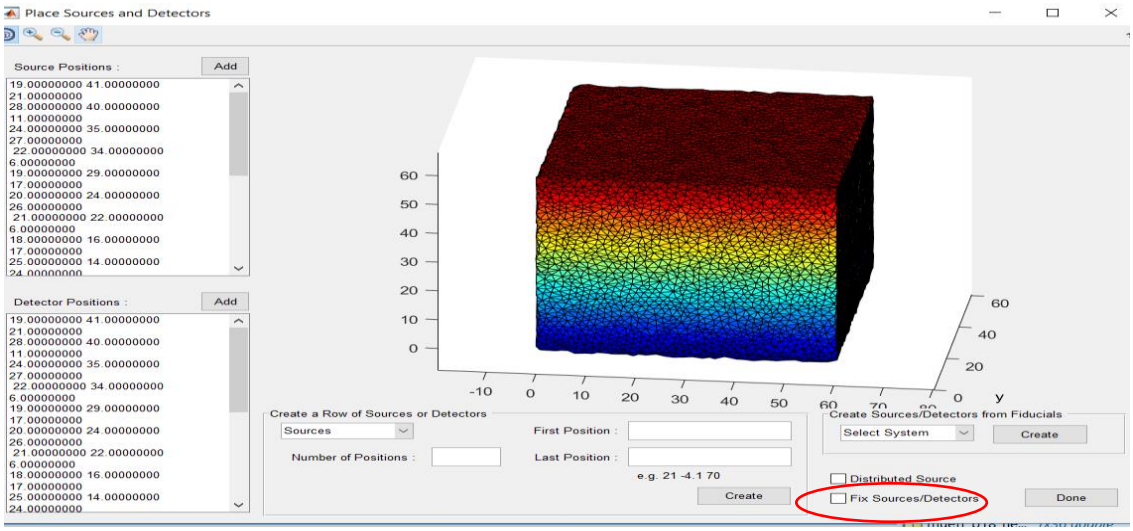

Figure 4: Creation of the mesh and positioning of the sources and detectors.

The next step is to create the mesh. To do that we select the parameters of the mesh, especially the cell size and radius. Those parameters will influence later on our results. The choice of a finer mesh increases the computation time but increases also the precision of the results. The standard parameters were chosen to realize the mesh in this master thesis. In Figure 4, we can see that it is during that mesh creation step that we have to position the fibres. The positioning of the fibres is done by an independent matlab script called MainfibrePositioning and the results (which correspond to the fibre positions) are written in the tables on the left of Figure 4. MainfibrePositionning work in the following way: basically, it starts by placing the fibres randomly in the prostate. This constitutes the only constraint for the fibres at the beginning: being placed inside the prostate and not occupy the same position as other fibres. Then, the best positioning is obtained by doing some steps in random directions until a good position is obtained. This good position is evaluated thanks to a fitness value that calculates the light distribution thanks to the diffusion approximation and tries to see if the high values are obtained within the area that we want to treat (prostate) and not outside this tissue (for example in the rectum). Then, the positions of the center point of the diffuser fibre is given. In the case of the positioning, we have decided to set a value high enough for the fibre resolution so that the positioning is independent of the fibre resolution and this parameter is constant for the positioning. It was set to 31 because it was observed that if the fibre resolution was inferior to the number of voxels

corresponding to the fibre length (given that the voxel size is 1mm) then the fibre resolution had an influence on the positioning.

So, now, we have the position of the center point of the diffuser. Nonetheless in the case of diffuser fibres, in order to create an array of point sources in Nirfast, the positions of all the points constituting the fibres must be entered in Figure 4 or the extreme positions of the fibres must be known. Another script calculates the positions of all the points based on the position of the middle point, on the length of the diffuser and on the number of points per fibre. The number of points per fibre is only a way of modelling the continuous diffuser by a discrete array of point sources. One important conclusion that we would be interested by, would be to determine if the fibre resolution has an impact on the results. We know that the fibre resolutions influence the computation time, so even though the best approximation of a continuous line would be to set the fibre resolution to a high value, we would like to see which changes, a change in fibre resolutions will cause on the light distribution. We will give a particular attention to the light dose delivered in the tissues.

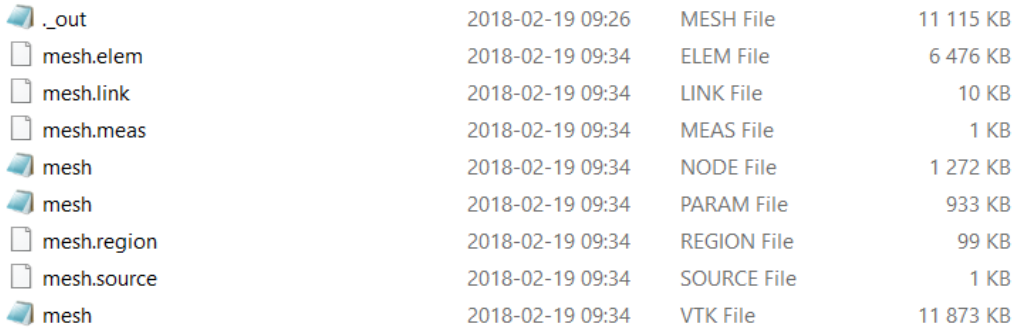

Figure 5: Mesh Files.

- Nirfast with Matlab

Nirfast is not only limited to Nirfast Slicer but it has an interface with Matlab and particularly a toolbox to process the data from Nirfast Slicer. Indeed, Nirfast has a GUI interface already implemented with Matlab. However, this GUI limits the field of action that we can have with the data generated. That is the reason why, instead of using that GUI, a Matlab script has been written to simulate the light propagation in our prostate model while using the toolbox function from Nirfast.

To be able to read the files in Figure 5, that contain information related to the mesh, a function called load_mesh, from the Nirfast toolbox, is used. This created a mesh structure in matlab whose data can be easily processed in Matlab.

```
          name: 'mesh'
         nodes: [50341×3 double]
        bndvtx: [50341×1 double]
          type: 'stnd'
           mua: [50341×1 double]
         kappa: [50341×1 double]
            ri: [50341×1 double]
           mus: [50341×1 double]
      elements: [286302×4 double]
     dimension: 3
        region: [50341×1 double]
        source: [1×1 struct]
          meas: [1×1 struct]
          link: [324×3 double]
             c: [50341×1 double]
           ksi: [50341×1 double]
element_area: [286302×1 double]
       support: [50341×1 double]
```

Figure 6: Mesh Structure in matlab.

We start by setting out the optical properties (μ_a and μ_s') for each node of the mesh and the dampening coefficient for each point source. The dampening might be due to the formation of blood around the fibre when it is inserted in the tissue and this might influence the light distribution received or emitted by the fibre. Then, we simulate data by running the function femdata_ipdt which solves the forward problem by solving equation (8) (or in other words, which answers to the question: if the optical properties are known, what is the light distribution?). During the treatment of the patient, this light distribution is not known everywhere in the patient's body but only at the positions where the fibres were inserted (the fibres act both as emitter and receiver). In order to simulate this real situation, we calculate the light distribution only at the positions of the fibres. This data, called fluence rate, in Figure 4.8 constitutes our original data with which our inverse problem (determining the optical properties if the light distribution is known) will be solved.

The data coming from the known optical properties will be referred as the FEM data and will be represented in the results section in red. This data is not accessible in reality because we do not know the real values of the optical properties.

Therefore, starting from the Fluence Rate data, we would like to calculate the optical properties by using the linear least square method. In our case we will consider two situations: on one hand, the only unknowns are the μeff at each point sources of the fibres, on the other hand, the unknowns are both those μeff coefficients but also some attenuation coefficients (named att_... in the matlab script). Those new unknown coefficients help to describe the dampening coefficients. Nonetheless, in the absence of dampening in the simulated cases, we expect those coefficients to be close to 1. We want to see the influence of the presence of those unknowns in the estimation of the inverse problem.

For the remaining part of the thesis, the method with the attenuation coefficients will be referred as Linear method and will be represented in green in all the graphics. The other method (with only the μeff coefficients) will be referred as the P18 method because it is the method currently used in the P18 system designed by Spectracure AB and the results related to this method will be illustrated in blue.

- Cimmino Algorithm: the lambda parameters

The orthogonal projection of a vector y∈ $\mathbb{R}^T$ onto an hyperplane defined as in (4.1) is given by:

$$p_{Qj} = y + c_j(y)\, a_j$$

where $c_j(y) = \min\left(0, \frac{b_j - \langle a^j, y\rangle}{\|a^j\|^2}\right)$

To calculate the irradiation times, we take the weighted projections of the irradiation times on each hyperplane. This gives the next step irradiation times. It is represented in Figure 4.1 and in the formula below:

$$x^{k+1} = x^k + \lambda_k \sum_{j=1}^{J} w_j c_j(x^k) a^j$$

$$0 < w_j < 1, \qquad j = 1, 2, \ldots, J, \qquad \sum_{j=1}^{J} w_j = 1$$

And the λ_k are some arbitrary constants called relaxation parameters. They are supposed to be in the following interval to ensure convergence with ξ a small positive quantity.

$$0 < \xi \leqslant \lambda_k \leqslant 2 - \xi$$

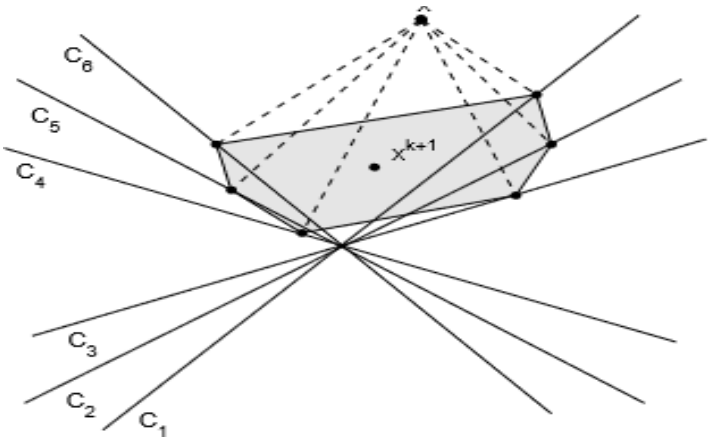

Figure 7: Cimmino algorithm ([16]).

The Block Cimmino consists in dividing the system of equations into blocks of equations. The process is illustrated in Figure 4.18 in comparison with the Cimmino algorithm represented in Figure 4.17.

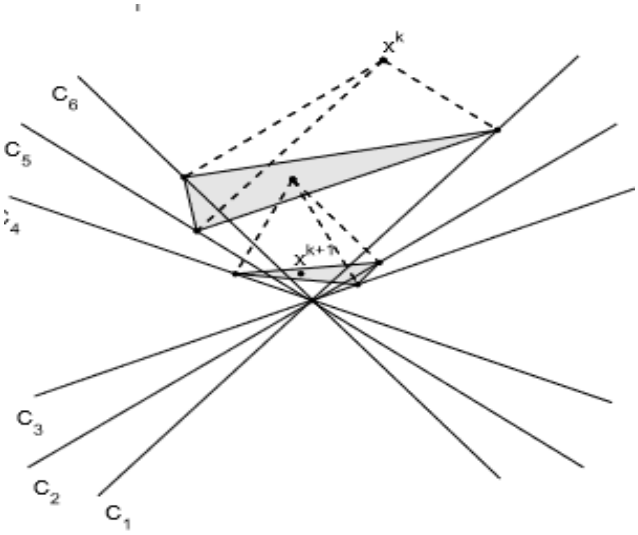

Figure 8: Block Cimmino ([16]).

In the following report, we will compare the results between a value of λ_k equal to 20 (the one set previously in the Cimmino algorithm) compared to a value of λ_k equal to 2. We will refer to the method using λ_k equal to 2 as Block Cimmino 2 and the other as Block Cimmino 20.